2011

Two-photon Cross Section Enhancement of Photochromic Compounds for Use in 3D Optical Data Storage

Gheorghe Luchita
University of Central Florida

TWO-PHOTON CROSS SECTION ENHANCEMENT OF PHOTOCHROMIC COMPOUNDS FOR USE IN 3D OPTICAL DATA STORAGE

by

GHEORGHE LUCHITA
B.S. Moldova State University, 2004
M.S. Moldova State University, 2005

A dissertation submitted in partial fulfillment of the requirements
for the degree of Doctor of Philosophy
in the Department of Chemistry
in the College of Sciences
at the University of Central Florida
Orlando, Florida

Summer Term
2011

Major Advisor: Kevin D. Belfield

ABSTRACT

Rewritable photochrome-based 3D optical data storage requires photochromic molecules with high two-photon absorption (2PA) cross sections. Currently, the low value of two-photon absorption cross sections of existing photochromes makes them unsuitable for practical application in 3D data storage. Worldwide attempts to increase the cross section of photochromic molecules by altering the chemical structure have yielded poor results. In this work, two ways to increase the two-photon absorption cross sections of photochromes were investigated. In the first method, partial success demonstrated by extending the conjugation of a photochromic molecule, a high two-photon absorption cross section of the closed form isomer and high photoconversion to the closed form were realized. At the same time, a decrease in photoswitching quantum yield and low photoconversion to open form was observed. A discussion is provided to explain the results, suggesting that the proposed method of extending the conjugation may not solve the problem. For this reason a new method for effective two-photon absorption cross section enhancement of photochromes was proposed. As a proof of principle, a new two-photon absorbing dye with a hydrogen bonding moiety was synthesized and used for the formation of supramolecular structures with a photochromic compound. Theoretical reasoning and experimental demonstration of energy transfer from the dye to the photochrome under one and two-photon excitation confirmed the practical value of the method. The effects of a 2PA dye on the photochromic properties of a diarylethene were investigated using a model compound to simplify data analysis. Formation of supramolecular structures was revealed using ^{1}H NMR spectroscopic methods. The model compound, having the same hydrogen bonding moiety as 2PA dye,

has been demonstrated to bind with photochrome molecules at very low concentrations. Photochromic properties of 2,3-bis(2,4,5-trimethyl-3-thienyl)maleimide, including conversions at the photostationary state, extinction coefficients, photoisomerization reaction rates and quantum yields, were shown to be affected by hydrogen bonding with the model compound - 2,6-bis-(acetamido)pyridine. The extent of this change was determined and discussed, demonstrating a balanced supramolecular strategy to modulate photochemical and photophysical properties of this important class of photochromic material.

TABLE OF CONTENTS

LIST OF FIGURES

LIST OF TABLES

LIST OF EQUATIONS

LIST OF ACRONYMS/ABBREVIATIONS

1PA One photon absorption

2PA Two photon absorption

2,6-BAP 2,6-bis-(acetamido)pyridine

3D Three dimensional

9,10-DPA 9,10-diphenylanthracene

AU Arbitrary units

CAD Computer aided design (software)

CD Compact disk

CD-R Compact disk recordable

CD-RW Compact disk rewritable

CF Closed form

CW Continuous wave (laser)

DVD Digital versatile disk

DCM Dichloromethane

FRET Förster resonance energy transfer, same as RET

GM Göppert-Mayer (units), 10^{-50} cm^4 sec $photon^{-1}$ $molecule^{-1}$

MCU Microcontroller unit

OF Open form

PEG Polyethylene glycol

PMMA Poly(methylmethacrylate)

PMT Photomultiplier tube

PSS Photostationary state

QY Fluorescence quantum yield

RET (Förster) resonance energy transfer

THB Triple hydrogen bonding

WORM Write once, read many (data storage type)

CHAPTER 1. INTRODUCTION

Three dimensional optical data storage, based on two-photon absorption (2PA), has been regarded as a possible means of information storage since 1989.[1] A multitude of different materials have been proposed[2-5] to be used in 3D optical data storage, nevertheless this technology struggles with severe unresolved problems that prohibit its commercial realization. The majority of these problems derive from the simple fact that 2PA is a very weak process, requiring molecules with high two-photon absorption cross sections. A systematic study[6] of the requirements imposed on the 2PA cross section of chromophores in 3D data storage applications has shown that a minimum of 1000 GM is required[7] with the use of ultrashort (100 fs) pulsed high power laser for readout at 12 Mbytes/sec. Since the high cost of such lasers makes 3D optical data storage less competitive with alternative data storage solutions, the use of continuous-wave (CW) laser diodes was proposed.[8,9] The demonstrated WORM type[10] data storage is an intriguing possibility, but the calculated write/readout speeds (based on exposure times) of under 1 Kbyte/sec is slow for practical high capacity data storage. To have the same signal-to-noise ratio with CW lasers at readout speeds in the range of several Mbytes/sec, as with high power pulsed lasers, the 2PA cross section of the chromophores has to be orders of magnitude higher.

In the case of the re-writable 3D optical data storage, the 2PA cross section of commercial fluorescent probes does not exceed 200 GM[6, 11] (and is typically below 100 GM) at the write/read wavelength, which is not sufficient for practical use even in conjunction with high power pulsed lasers. As a general rule, higher 2PA cross sections can be achieved by designing molecules with increased conjugation lengths,[12] particularly new photochromic

materials.[13,17] Some research done in this direction has shown that such modifications in the structure, in most of the cases, greatly decrease photoswitching quantum yields,[14,15] and in other cases completely disables photoswitching properties.[16] Taking into account that photochromes have to fulfill additional requirements for data storage applications,[15,17] alteration of the basic photochromic structure creates questionable chance for success.

In this work a different approach to the problem of low 2PA cross section of the photochromes is considered. The working principle has been exemplified on a photochrome from the diarylethene family, which has good thermal stability and fatigue resistance[18] but a low 2PA cross section. Figure 1 demonstrates the principle.

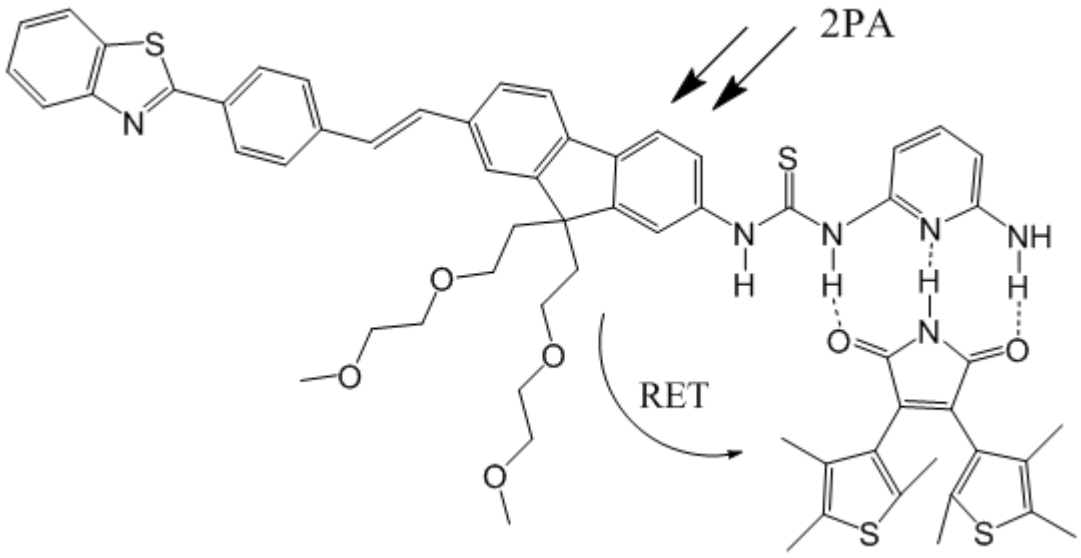

Figure 1. Hydrogen bonding formation between the photochromic molecule and the two photon absorbing dye. Close proximity of the two compounds makes it possible for an efficient resonance energy transfer to both open and closed forms of the photochrome

The photochrome is paired with a fluorescent molecule with a higher 2PA cross section, to form a supramolecular structure via hydrogen bonding. In this case, the fluorescent molecule transfers the absorbed energy of two photons to the photochrome via

Förster Resonance Energy Transfer (FRET or RET).[19] The write/readout process for data storage application using FRET has been described previously[20] on simple molecules, however it required high concentrations of photochrome used in polymer films. In contrast, the formation of a hydrogen bonded complex, may allow the use of low concentration formulations with efficient energy transfer from the dye to the photochrome. Also, the FRET approach partially addresses the destructive readout issue, which is commonly viewed by as a significant problem for photochromic optical data storage.[21] In the same work[20] it was shown that FRET-based compositions increase the number of readout cycles, before data refreshing was needed.

The formation of a supramolecular structure is expected to change the photoswitching properties of the photochromic molecule as well, because the optical properties of any molecule depend on their environment, e.g., solvent, polymer matrix, and the presence of other molecular species. In case of some of the diarylethenes, a decrease in photoisomerization quantum yields with increase of solvent polarity was reported by Irie and Sayo.[22] Their work was followed by Rappon and Syvitski who conducted a research on photochemical kinetics, and observed the effects of the solvent polarity on the rate of photo-isomerization.[23] A detailed quantitative study on the effect of the polarity of solvents and polymers upon for photophysical properties of some new photochromes was reported by Min Li and coworkers.[18] It was also expected that the presence of some impurities, complexing agents, or other additives in very small quantities can also alter the optical properties of other molecular species. However, the content of this change was not measured, until recently, when Hecht and colleagues in their work[24] on "photoswitchable triple hydrogen-bonding motif" observed a minor decrease in photoswitching quantum yields upon formation of a

supramolecular structure. Since the photochromic molecule and supramolecular complex are completely different than the ones in this work, their results may be useful as a guide.

1.1 Dissertation objectives

This dissertation has two primary objectives. The first objective is to demonstrate that the proposed new method of virtual two-photon cross section enhancement via FRET is viable. To accomplish this objective, complex formation (as in Figure 1) and the resulting side-effects are investigated. The second objective is to investigate the possibilities for use of similar complexes or new photochromes in applications such as 3D optical data storage. An example of two-photon recording and readout is presented, however the 2PA cross section of the used dye was shown to be lower than expected. Nevertheless, a quantitative evaluation of FRET effect was performed in order to determine the requirements for the two-photon absorbing dyes for future practical applications.

1.2 Dissertation outline

The current dissertation consists of six distinctive parts. The first part (background chapter), describes the basics of the technological principles of 3D data storage, two-photon absorption, measurements of two-photon absorption cross sections, photochromism and resonance energy transfer. It serves as a handy resource for those readers who are not specialists in all the topics covered in this dissertation.

In the second part of this dissertation, a new photochromic compound with extended conjugation is described, as an additional attempt to solve the low two-photon absorption cross section problem of photochromic compounds via synthetic methods. A discussion is

provided to explain the results and gain a better understanding of the limitations of this method. Based on this knowledge, a better method has been proposed and investigated in the following parts of the dissertation.

The third part of this work describes a study on supramolecular complexation between a photochromic compound and a model pyridinyl compound. As a model, a relatively simple compound was used. The model compound did not absorb in visible region as not to interfere with absorption by the photochromic compound. The use of the model pyridinyl compound also simplified the ^{1}H NMR analysis that was used in the study of hydrogen bonding effects. A quantitative investigation in the change of optical switching properties of the photochrome upon complexation is presented.

The fourth part of the work provides experimental evidence of energy transfer with a supramolecular complex. This was achieved by a comparative optical study of two photochromic systems: one with high probability of complex formation at the molecular level (with a dye containing the same H-bonding motif as the model pyridinyl compound) and the other with low probability. An additional study to estimate the ratio of complexed photochromic molecules at a concentration suitable for practical applications was performed using computer simulations. The results allows for a better understanding of the alteration or modulation of the photophysical properties of the photochrome.

The fifth part of this dissertation presents the results of two-photon absorption cross section measurements of the dyes and the photochromes used in the study. A few improvements to Z-Scan methods are described. It also includes an attempt to discuss some of the issues of two-photon absorption cross section measurements of photochromic compounds by the Z-scan method. An alternative method for two-photon absorption cross

section determination of photochromes is disclosed. Following the results of two-photon absorption cross section data for serveral dyes, data recording under two-photon absorption with the proposed systems was demonstrated under optimized experimental conditions.

The sixth part of the dissertation provides a conclusion of the work.

References

[1] Parthenopoulos D. A.; Rentzepis P.M. *Science* **1989**, *245*, 843.

[2] Belfield, K. D.; Yao, S.; Bondar, M. V. *Adv. Polym. Sci.* **2008**, *213*, 97-156

[3] Li, X.; Bullen, C.; Chon, J. W.; Evans, R. A.; Gu, M. *Appl. Phys. Lett.* **2007**, *90*, 161116/1-161116/3.

[4] Shipway, A. N.; Greenwald, M.; Jaber, N.; Litwak, A. M.; Reisman, B. J. *Jpn. J. Appl. Phys., Part I:* **2006**, *45*, 1229-1234

[5] Li, F.; Zhuang, J.; Jiang, G.; Tang, H.; Xia, A.; Jiang, L.; Song, Y.; Li, Y.; Zhu, D. *Chem. Mater.* **2008**, *20*, 1194-1196

[6] Makarov, N. S.; Rebane, A.; Drobizhev, M.; Wolleb, H.; Spahni, H. *J. Opt. Soc. Am. B* **2007,** *24*, 1874-1885

[7] The measured values of 2PA depends on the laser pulse width, the difference in 2PA cross sections can be orders in magnitude with different lasers. The value of 1000 GM is taken, assuming a 100 femtosecond pulsed laser is used.

[8] Gu, M.; Day, D. *Opt. Lett.* **1999**, *24*, 288-90.

[9] Ganic, D.; Day, D.; Gu, M. *Optics and Lasers in Engineering* **2002**, *38*, 433–437

[10] Yanez, C. O.; Andrade, C. D.; Yao, S.; Luchita, G.; Bondar, M. V.; Belfield, K. D. *ACS Appl. Mater. & Interfaces* **2009**, *1*, 2219-2229

[11] Corredor, C.; Huang, Z.-L.; Belfield, K.D. *Polym. Prepr. (Am. Chem. Soc. Div. Polym. Chem.)* **2006,** *47*, 1058-1059

[12] Drobizhev, M.; Stepanenko, Y.; Dzenis, Y.; Karotki, A.; Rebane, A.; Taylor, P. N.; Anderson, H. L. *J. Phys. Chem. B* **2005**, *109*, 7223-7236.

[13] Foelling, J.; Belov, V.; Riedel, D.; Schoenle, A.; Egner, A.; Eggeling, C.; Bossi, M.; Hell, S. W. *ChemPhysChem* **2008**, *9*, 321-326

[14] Ogawa, K.; Kobuke, Y. *Org. Biomol. Chem.* **2009**, *7*, 2241-2246

[15] Saita, S.; Yamaguchi, T.; Kawai, T.; Irie, M. *ChemPhysChem* **2005**, *6*, 2300-2306

[16] Mikhailov, I. A.; Belfield, K. D.; Masunov, A. E. *J. Phys. Chem. A* **2009**, *113*, 7080-7089

[17] Tian, H.; Feng, Y. *J. Mater. Chem.* **2008**, *18*, 1617-1622

[18] Li, M.; Pu, S.; Zheng, C.; Luo, M.; Le, Z. *Surf. Rev. Lett.* **2008**, *15*, 145-151

[19] Wen, Y.; Liu, Y.; Yang, Y.; An, L.; Song, W.; Yang, Z. *J. of Micro/Nanolithography, MEMS, and MOEMS* **2010**, *9*, 031003/1-031003/4.

[20] Corredor, C. C.; Huang, Z.-L.; Belfield, K. D. *Adv. Mater.* **2006**, *18*, 2910-2914

[21] Liu, H.-H.; Chen, Y. *J. Photochem. Photobiol., A* **2010**, *215*, 103-107.

[22] Irie, M.; Sayo, K. *J. Phys. Chem.* **1992**, *96*, 7671-4

[23] Rappon, M.; Syvitski, R. T. *J. Photochem. Photobiol., A* **1996**, *94*, 243-7

[24] Herder, M.; Patzel, M.; Grubert L.; Hecht S. *Chem. Commun.*, **2010**, *Advance Article*

CHAPTER 2. BACKGROUND

The background chapter does not contain any new ideas or discoveries other than the ones found in the literature and can be skipped by readers who are familiar with topics in 3D optical data storage, two-photon absorption, 2PA cross section measurements, photochromism and resonance energy transfer. The purpose of this chapter is to provide some background information in the listed topics that may help for a better understanding of the presented research.

2.1 Physical and technological principles of optical 3D data storage

The progress of laser technology led to a technological bloom in many fields including data storage. Several generations of optical data storage have changed since 1982 when the first commercial CD was presented to the public by SONY and Philips. The increase of laser diode output power and specific organic dyes made possible CD-R (recordable) and CD-RW (rewritable) to reach the market. Later, the use of shorter wavelength laser diode (640 nm vs. 780 nm for CD) led to the DVD. With the development of the 405 nm laser diode, the “Blue Ray” disk was introduced to the market in 2006. Each generation of optical disks offered an increasingly higher data storage density. Further increase of data density on the optical disk became problematic (no cheap ultraviolet laser diodes are currently available nor are high numerical aperture lenses), inspiring investigation of a new solution for the problem – the possibility to use the third dimension for data recording (recording in multiple layers).

Data recording and readout in three dimensions in the current research is based on the phenomenon of two-photon absorption (2PA).[1-3] This is a nonlinear optical effect that occurs at extremely high intensities of light. Practically, such intensities are achieved by focusing a powerful laser beam into a small spot. Because 2PA has a quadratic dependence on the intensity of light, with proper conditions, it is possible to localize the absorption almost entirely in the laser focal spot (see Figure 2).

Figure 2. Demonstration of excitation under conventional one-photon absorption (lower) in a comparison with two-photon absorption (upper). Note: in case of 2PA, the excitation is localized in a spot smaller than the fluorescent spot seen in the picture. The solution contains $5*10^{-5}$ M of fluorescein. Other experimental conditions can found on the research group website.[4]

The 2PA process can be viewed as the simultaneous absorption of two photons in which the sum of the energy of the two photons is the same energy of one photon of half the

wavelength. This is an oversimplified description, in reality electronic transitions in the case of two-photon absorption are different from those of single photon absorption,[5,6] resulting in a different 2PA spectral contour in comparison with one-photon absorption (1PA). In the particular case of centro-symmetrical compounds, as an example, transitions allowed by one-photon absorption are prohibited by two-photon absorption.[7] Once the energy is absorbed by 2PA, molecules are promoted into the excited state from where they can relax to the ground state through multiple mechanisms (depending on the molecule type): fluorescence, intersystem crossing, phosphorescence, thermal dissipation, energy transfer to other molecular species. In some cases this energy can induce photoreactions, such as photoisomerization and photodegradation. In most recording media considered for 3D optical data storage, molecules that express two properties are required: fluorescence (for signal detection) and photoreactivity (for signal modulation). This function can be carried by one molecular species (e.g. photobleaching of fluorescent dyes) or by several molecular species (e.g. photoactive photochromes or photoacid generating molecules[8] and a separate fluorescent dye).

From a technological point of view, there are several differences between 2D and 3D data storage. The most significant difference lies in signal registration. In the case of 3D optical data storage, because of low intensity of the fluorescence signal, an amplification of the signal is needed. This can be done with a compact photomultiplier tube (PMT)[9] or using an avalanche photodiodes (cheaper). In case of the avalanche photodiodes, additional optics is required to focus the fluorescence on the small active area of the photodiode.

A second major difference is found in the laser positioning system. 3D optical data storage requires an additional axis for depth control or layer selection. Although Figure 3

displays a classical disk (where the Y-position is controlled through rotation of the disk), 3D optical data storage is not limited to this particular shape. At smaller size scales, it can be produced in any shape, for example cube or spherical.

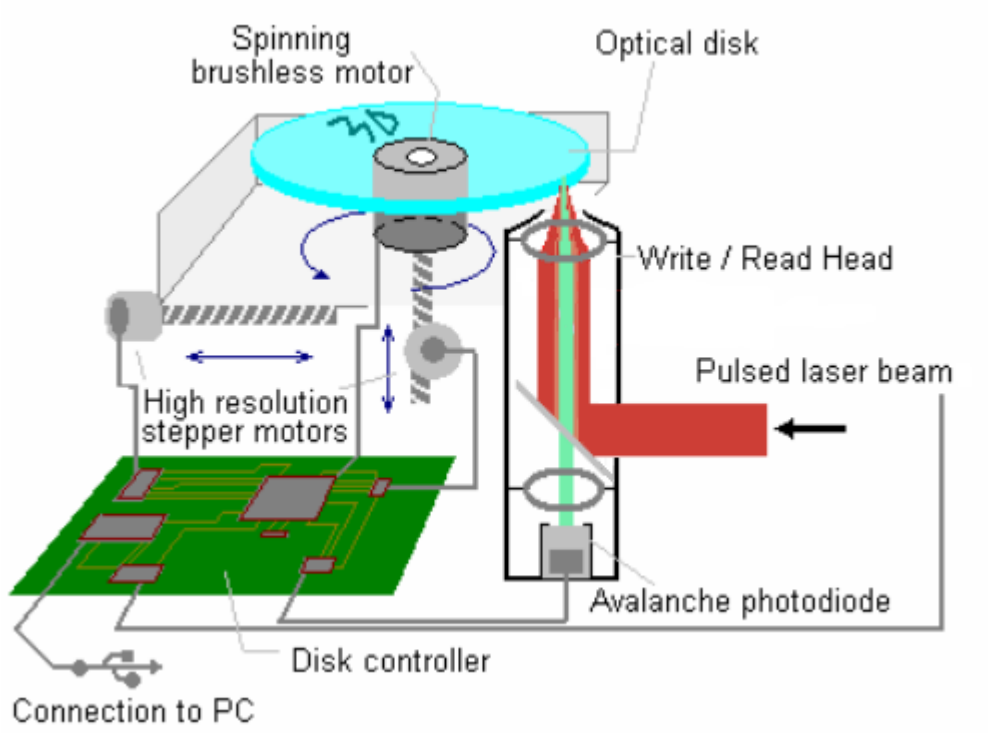

Figure 3. Schematic representation of 3D optical data storage components. In addition to the XY positioning system found in 2D optical disk drives, a third axis is used to focus the laser beam in Z-direction. The two-photon upconverted fluorescence (in light green color) is partially collected by a lens into the avalanche photodiode, where the optical signal is converted to an electrical signal. Differences in fluorescence signal conventionally represent 0 and 1 in binary code.

Probably the most important component of 3D optical data storage is the laser. Currently, there are not many choices for commercial laser sources that can meet most of the requirements (high pulse repetition rate, high power, compact size, suitable wavelength, competitive price) for this application. Nevertheless, worldwide research has been conducted

in mode-locked semiconductor-based lasers[10-13] that may change the situation and make this important component available in the near future.

2.2 Measurements of 2PA cross sections

3D optical data storage is based on the weak 2PA effect, and identifying molecules with large 2PA cross sections is an essential research pursuit. Currently, there is only a partial understanding of the relationship between molecular structure of compounds and their nonlinear optical properties. This is a primary reason that this research relies on precise experimental measurements.

Measuring accurately nonlinear optical properties of materials, in general, is not a simple task. It requires significant investments in commercially available and custom-made equipment, as well as highly trained personal. Even so, there are discrepancies in results across different research groups and different methods.[14] This is due to a difference in equipment, standards, experience, human factors, misunderstanding of related keen effects etc.

In this research two described methods for 2PA cross section measurements have been used: Z-Scan and relative fluorescence methods. The relative fluorescence method,[7] as the name suggests, is suitable only for fluorescent molecules. In this method, the fluorescence intensity (number of emitted photons) of the sample under 2PA is compared with that of a standard. With some additional data (fluorescence quantum yield, sample concentration) the relative 2PA cross section can be computed. Another technique used is the Z-Scan method.[16] Though less sensitive than the fluorescence method, it is universal and suitable for 2PA cross section measurements of all compounds (fluorescent and

nonfluorescent). The 2PA cross section value is extracted from transmittance plots, such as the one shown in Figure 4.

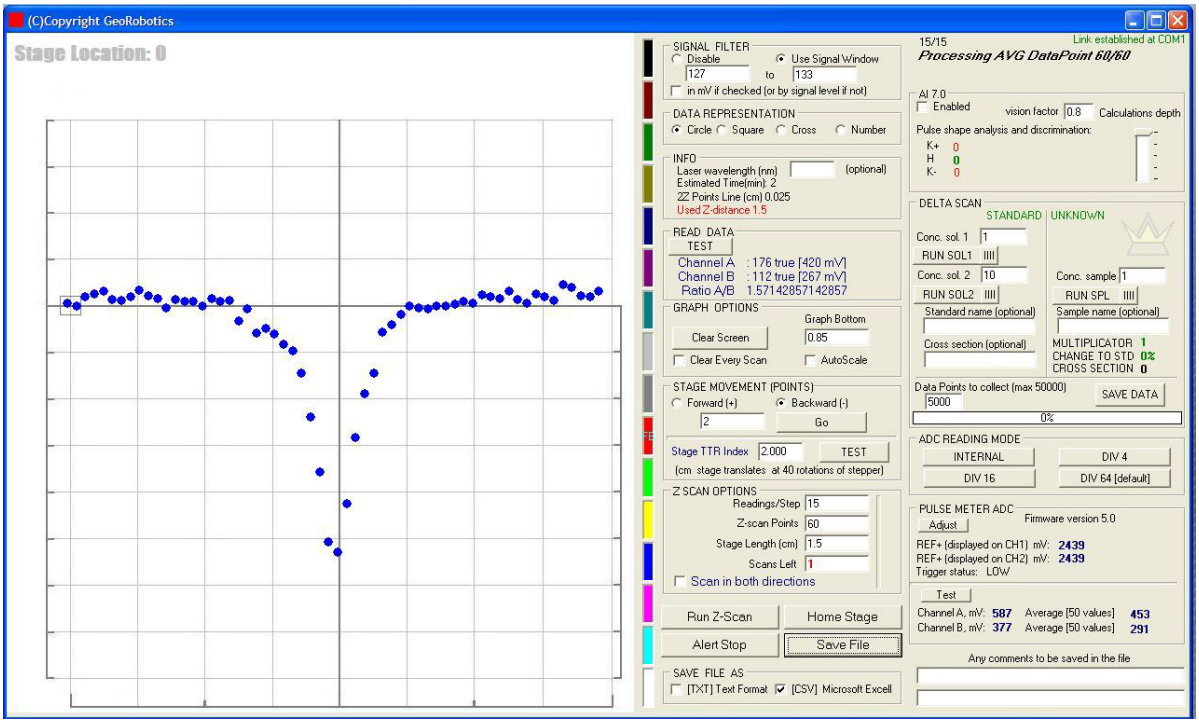

Figure 4. Screenshot from MK7 software, displaying a typical Z-Scan curve on the left side. The plot shows the sample transmittance (T) as function of the sample position (z). The sample is translated along a converging laser beam. As the sample approaches the laser focus, 2PA increases and a decline in transmittance is observed. A minimum in transmittance occurs when sample is centered on the focal volume of the laser, after which the transmittance increases again.

The nonlinear optical coefficient β is obtained by fitting from values of experimental transmittance, T(z), according to the known equation:[17]

$$T(z) = \frac{1}{\sqrt{\pi} \cdot \beta \cdot I_0(z) \cdot L} \cdot \int_{-\infty}^{+\infty} ln\left[1 + \beta \cdot I_0(z) \cdot L \cdot exp(-t^2)\right] dt$$

As one of the most popular methods for 2PA measurements, Z-Scan is constantly evolving. Several variations of the method exists, including L-Scan and double L-Scan.[18] A minor improvement to the method was realized by the author as well (in Chapter 6).

2.3 Photochromism

The property of some substances to change their color upon light exposure in a reversible way has been known for a long time. This phenomenon was scientifically explained at the end of 19th century as a reversible photo-isomerization reaction, in which the two isomers have different optical properties. Today we know it as “photochromism”, a term introduced by Yehuda Hirshberg in the 1950s. Compounds that exhibit this property are known as “photocromic compounds” or “photochromes”. There are known several classes of photochromes (e.g. azobenzenes,[19] spiropyrans,[20] fulgides[21]) and the number of classes continuously grow in numbers.

The processes of one- and two-photon photochromic transformations in organic molecules are currently a subject of great interest for various applications, such as the development of optoelectronics,[22-26] optical signal processing,[27,28] and high-density 3D optical data storage.[29-32]

Among the wide variety of photochromic compounds, diarylethene derivatives are a promising class of thermally irreversible photochromic molecules developed by Irie *et al.*[33,34] and Lehn *et al.*[35,36] for potential use in high-density optical memory devices. These compounds are characterized by efficient photoisomerization and excellent thermal stability, write-erase fatigue resistance, high sensitivity, fast response, and nondestructive readout capability.[37-40]

However, little has been reported on diarylethene derivatives with large values of 2PA cross sections and high quantum yield of the photochromic transformation. For example, diarylethene dimer derivatives with 1,4-bis-(ethynyl)benzene or 1,4-bis(ethenyl)benzene as π-conjugated chain units were described.[41] These compounds

exhibited efficient phototransformation (with corresponding quantum yields of ~0.3-0.7) but relatively small values of 2PA cross sections (~ 23-44 GM). The main difficulties in the development of photochromic 2PA diarylethenes involve the high sensitivity of cyclization and cycloreversion quantum yields on the molecular geometry of diarylethene core,[42,43] which typically changes even upon subtle structural modifications of the photochromic molecule.[44,45] Therefore, introduction of an extended π-electron system, with large 2PA, in the diarylethene-based structure often leads to a dramatic decrease in the photoisomerization quantum yield.

2.4 Resonance Energy Transfer

The close proximity of two molecules, under certain conditions, makes it possible for the energy of the excited state of one molecule (donor) to be transferred to the other molecule (acceptor) nonradiatively. The mechanism for this process is known as Forster resonance energy transfer (FRET), and has been extensively studied and applied.[46-49] For the FRET to efficiently take place, several conditions are required, but only two of them can be deliberately controlled. The first is the distance between 2 species, which should be as small as possible, typically less than 5 nm. The second is the spectral overlap; the donor emission spectrum has to, at least partially, overlap the absorption spectrum of the acceptor. Other factors that affect the efficiency of FRET, such as relative molecular dipole orientations, are difficult or impossible to control.

References

[1] Webster, S.; Fu, J.; Padilha, L. A.; Przhonska, O. V.; Hagan, D. J.; Van Stryland, E. W.; Bondar, M. V.; Slominsky, Y. L.; Kachkovski, A. D., *Chem. Phys.* **2008,** *348*, 143-151.

[2] Gu, B.; Ji, W.; Patil, P. S.; Dharmaprakash, S. M., *J. Appl. Phys.* **2008,** *10*, 103.

[3] Allain, C.; Schmidt, F.; Lartia, R.; Bordeau, G.; Fiorini-Debuisschert, C.; Charra, F.; Tauc, P.; Teulade-Fichou, M. P., *Chembiochem* **2007,** *8*, 424.

[4] Kevin D. Belfield research group website: belfield.cos.ucf.edu

[5] Belfield, K. D.; Bondar, M. V.; Yanez, C. O.; Hernandez, F. E.; Przhonska, O. V. *J. Mater. Chem.* **2009**, *19*, 7498

[6] Mikhailov, I. A.; Bondar, M. V.; Belfield, K. D.; Masunov, A. E. *J. Phys. Chem. C* **2009**, *113*, 20719

[7] Belfield, K. D.; Bondar, M. V.; Hernandez, F. E.; Przhonska, O. V.; Wang, X.; Yao, S. *Phys. Chem. Chem. Phys.* **2011**, *13*, 4303

[8] Yanez, C. O.; Andrade, C. D.; Yao, S.; Luchita, G.; Bondar, M. V.; Belfield, K. D. *ACS Appl. Mater. Interfaces* **2009**, *1*, 2219

[9] Joseph R. L. *Principles of Fluorescence Spectroscopy,* Springer Science: New York, **2006,** p.118

[10] Quinlan, F.; Ozharar, S.; Gee, S.; Delfyett, P. J.. *J. Optics A* **2009**, *11*, 103001

[11] Yang, W. *Adv. OptoElectron.* **2011**, *11*, 780373

[13] Zhao, X.; Zheng, Z.; Liu, L.; Liu, Y.; Jiang, Y.; Yang, X.; Zhu, J. *Optics Express* **2011**, *19*, 1168

[14] Makarov, N. S.; Drobizhev, M.; Rebane, A. *Optics Express* **2008**, *16*, 4029

[16] Sheik-Bahae, M.; Said, A.A.; Wei, T. H.; Hagan, D. J.; Van Stryland, E. W. *IEEE J. Quantum Electron.* **1990**, *26*, 760

[17] Belfield, K. D.; Bondar, M. V.; Hernandez, F. E.; Przhonska, O. V.; Yao, S. *J. Phys. Chem. B* **2007**, *111*, 12723

[18] Hernandez, F.E.; Rizzo, A. *Molecules* **2011**, *16*, 3315

[19] Wei, F. K., H.; Mei-Xiang, W. *Chinese Phys.* **2005**, *14*, 306.

[20] Berkovic, G.; Krongauz, V.; Weiss, V. *Chem. Rev.* **2000**, *100*, 1741.

[21] Liang, Y. C.; Dvornikov, A. S.; Rentzepis, P. M. *Macromolecules* **2002**, *35*, 9377.

[22] Yassar, A.; Garnier, F.; Jaafari, H.; Rebiere-Galy, N.; Frigoli, M.; Moustrou, C.; Samat, A.; Guglielmetti, R. *Appl. Phys. Lett.* **2002**, *80*, 4297.

[23] Berkovic, G.; Krongauz, V.; Weiss, V. *Chem. Rev.* **2000**, *100*, 1741.

[24] Yun, C.; You, J.; Kim, J.; Huh, J.; Kim, E. *J. Photochem. Photobiol. C Photochem. Rev.* **2009**, *10*, 111.

[25] Xu, L.; Zhao, Z. J.; Xing, Y. J.; Lu, P. *J. Zhejiang University-Science A* **2008**, *9*, 1590.

[26] van der Molen, S. J.; Liao, J. H.; Kudernac, T.; Agustsson, J. S.; Bernard, L.; Calame, M.; van Wees, B. J.; Feringa, B. L.; Schonenberger, C. *Nano Lett.* **2009**, *9*, 76.

[27] Paterson, J.; Natansohn, A.; Rochon, P.; Callender, C. L.; Robitaille, L. *Appl. Phys. Lett.* **1996**, *69*, 3318.

[28] Rochon, P.; Natansohn, A.; Callender, C. L.; Robitaille, L. *Appl. Phys. Lett.* **1997**, *71*, 1008.

[29] Kawata, S.; Kawata, Y. *Chem. Rev.* **2000**, *100*, 1777.

[30] Liang, Y. C.; Dvornikov, A. S.; Rentzepis, P. M. *Tet. Lett.* **1999**, *40*, 8067.

[31] Toriumi, A.; Herrmann, J. M.; Kawata, S. *Opt. Lett.* **1997**, *22*, 555.

[32] Chen, B. Z.; Wang, M. Z.; Li, C.; Xia, H. M.; Tian, H. *Syn. Metals* **2003**, *135*, 491.

[33] Irie, M.; Mohri, M. *J. Org. Chem.* **1988**, *53*, 803.

[34] Irie, M. *Chem. Rev.* **2000**, *100*, 1683.

[35] Gilat, S. L.; Kawai, S. H.; Lehn, J. M. *J. Chem. Soc. Chem. Commun.* **1993**, 1439.

[36] Tsivgoulis, G. M.; Lehn, J. M. *Angew. Chem. Internat. Ed. Eng.* **1995**, *34*, 1119.

[37] Cho, H. G.; Cheong, B. S. *Bull. Korean Chem. Soc.* **1998**, *19*, 308.

[38] Higashiguchi, K.; Matsuda, K.; Kobatake, S.; Yamada, T.; Kawai, T.; Irie, M. *Bull. Chem. Soc. Jpn.* **2000**, *73*, 2389.

[39] Miyasaka, H.; Araki, S.; Tabata, A.; Nobuto, T.; Mataga, N.; Irie, M. *Chem. Phys. Lett.* **1994**, *230*, 249.

[40] Kim, E. P., J.; Cho, S. Y.; Kim, N.; Kim, J. H. *ETRI Journal* **2003**, *25*, 253.

[41] Saita, S.; Yamaguchi, T.; Kawai, T.; Irie, M. *ChemPhysChem* **2005**, *6*, 2300.

[42] Shim, S.; Eom, I.; Joo, T.; Kim, E.; Kim, K. S. *J.f Phys. Chem. A* **2007**, *111*, 8910.

[43] Clark, A. E. *J. Phys. Chem. A* **2006**, *110*, 3790.

[44] Chen, D. Z.; Wang, Z.; Zhang, H. H. *J. Mol. Struct. Theochem* **2008**, *859*, 11.

[45] Laurent, A. D.; Andre, J. M.; Perpete, E. A.; Jacquemin, D. *J. Photochem. Photobiol. A Chem.* **2007**, *192*, 211.

[46] Schroeder, W. F.; Liu, Y.; Tomba, J. P.; Soleimani, M.; Lau, W.; Winnik, M. A. *J. Phys. Chem. B* **2010**, *114*, 3085-3094

[47] Gao, X.; Zhang, J. *ChemBioChem* **2010**, *11*, 147-151

[48] Basham, J. I.; Mor, G. K.; Grimes, C. A. *ACS Nano* **2010**, *4*, 1253-1258

[49] Rogach, A. L.; Klar, T. A.; Lupton, J. M.; Meijerink, A.; Feldmann, J. *J. Mater. Chem.* **2009**, *19*, 1208-1221

CHAPTER 3. CROSS SECTION ENHANCEMENT OF PHOTOCHROMES VIA CONJUGATION EXTENSION

In this chapter a new photochromic compound with extended conjugation is described. The presented data and discussions allow for a better understanding of the problems and challenges in the quest for excellent photochromic properties required by 3D optical data storage.

3.1 Materials and methods

The synthesis of the photochromic diarylethene 1 is shown in Figure 5. 1,2-Bis(5-chloro-2-methylthiophen-3-yl)cyclopent-1-ene (2) was converted to boronic acid *in situ* and directly coupled with 9, 9-didecyl-2-iodo-7-nitro-9H-fluorene (3) using $Pd(PPh_3)_4$ and ethylene glycol as catalysts in a one-pot reaction to give the product 1 with a yield of 77%, as described below. The structure was confirmed by ^{1}H, ^{13}C NMR as well as high resolution MS. Intermediates 2 and 3 were prepared according to literature methods.[1,2]

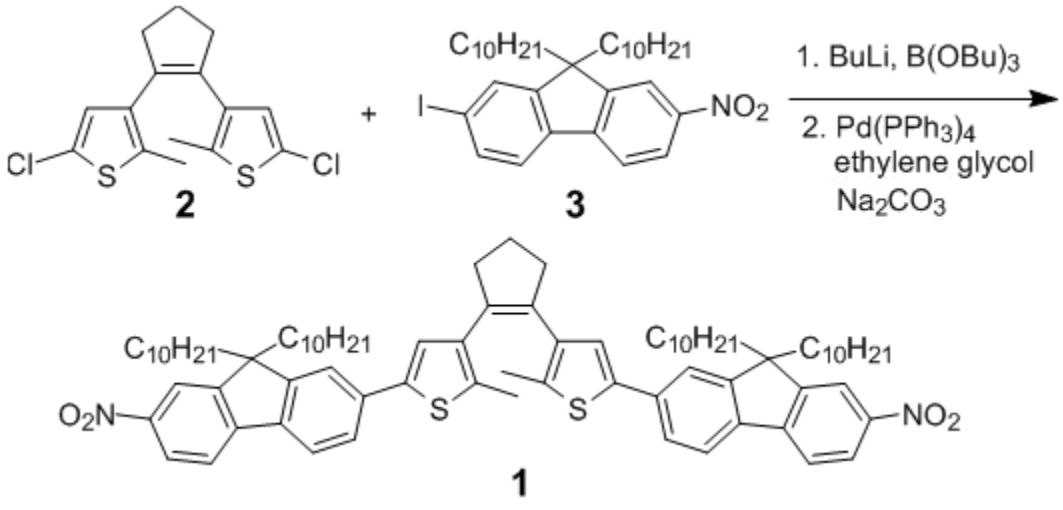

Figure 5. Synthesis of diarylethene 1.

3.1.1 Synthesis of diarylethene 1.

1,2-Bis(5-chloro-2-methylthiophen-3-yl)cyclopent-1-ene 2 (0.66g, 2.0 mmol) in dry THF was added to n-BuLi (1.6 M in hexane, 2.5 mL, 4.0 mmol) at -78 ˚C under Ar and stirred for 30 min. The mixture was then stirred at room temperature for 20 min before addition of $B(OBu)_3$ (1.73 mL, 6.4 mmol), and the reaction was continued at room temperature for one more hour. Meanwhile 9, 9-didecyl-2-iodo-7-nitro-9H-fluorene 3 (2.78g, 4.5 mmol) in THF and ethylene glycol (10 drops) mixed with 2M Na_2CO_3 aqueous solution (10 mL) was purged with Ar for 30 min. The above mentioned two solutions and $Pd(PPh_3)_4$ (0.126g, 0.11 mmol) were mixed under Ar and heated at reflux for 16 h. Water was added, and the product was extracted with hexane, washed with water, and dried over $MgSO_4$. The crude product was purified by column chromatography using hexanes/CH_2Cl_2 (from 6/1 to 3/1) to afford 1.92 g of product 1 as yellow sticky oil (77% yield). ^{1}H NMR (300 MHz, $CDCl_3$) δ 8.18 (m, 2H), 8.11 (s, 2H), 7.66 (m, 4H), 7.49 (m, 2H), 7.41 (s, 2H), 7.11 (s, 2H), 2.84 (t, J = 7.5 Hz, 4H), 2.06 (m, 2H), 2.01 (s, 6H), 1.94 (t, J = 9.0 Hz, 8H), 1.18-0.97 (m, 56H), 0.76 (t, J = 6.0 Hz, 12H), 0.54 (m, 8H). ^{13}C NMR (75 MHz, $CDCl_3$) δ 153.4, 152.2, 147.4, 147.2, 139.9, 137.9, 137.2, 135.7, 135.5, 134.9, 125.0, 124.9, 123.6, 121.8, 119.8, 118.4, 105.0, 56.0, 40.3, 38.8, 32.1, 30.1, 29.7, 29.5, 29.4 24.0, 22.9, 14.9, 14.3. HRMS (ESI) for $C_{81}H_{110}N_2O_4S_2$ theoretical m/z $[M+Na]^+$=1261.7799, found $[M+Na]^+$=1261.7790.

3.1.2 Linear photophysical measurements

All photophysical parameters of 1 were obtained in spectroscopic grade hexane, cyclohexane and dichloromethane (DCM) at room temperature. The steady-state absorption spectra of 1 were measured with an Agilent 8453 UV-visible spectrophotometer in 1 and 10

mm path length quartz cuvettes with dye concentrations $2 \cdot 10^{-5}$ M $\leq C \leq 2.5 \cdot 10^{-4}$ M. The steady-state fluorescence and excitation spectra were obtained with a PTI QuantaMaster spectrofluorimeter in 10 mm spectrofluorometric quartz cuvettes with $C \sim 1\text{-}2 \cdot 10^{-6}$ M. All fluorescence spectra were corrected for the spectral responsivity of the PTI detection system (emission monochromator and PMT). The values of fluorescence quantum yields of 1 were measured in dilute solutions by a standard method relative to 9,10-diphenylanthracene in cyclohexane.[3] Cyclization and cycloreversion reaction quantum yields of 1 were obtained by known experimental methodology[4] under cw 405 and 532 nm low intensity laser irradiation, respectively.

3.1.3 Transient absorption measurements

Investigations of dynamic processes in photochrome 1 were performed based on pump-probe transient absorption methodology[5,6] using the femtosecond laser system depicted in Figure 6a. The output of a mode-locked Ti:sapphire laser (Mira 900-F, Coherent, wavelength 800 nm, average power ≈ 1.1 W, pulse duration 200 fs, repetition rate 76 MHz) pumped by the SHG of cw Nd^{3+}:YAG laser (Verdi-10, Coherent) was regeneratively amplified with 1 kHz repetition rate (Legent Elite USP, Coherent) providing ≈ 100 fs pulses (FWHM) withan energy of ≈ 2.8 mJ/pulse. This output was split into two separate laser beams with ≈ 1.8 W and ≈ 0.8 W average powers, respectively. The first beam pumped an ultrafast optical parametric amplifier (OPerA Solo, Coherent) with a tuning range 240 nm to 20 μm, pulse duration τ ≈ 100 fs (FWHM) and pulse energies, E, up to ≈ 40 μJ. The second laser beam (800 nm) was converted via SHG for use as a 400 nm pump source. The time profile of the transient absorbance of the OF of 1 excited at 400 nm (≈ 2.5 μJ, pump pulse)

was obtained with monitoring at 425 nm (< 2 nJ, probe pulse). The polarization of the two pulses was linear and oriented at the magic angle relative to each other for all measurements. The pump and probe beams were focused to waists of radii ~ 0.7 mm and 0.2 mm (FWHM), respectively, and recombined at a small angle (< 5-7°) within the sample solutions in a 1 mm path length quartz cell. The transient absorbance profile of the CF of 1 was measured with the pump (≈ 2.5 μJ) and probe (< 2 nJ) pulses at the same wavelength (600 nm) from the OPA output split in two beams. The absorbance of the samples at the excitation wavelengths was set to be ~ 0.8-1.0 and the sample solution was circulating through a 1 mm quartz cell at a flow rate of ≈ 200 mL/min. The duration of the cross-correlation between pump and probe pulses, τ_{CC}, were measured with a pump-probe technique based on the optical Kerr effect[7,8] in a 1 mm optical pathlength quartz cell filled with CCl_4 and corresponded to ≈ 100 fs (FWHM) Gaussian pulses. A typical example of the cross-correlation trace monitored at the sample position is shown in Figure 6b.

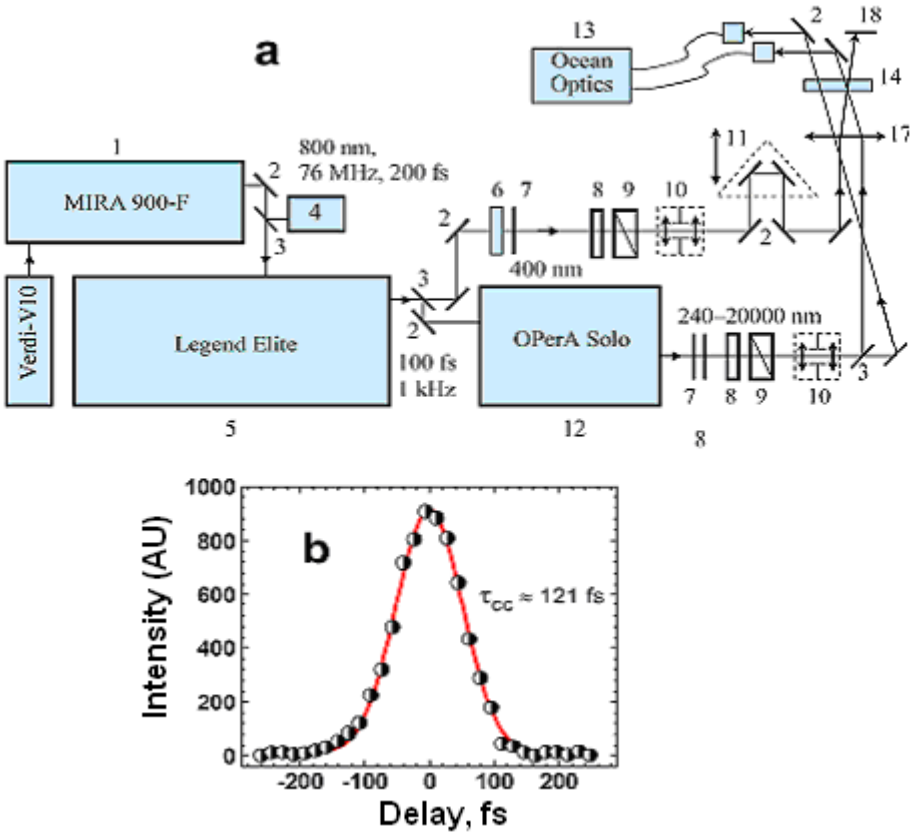

Figure 6. (a) Schematic diagram of the experimental setup: 1 - femtosecond 76 MHz laser; 2 - 100% reflection mirrors; 3 - beam splitters; 4 - spectrometer; 5 - regenerative amplifier; 6 - BBO crystal; 7 - set of neutral and/or interferometric filters; 8 - wave plates $\lambda/2$; 9 - polarizers; 10 - space filters; 11 - optical delay line with retro-reflector; 12 - optical parametric amplifier; 13 - fiber optic dual-channel spectrometer SD2000 (Ocean Optics, Inc.); 14 - 1 mm quartz cuvettes with investigated solutions; 17 - focusing lenses; 18 - beam dump. (b) Cross-correlation trace for pump-probe pulses at 600 nm. The solid curve is a fit to Gaussian pump-probe pulses with $\tau \approx 100$ fs (FWHM).

3.2 Results and discussion

3.2.1 Linear spectral properties of 1 and photoisomerization

The photoisomerization process for diarylethene 1 are shown in Figure 7. A solution of the OF is colorless (no absorption bands in the visible spectral range) and becomes colored

during the cyclization reaction OF $\rightarrow$ CF induced by UV irradiation. The reverse process CF $\rightarrow$ OF also was observed under irradiation in the visible region. The steady-state absorption spectra of the individual OF and CF of 1 and their kinetic transformations OF $\rightarrow$ CF in hexane and DCM are presented in Figure 8. The values of the direct, Φ_{OC}, and reverse, Φ_{CO}, photochromic quantum yields of 1 are indicated in Table 1 along with other major photophysical parameters. According to this data, photochrome 1 exhibited extremely high values of $\Phi_{OC} \approx 0.9\text{-}1.0$ in nonpolar solvents (hexane, cyclohexane), whereas the efficiency of the reverse reaction was lower than the ring closure by up to 3-3.5 orders of magnitude. Thus, the conversion efficiency of the direct photochromic transformation (OF $\rightarrow$ CF) exceeds 99% upon irradiation at λ_{abs}^{max} of the OF in nonpolar solvents. This high value may indicate fast interconversion between photochemically active and inactive isomers of 1. The latter, as will be shown, is also present in the mixture. No essential dependence of Φ_{OC} and Φ_{CO} on solvent viscosity was observed in nonpolar solvents. In polar DCM the efficiency of direct photochromic transformation of 1 decreased significantly ($\Phi_{OC} \approx 4 \cdot 10^{-2}$) in contrast to the reverse quantum yield Φ_{CO} which decreased 2-3 fold relative to use of nonpolar solvents.

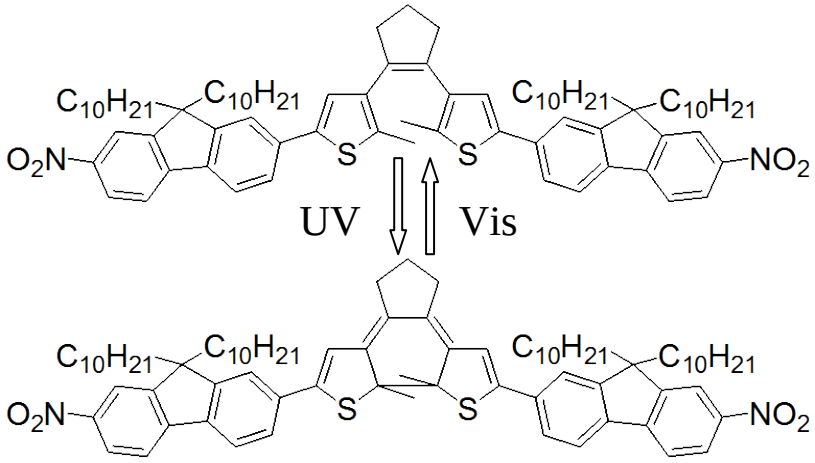

Figure 7. Molecular structures of the OF and CF isomers of photochrome 1.

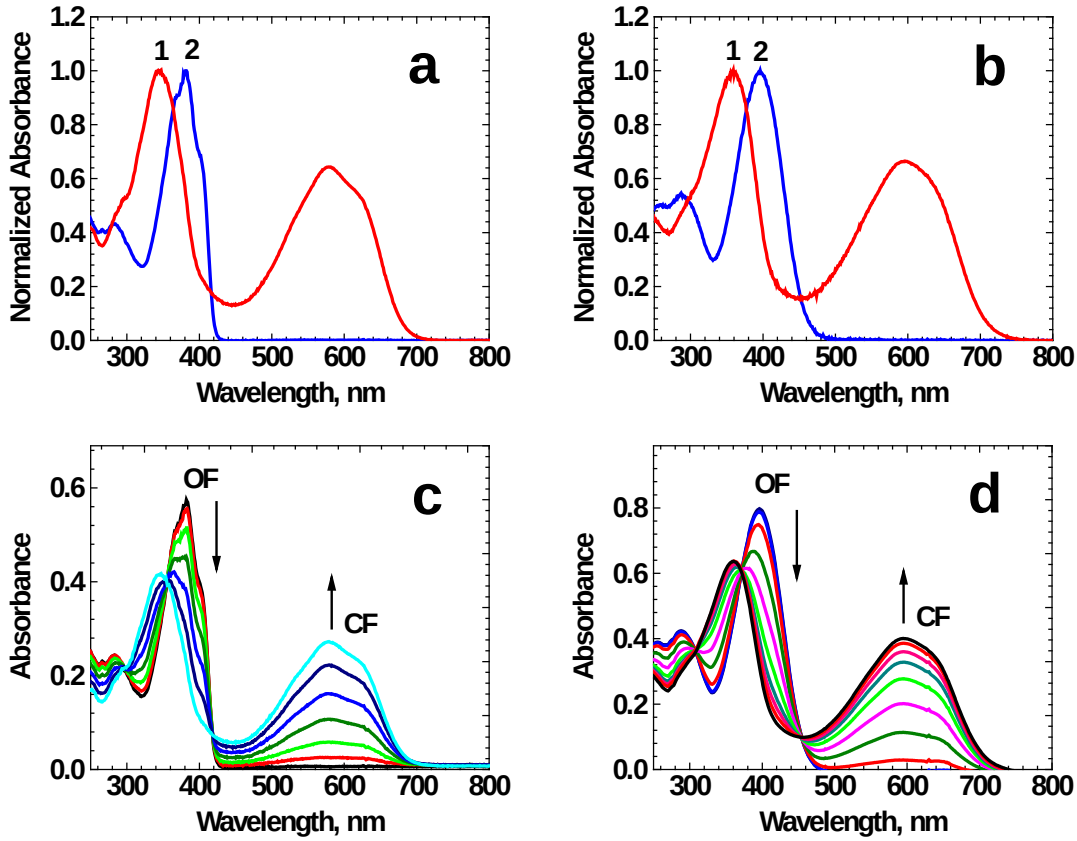

Figure 8. Normalized steady-state absorption spectra of the OF (1) and CF (2) of 1 (a, b) and kinetic changes OF → CF (c, d) under CW laser irradiation at 405 nm in hexane (a, c) and DCM (b, d), respectively.

Table 1. Major photophysical parameters of 1 in organic solvents with different polarity, Δf^*, and viscosity, η: absorption maxima, λ_{abs}; maximum extinction coefficients, ε^{max}; quantum yields of the photochromic transformations, Φ_{OC}, Φ_{CO}, at corresponding excitation wavelengths, λ_{exc}, and fluorescence quantum yields, Φ_{OF}^{FL}, Φ_{CF}^{FL}, of the open form and closed form, respectively.

N/N	Hexane	Cyclohexane	DCM
Δf^*	$8 \cdot 10^{-5}$	$2.5 \cdot 10^{-4}$	0.217
η, cP	0.313	0.97	0.4
λ_{abs}^{max}, nm (OF)	381 ± 1	385 ± 1	396 ± 1
λ_{abs}^{max}, nm (CF)	345 ± 1	347 ± 1	359 ± 1
$\varepsilon^{max} \cdot 10^{-3}$, $M^{-1} \cdot cm^{-1}$ (OF)	54 ± 5	62 ± 5	52 ± 5
$\varepsilon^{max} \cdot 10^{-3}$, $M^{-1} \cdot cm^{-1}$ (CF)	39 ± 4	46 ± 4	42 ± 4
Φ_{OC} (λ_{exc} = 405 nm)	1.0 ± 0.2	0.9 ± 0.2	0.04 ± 0.004
Φ_{CO} (λ_{exc} = 532 nm)	$(8.3 \pm 1) \cdot 10^{-4}$	$(4.8 \pm 0.6) \cdot 10^{-4}$	$(2.3 \pm 0.3) \cdot 10^{-4}$
Φ_{OF}^{FL}	$(3.3 \pm 2) \cdot 10^{-4}$	$< 10^{-4}$	$(1.2 \pm 0.4) \cdot 10^{-2}$
Φ_{CF}^{FL}	$(3 \pm 2) \cdot 10^{-4}$	$(2 \pm 1) \cdot 10^{-3}$	$(5 \pm 2) \cdot 10^{-3}$

*orientation polarizability $\Delta f = (\varepsilon - 1)/(2\varepsilon + 1) - (n^2 - 1)/(2n^2 + 1)$ (ε and n are the dielectric constant and refraction index of the medium, respectively).[3]

The reliable analysis of the steady-state fluorescence and excitation spectra of 1 (Figure 9) was performed only in more polar DCM, where the value of Φ_{OC} << 1.0 and fluorescence quantum yields of the OF, Φ_{OF}^{FL}, and CF, Φ_{CF}^{FL}, were not extremely low (see Table 1). As follows from Figure 9a, the excitation spectrum of the OF in DCM (curve 3) nicely overlapped with the corresponding absorption contour (curve 1). At first thought, the fluorescence spectrum with maximum at≈ 620 nm (curve 2) should be a weak emission of the OF in DCM. On the other hand, nearly identical excitation and emission spectra (Figure 9b, curves 2, 3) were observed from the same solution after its full photochromic transformation OF → CF (> 98 %). This suggests that a small amount (1–2%) of highly fluorescent unconverted isomers of 1 exist in solution. These isomers were likely responsible for the weak emission properties of 1 but did not effect photochromic reaction of the convertible isomers.

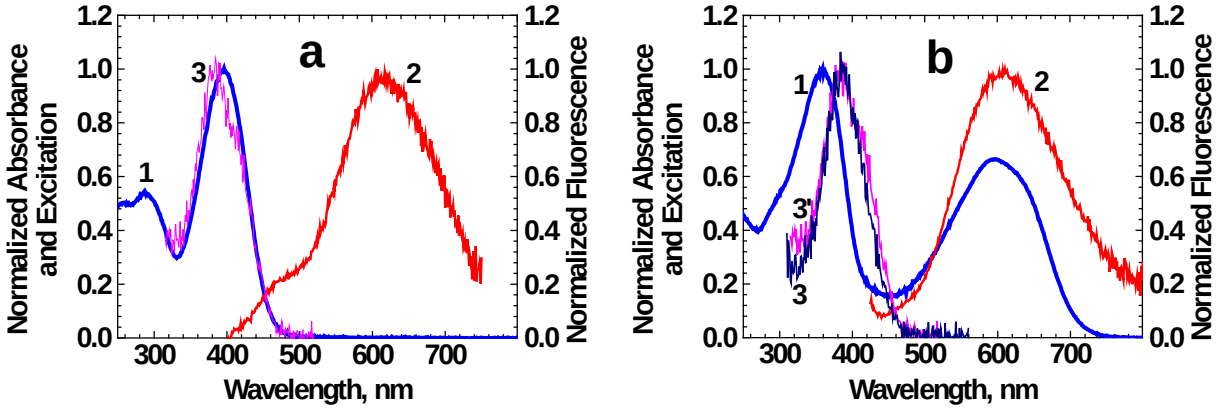

Figure 9. Steady-state absorption (1), fluorescence (2) and excitation (3, 3') spectra of the OF (a) and CF (b) of 1 in DCM. Curve 3' (b) is identical to curve 3 (a) and presented for comparison with 3 (b). The observed wavelength for all excitation spectra was ≈ 620 nm.

3.2.2 Transient absorption kinetics

Transient absorption measurements were performed in order to estimate the corresponding rate constants of the cyclization and cycloreversion reactions of 1 and better understand the fast photoisomerization that was observed. The time profiles of transient absorbance of the OF and CF of 1 in DCM, obtained by a femtosecond pump-probe technique, are presented in Figure 10. Corresponding solutions with pure OF and CF were prepared before pump-probe measurements. The negative absorption signals observed at 425 (Figure 10a) and 600 nm (Figure 10b) exhibited nearly monoexponential decay and can be ascribed to the depopulation of the OF and CF to the ground states, respectively. In the case of sufficiently low photochromic quantum yields ($\{ \Phi_{OC}, \Phi_{CO} \} << 1.0$) the time constants of the recovering processes for OF, $\tau_{OF} \approx (0.7 \pm 0.1)$ ps, and CF, $\tau_{CF} \approx (0.9 \pm 0.1)$ ps, should be consistent with corresponding lifetimes of the first excited state S_1 of OF and CF, respectively. It should be noted that no long components (~ 5-10 ps) in the negative absorbance decay that can be associated with vibrational thermalization effects in the ground state[9,10] were observed. The obtained lifetimes, τ_{OF} and τ_{CF}, along with the quantum yields Φ_{OC} and Φ_{CO}, allowed determination of the rate constants of the photochromic transformation, $k_{OF} \approx 5.7 \cdot 10^{10}$ s^{-1} (OF $\rightarrow$ CF) and $k_{CF} \approx 2.6 \cdot 10^{8}$ s^{-1} (CF $\rightarrow$ OF) for 1 in DCM. A comprehensive analysis of the data in Table 1 allows for the estimation of the corresponding rate constant for 1 in hexane as $k_{OF} > 10^{12}$ s^{-1}.

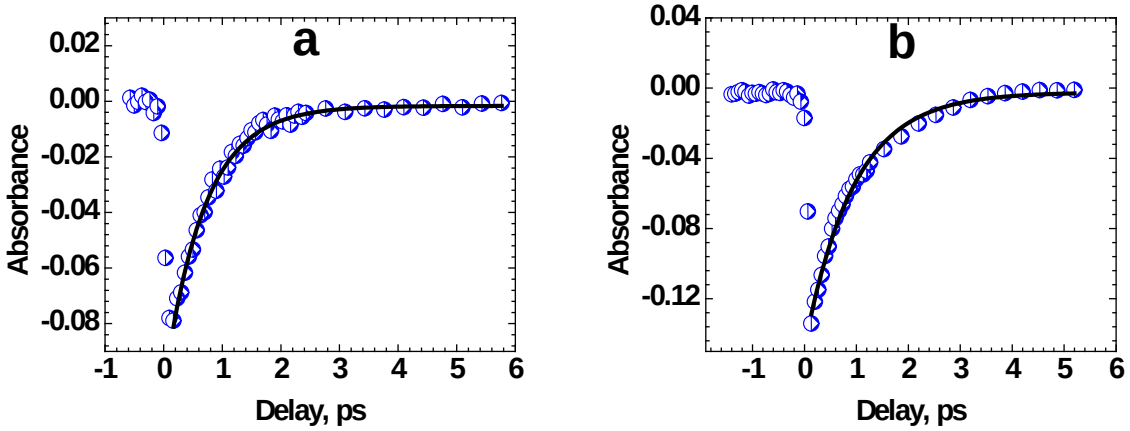

Figure 10. Transient absorbance profiles of 1 in DCM. (a) OF pumped at 405 nm and monitored at 425 nm. (b) CF pumped and monitored at 600 nm. Solid curves are the single exponential fits (see text).

References

[1] Lucas, L. N.; de Jong, J. J. D.; van Esch, J. H.; Kellogg, R. M.; Feringa, B. L. *Eur. J. Org. Chem.* **2003**, 155.

[2] Belfield, K. D.; Schafer, K. J.; Mourad, W.; Reinhardt, B. A. *J. Org. Chem.* **2000**, *65*, 4475.

[3] Lakowicz, J. R. *Principles of Fluorescence Spectroscopy*; Kluwer: New York, **1999**.

[4] Corredor, C. C.; Huang, Z. L.; Belfield, K. D.; Morales, A. R.; Bondar, M. V. *Chem. Mater.* **2007**, *19*, 5165.

[5] Lepkowicz, R. S.; Przhonska, O. V.; Hales, J. M.; Hagan, D. J.; Van Stryland, E. W.; Bondar, M. V.; Slominsky, Y. L.; Kachkovski, A. D. *Chem. Phys.* **2003**, *286*, 277.

[6] Miyasaka, H.; Murakami, M.; Okada, T.; Nagata, Y.; Itaya, A.; Kobatake, S.; Irie, M. *Chem. Phys. Lett.* **2003**, *371*, 40.

[7] Bradley, C. W. W.; Taylor, R. A.; Ryan, J. F.; Mitchell, E. W. J. *J. Phys. Cond. Mat.* **1989**, *1*, 2715.

[8] Idrissi, A.; Ricci, M.; Bartolini, P.; Righini, R. *J. Chem. Phys.* **1999**, *111*, 4148.

[9] Ishibashi, Y.; Murakami, M.; Miyasaka, H.; Kobatake, S.; Irie, M.; Yokoyama, Y. *J.f Phys. Chem. C* **2007**, *111*, 2730.

[10] Ishibashi, Y.; Okuno, K.; Ota, C.; Umesato, T.; Katayama, T.; Murakami, M.; Kobatake, S.; Irie, M.; Miyasaka, H. *Photochem. Photobiol. Sci.* **2010**, *9*, 172.

CHAPTER 4. CHARACTERIZATION OF PHOTOCHROMIC SUPRAMOLECULAR ASSEMBLY

In this work, 2,3-bis(2,4,5-trimethyl-3-thienyl)maleimide was selected as the photochromic compound or photochrome for its property to form hydrogen bonds with other compounds such as 2,6-bis-(acetamido)pyridine (see Figure 11). Formation of complexes through hydrogen bonding is a dynamic process. At equilibrium, the concentration of the complexed photochrome depends on several factors, including concentration of both complexing species and solvent. The formation of three hydrogen bonds per complex allows one to expect a strong interaction and, therefore, a reasonable concentration of photochromic complex in solution. In this chapter some evidence of complex formation will be presented, along with a quantitative study of the complexation effect upon photochromic properties.

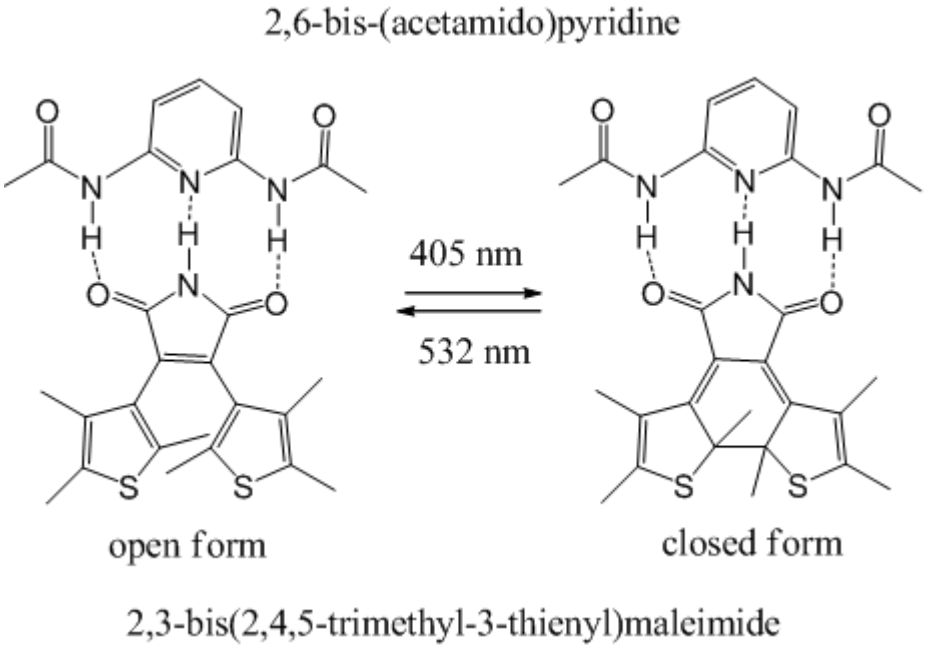

Figure 11. Intermolecular complexes formed by the open and closed-forms photoisomers of the photochrome and 2,6-BAP.

4.1 Materials and methods

The photochromic compound 2,3-bis(2,4,5-trimethyl-3-thienyl)maleimide (MW=345.48 g/mol) was purchased from TCI America and 2,6-bis-(acetamido)pyridine (2,6-BAP, MW=193.21 g/mol) from Sigma-Aldrich (from the collection of rare chemicals) and used without any additional purification. NMR experiments were performed in $CDCl_3$ using at either 300 or 500 MHz for ^{1}H or 75 MHz for ^{13}C on Varian NMR spectrometers.

4.1.1 Preparations of solutions for hydrogen-bonding study by NMR

2,6-Bis-(acetamido)pyridine (4.9 mg, $2.5 * 10^{-5}$ mol) and 2,3-bis(2,4,5-trimethyl-3-thienyl)maleimide (8.7 mg, $2.5 * 10^{-5}$ mol) were dissolved in 400 μL of $CDCl_3$. From this solution, using a micro-syringe, small volumes were subsequently added to an NMR tube, which already contained 0.45 mL of $CDCl_3$. A ^{1}H NMR spectrum was recorded following every addition. The total volumes of initial solution that resulted (in addition to 0.45 mL of $CDCl_3$) were: 5, 25, 35, 45, 55, 75, 150, 200, and 300 μL. The resulting concentrations of the photochrome and 2,6-BAP used for ^{1}H NMR are shown in Figure 14.

4.1.2 Switching properties of 2,3-bis(2,4,5-trimethyl-3-thienyl)maleimide

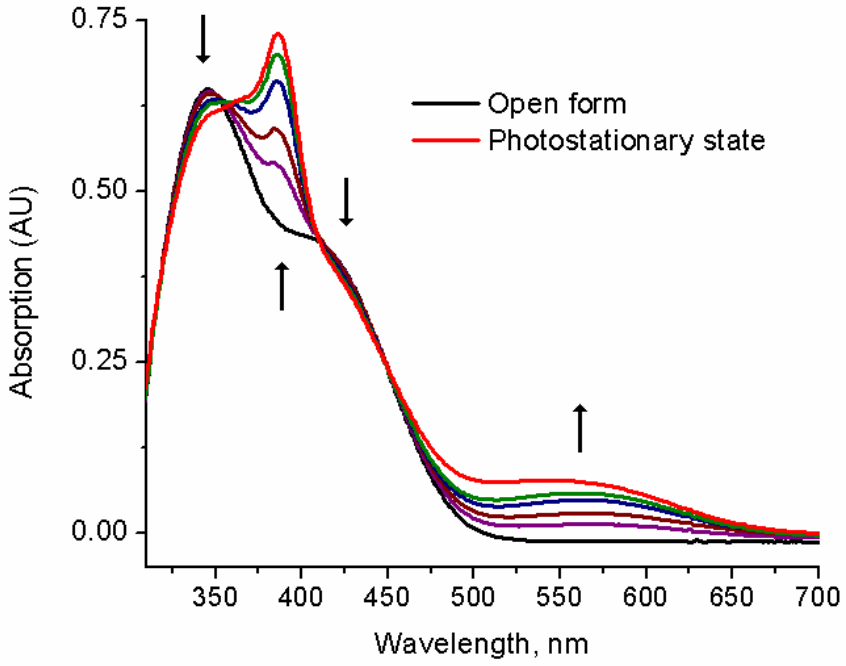

Figure 12. Absorption spectra of the open form of 2,3-bis(2,4,5-trimethyl-3-thienyl)maleimide (black line) and the photostationary state (red line) in $CHCl_3$ upon irradiation at 405 nm

2,3-Bis(2,4,5-trimethyl-3-thienyl)maleimide is commercially available in its open form isomer. It was handled under red light to avoid conversion to the closed form isomer. Absorption of the open form was recorded in a 1 mm cuvette (see Figure 10). Next, the solution was irradiated at 405 nm with a laser diode in its far field. After every 5-10 seconds an absorption spectrum was recorded until it no further change was observed (the photostationary state – PPS was achieved). The absorption at PSS, at any wavelength, is given by the following expression:

$$A_{PSS} = A_{OF} \cdot (1 - \eta) + A_{CF} \cdot \eta$$

where A_{OF} is the absorption of the open form, A_{CF} is the absorption of the closed form, and η is conversion to the closed form at photostationary state. If η is known, the absorption of the closed form is computed as:

$$A_{CF} = \frac{A_{PSS} - A_{OF} \cdot (1 - \eta)}{\eta}$$

Equation 1. Absorption of the closed form

Using the calculated conversion η=0.12 (from ^{1}H NMR data), the spectrum of the closed form was mathematically computed using above equation for every wavelength (see Figure 13). Several numerical values for extinction coefficients are presented in Table 2.

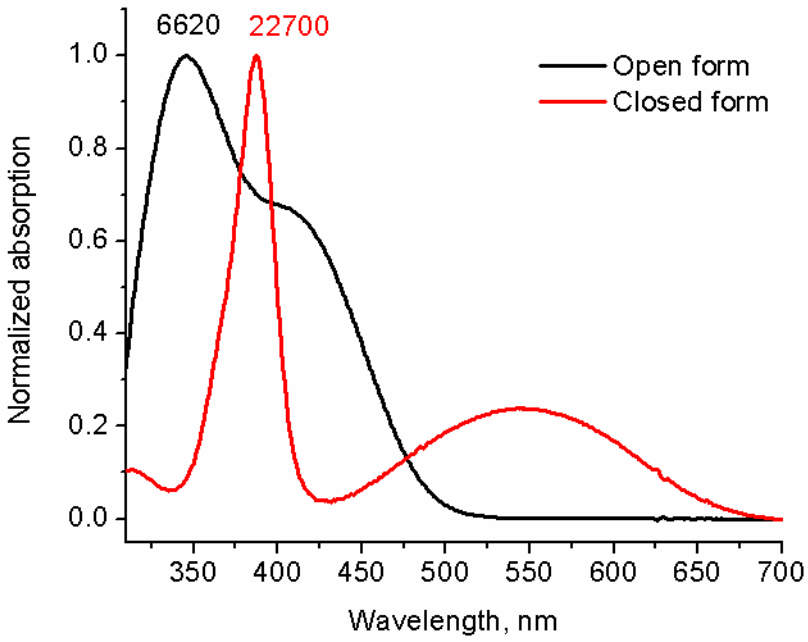

Figure 13. Normalized absorption spectra of photochrome in $CHCl_3$. Numbers indicate the value of extinction coefficients at 345 nm and 387 nm.

Table 2. Value of extinction coefficients of photochrome for selected wavelengths, M^{-1} cm^{-1}

Open form	ε_{345}=6620	ε_{405}=4450		
Closed form	ε_{387}=22700	ε_{405}=5800	ε_{532}=5300	ε_{542}=5420

4.1.3 Photophysical studies of photochrome complex with model compound (2,6-BAP)

Solutions used for determination of conversion at the photostationary state and extinction coefficients of the closed photoisomer form were prepared by the method described below. 2,3-Bis(2,4,5-trimethyl-3-thienyl)maleimide (17.7 mg, 5.1 * 10^{-5} mol) was dissolved in 2 mL of $CDCl_3$ to form a solution with the concentration of 2.6 * 10^{-2} mol/l; 0.5 mL of this solution was placed in an NMR tube, 0.5 mL in a 1 mm quartz cuvette, and 1 mL of this solution was added to a glass vial that contained 5.0 mg (2.6 * 10^{-5} mol) of 2,6-BAP. The closed vial was sonicated until the powder dissolved, and 0.5 mL of this solution was placed in an NMR tube, while 0.5 mL was placed in a 1 mm quartz cuvette. In this way, all NMR tubes and quartz cuvettes contained the same concentration of photochrome.

Absorption spectra were recorded with Agilent 8453 spectrophotometer using 1 mm path length quartz cuvettes. Before irradiation, spectra were recorded, including a blank and $CDCl_3$. Time was recorded during irradiation, until the photostationary state was reached. After 15 min of irradiation there was no change in absorption in both solutions (with and without 2,6-BAP). ^{1}H NMR spectra were recorded before irradiation as well. The NMR tubes were irradiated for 1 h, manually shaking the solutions from time to time. It has been assumed that during this time the photostationary state was achieved. ^{1}H NMR spectra were recorded again (spectra in Figure 16 and Figure 17).

The optical setup was adjusted to uniformly irradiate the sample. The irradiation of the sample (to convert the open form of the photochrome to the closed form) was done using a 405 nm laser diode with maximum output of 150 mW. The light irradiance incident on the sample was reduced with a beam expander to 18 mW/cm^2.

Preparation of the solution for photoisomerization kintetic studies was done in a similar way to the one described above in that 8.9 mg ($2.6 * 10^{-5}$ mol) of the photochrome was dissolved in 1 mL of chloroform, while 0.5 mL of this solution was placed in 1 mm quartz cuvette and the remaining solution (approximately 0.5 mL) was added to a glass vial that contained 2.5 mg ($1.3 * 10^{-5}$ mol) of 2,6-BAP in powder form. After dissolution, it was also placed in a quartz cuvette.

The same optical setup as described above was used to study the photoisomerization kinetics. Every 10 seconds the light path of the laser beam was interrupted by an electronic shutter. The cuvette was removed, manually shaken (to ensure the solution was homogeneous), and the absorption spectrum was recorded after every 10 s of irradiation (Figure 14). For the reverse process depicted in Figure 20 (closed form to open form of the photochrome), the sample was irradiated with a 532 nm laser with maximum output of 200 mW. A beam splitter and a beam expander were used to reduce the light irradiance to 4 mW/cm^2.

4.2 Results and discussions

Both substances (photochrome and 2,6-bis-(acetamido)pyridine, further in the text 2,6-BAP) can form hydrogen bonds with themselves alone, but mixed together three hydrogen bonds can be formed between the two substances, as depicted in Figure 11. In this

configuration, which has the maximum number of hydrogen bonds, the intermolecular structure is more likely to be the most stable. This means that at any given time, one would expect that more of the photochrome molecules will be hydrogen bonded to the 2,6-BAP, rather then with themselves.

To confirm the formation of hydrogen bonds between the photochrome and 2,6-BAP, an ^{1}H NMR study was conducted. The ^{1}H NMR spectra for a range of concentrations from $7*10^{-4}$ to $2.5*10^{-2}$ mol/L of open form of the photochrome and 2,6-BAP (1:1 molar ratio) were recorded (see Figure 14). The doublet that shifted from 8.3 ppm to 10 ppm, corresponded to the nitrogen-linked proton on the photochrome; the singlet that shifted with the increase of concentration corresponded to nitrogen-linked protons in the 2,6-BAP. The other peaks shown in the spectra are signals from protons on the pyridine ring. All the other NMR signals for the photochrome and 2,6-BAP are in the upfield region, exhibiting no significant dependence on concentration change (not displayed). The downfield change in chemical shift of some protons cannot be considered unambiguous proof that hydrogen bonding is formed between the two different substances in the mixture. Since direct methods of observation are not technologically accessible, one has to rely on indirect evidence of hydrogen bonding between the substances. Such indirect evidence can be the “doublet” signal of the proton on the maleimide ring (see Figure 14). This is not observed in the absence of 2,6-BAP, rather only a singlet is observed. The situation changes when 2,6-BAP is added and two signals are observed.

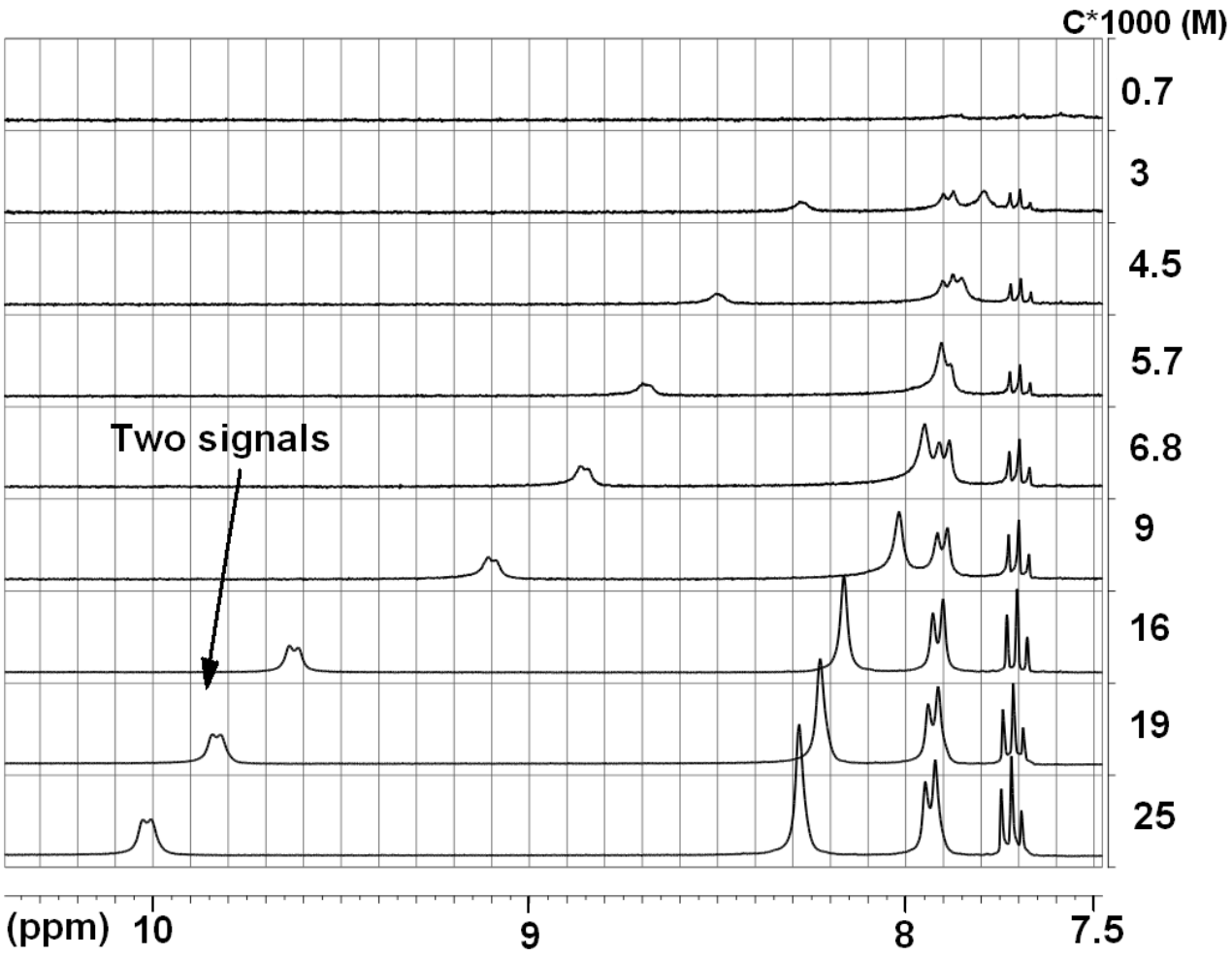

Figure 14. Partial ^{1}H NMR (300Mhz) spectra of the photochrome and 2,6-BAP at different concentrations of an equimolar mixture in $CDCl_3$. The concentration C*1000 (mol/L) is shown on the right.

Assuming that 2,6-BAP forms hydrogen bonds with the photochrome, an explanation for the "doublet" can be proposed. It has to be noted that thienyl rings in the photochrome molecule are in different planes (for simplicity noted as up and down). This is because the methyl groups in position 2 of the thienyl rings imposed restrictions on coplanarity (see Figure 15). Also, the proton on the nitrogen (marked with arrow in see Figure 15) is located on the vertex on the trigonal pyramidal geometry of the nitrogen. At room temperature, thermal energy is sufficient to let the proton swing up and down, changing its geometrical

location. In the case of being in the proximity of the photochrome, the molecule is able to form hydrogen bonds as depicted in see Figure 15. The proton becomes more confined, i.e., more energy is required for tunneling and one is able to distinguish the two protons by NMR. One proton is “up when the right ring is up” and the other is “up when the right ring is down”, relative to the reference molecule 2,6-BAP. Thus, the “doublet” is actually two different signals partially overlapped.

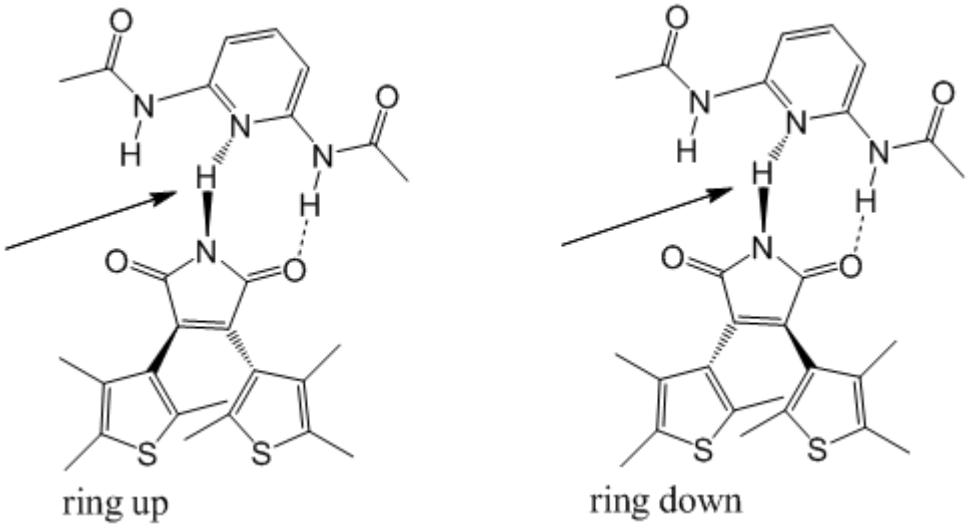

Figure 15. A possible explanation of the observed “doublet”. Formation of the hydrogen bonds “locks” the protons (with arrows), making then chemically nonequivalent.

Another rationale that can be used to support the formation of the hydrogen bonding between the two substances is the actual change in the optical properties of the photochrome, resulting from close inter-molecular interaction. The most distinguishing characteristic of photochromic molecules is photoisomerization. Photoisomerization can be characterized by several parameters, the most important is photoisomerization quantum yield. Changes in the photoisomerization quantum yield can provide a measure of the hydrogen bonding effect.

The photoisomerization quantum yield was calculated according to the following expression:[1]

$$\Phi_{1PA} = \frac{[A_{t0} - A_t] \cdot N_A}{10^3 \cdot \varepsilon_\lambda \cdot I_0 \cdot (1 - 10^{-D}) \cdot \Delta t}$$

Equation 2. Photoisomerization quantum yield

In the above expression, $A_{t0} - A_t$ is the difference in absorption at any arbitrary wavelength of observation λ_1, upon irradiation with a monochromatic light (λ_2) with intensity I_0 during Δt time. ε_λ is the extinction coefficient of the photochrome at wavelength of observation λ_1. N_A stands for the Avogadro number, and D is the average of optical densities in the photochrome absorption spectrum at λ_2, during irradiation interval.

The λ_1 was chosen in the region where only closed form of the photochrome absorbs (see Figure 13) and 532 nm is the arbitrary number used for calculations. To apply the above formula, the extinction coefficient at the wavelength of observation λ_1 had to be determined. The extinction coefficient of any substance depends on the surrounding environment, such as solvent and the presence of other substances in the solution. Thus, one would expect a difference in extinction coefficients for the cases with and without 2,6-BAP.

Technically, it is possible to isolate the closed form of the photochrome, and prepare a solution with known concentration then determine the extinction coefficient from the absorption spectrum. However, taking into account the photosensitive nature of the photochrome an indirect method is preferred. Since at 532 nm only one isomer absorbs, by knowing the concentration of the closed form at the photostationary state it was possible to calculate the extinction coefficient. The concentration of the closed form at the photostationary state was determined by ^{1}H NMR. Figure 16 shows the partial ^{1}H NMR spectra of the photochrome before irradiation and at the photostationary state.

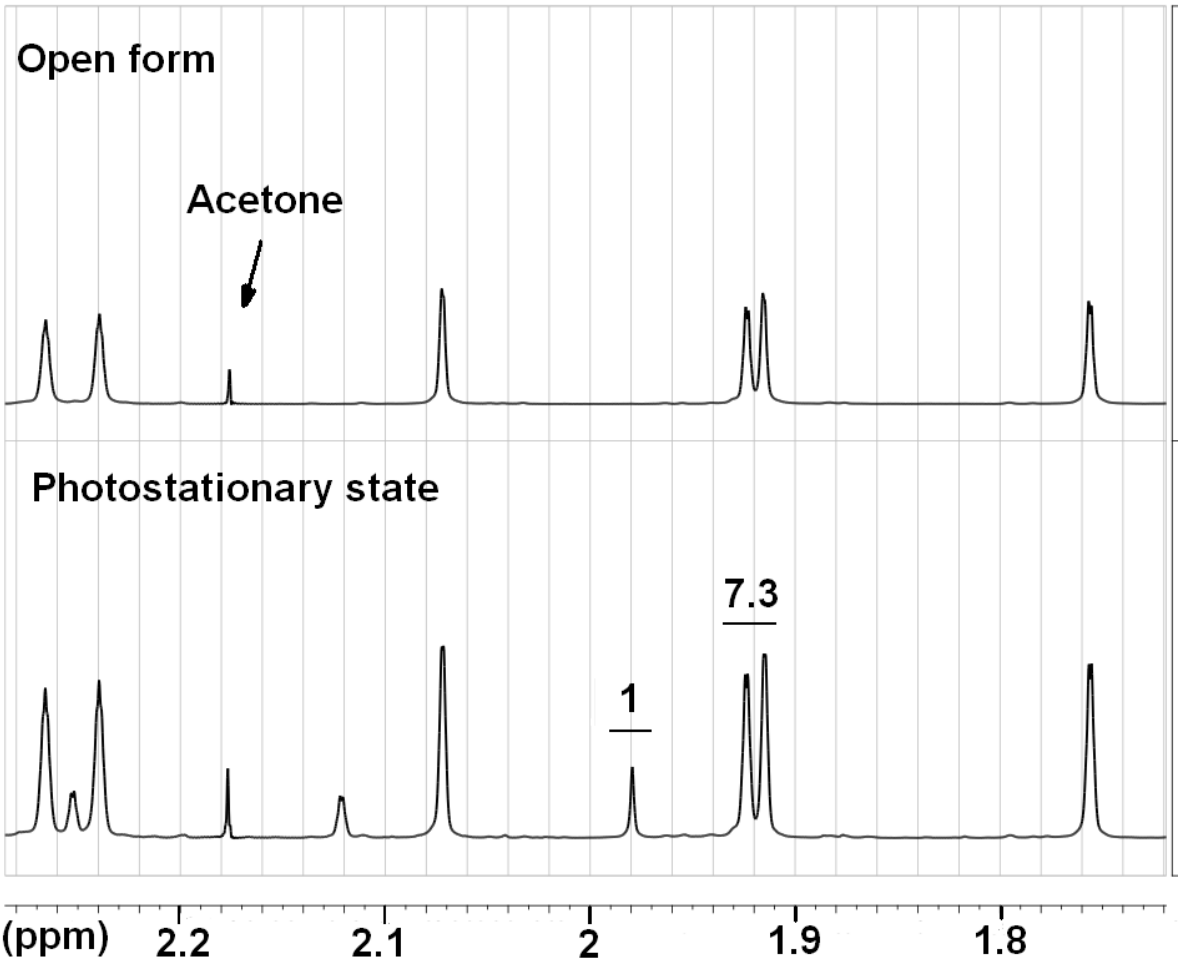

Figure 16. ^{1}H NMR (500Mhz) spectra of the photochrome in $CDCl_3$ before irradiation (top spectrum) and after irradiation at 405 nm, and photostationary state (bottom spectrum)

All six methyl groups on the photochrome molecule in the open form are distinguishable by ^{1}H NMR (as 6 singlets with same integrated area, Figure 16, top spectrum), because of the nonplanar structure of the molecule. Given sufficient time for irradiation, the photostationary state is established. At this point, the concentration of both closed and open form of the photochromic molecules does not change. In the case of the closed-form photochromic molecules, the thienyl rings are arranged symmetrically toward the maleimide ring, and the number of signals in ^{1}H NMR spectrum is reduced to 3 singlets (see Figure 16 for three additional signals). Therefore, the integral ratio between any one

small signal and 2 larger signals corresponds to the ratio of the closed form to the open form in the mixture. This ratio was found to be 1:7.3. For a nearly identical concentration of the photochrome (see experimental section for details), but in the presence of 2,6-BAP, the concentration ratio at the photostationary state between closed and open forms was found to be as 1:12 (see Figure 17).

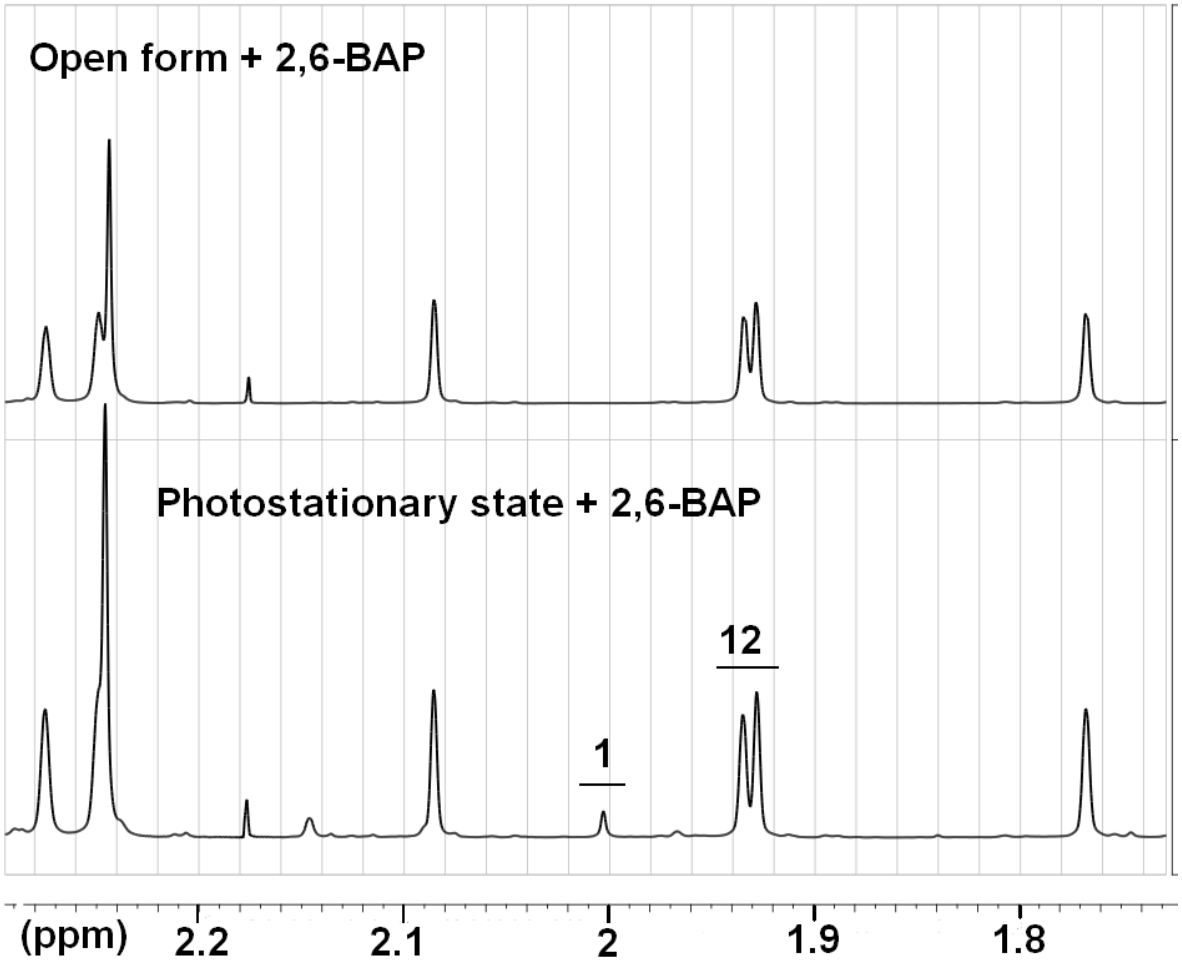

Figure 17. ^{1}H NMR (500 MHz) spectra of the mixture of photochrome and 2,6-BAP before irradiation (top spectrum) and same mixture after irradiation at 405 nm and photostationary state (bottom spectrum).

For the same concentration of photochrome that was used in the ^{1}H NMR study, absorption spectra were recorded at the photostationary state (Figure 18). The extinction coefficient for closed form was determined from the Beer–Lambert–Bouguer law (see Table 3). The presence of 2,6-BAP decreased the concentration of the closed form relative to open form in the photostationary state and increased the extinction coefficient of the closed form by approximately 15%. It can be noted from Figure 18 that the extinction coefficient for the open form also increased in the presence of 2,6-BAP (compare curve A and curve B). 2,6-BAP itself does not absorb in the visible region.

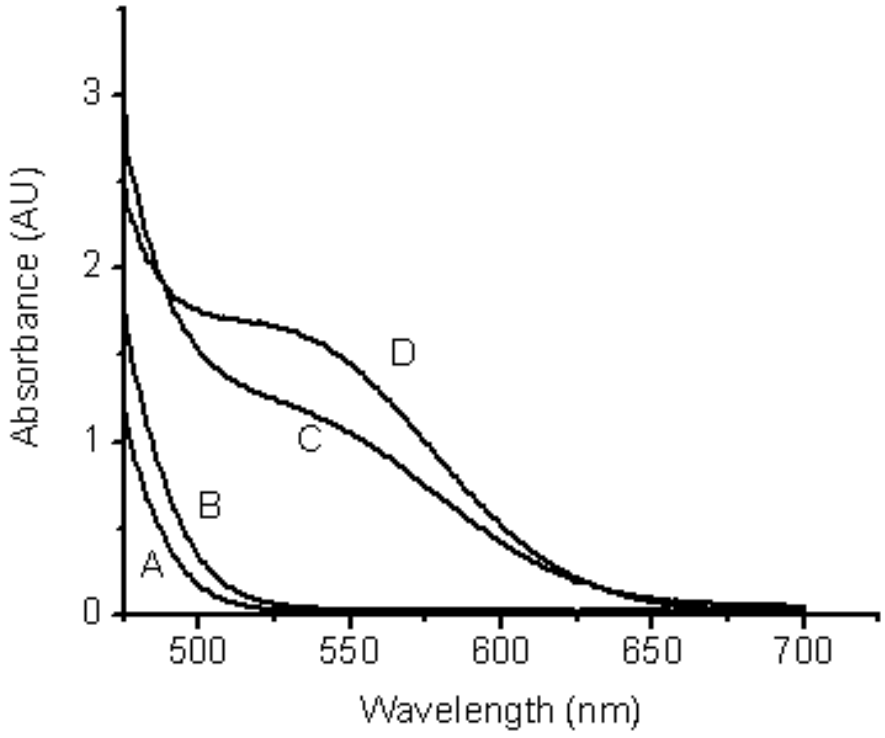

Figure 18. Absorption spectra in $CDCl_3$ of: A – photochrome open form without 2,6-BAP; B – photochrome open form with 2,6-BAP; C – photostationary state of photochrome with 2,6-BAP; D – photostationary state of photochrome without 2,6-BAP.

Knowledge of the extinction coefficient at λ_1 of the closed form facilitated photochemical kinetic studies and quantum yield calculations. The same concentration of the photochrome that was used for calculation of the extinction coefficient of the closed form was used for kinetics studies. Initial solutions (with and without 2,6-BAP) containing only the open form of photochrome were irradiated with a 405 nm laser and absorption spectra recorded after every 10 s of irradiation, for a total of three minutes irradiation time. The resulting spectra are shown in Figure 19. The same solutions were then irradiated over three minutes with a 532 nm laser, and the absorbance was recorded after every 10 s of irradiation (Figure 20). It was observed, in both cases, that in the presence of 2,6-BAP the photoisomerization rate decreased.

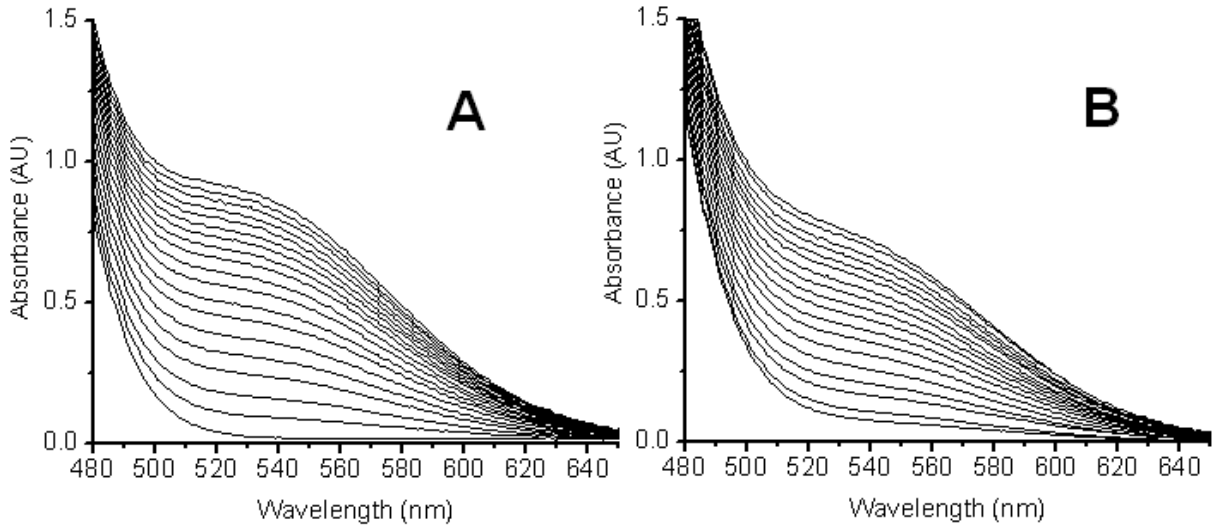

Figure 19. Kinetics of photoisomerization reaction in $CDCl_3$ with excitation at 405 nm; (A) photochrome without 2,6-BAP and (B) photochrome in the presence of 2,6-BAP.

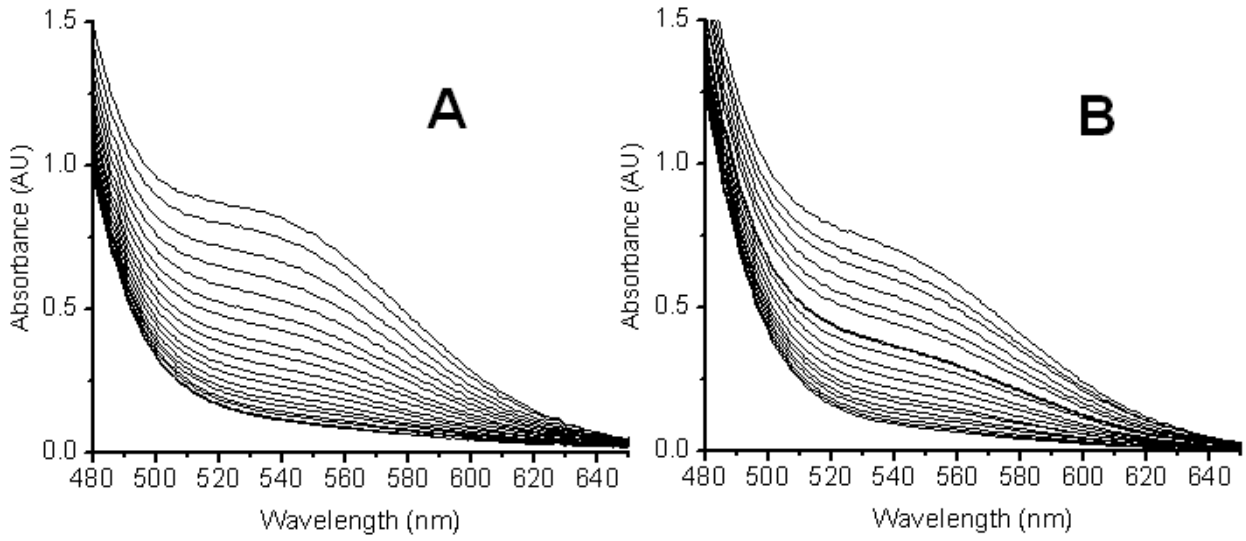

Figure 20. Kinetics of photoisomerization reaction in $CDCl_3$ with excitation at 532 nm; (A) photochrome without 2,6-BAP and (B) photochrome in the presence of 2,6-BAP.

For the concentration used, the absorbance of the photochrome at 405 nm was large and the factor $1\text{-}10^{-D}$ in the quantum yield formula can be taken as 1 for the process depicted in Figure 19. From the absorption spectra in Figure 13, one can see that, at 405 nm, both isomers absorb photons. As soon as some open-form molecules of the photochrome isomerizes to the closed-form, a reverse process can occur due to absorption of the closed form at 405 nm (from closed to open). This is the reason why the photoisomerization quantum yield for the open-to-closed process can be only estimated, based on the first data points. The actual quantum yield is expected to have a higher value. In the case of the closed-to-open process, the photoisomerization quantum yield can be determined with certainty, by averaging the values calculated with the quantum yield formula and using data from Figure 20 at 532 nm. Calculated photoisomerization quantum yields are presented in Table 4.

Table 3. Alteration of photochromic properties inside the supramolecular complex

Parameter	Photocrome without 2,6-BAP	Photochrome with 2,6-BAP
Absorption at 532 nm at photostationary state	1.63	1.20
Total concentration of photochrome in sol., mol/L	$2.6 * 10^{-2}$	$2.6 * 10^{-2}$
Closed to open form concentration ratio	1:7.3	1:12
Conversion to closed form, η %	12%	7.7%
Concentration of the closed form, mol/L	$3.1 * 10^{-3}$	$2.0 * 10^{-3}$
Cuvette optical path length, cm	0.1	0.1
Extinction coefficient for closed form at 532 nm, M^{-1} cm^{-1}	5300	6070

Table 4. Photochrome photoisomerization quantum yields

	Without 2,6-BAP	With 2,6-BAP
Open to Closed (first point only)	(2.3 ± 0.1) %	(1.9 ± 0.1) %
Closed to Open (averaged)	(7.8 ± 0.4) %	(6.5 ± 0.3) %

References

[1] Corredor, C. C.; Belfield, K. D.; Bondar, M.V.; Przhonska, O. V.; Yao, S. *J. Photochem. Photobiol., A* **2006**, *184,* 105–112.

CHAPTER 5. STUDY OF RESONANCE ENERGY TRANSFER WITHIN SUPRAMOLECULAR COMPLEX

This chapter provides experimental evidence of energy transfer with a supramolecular complex. This was achieved by a comparative optical study of two photochromic systems: one with high probability of complex formation at the molecular level (with a dye containing the same H-bonding motif as the model pyridinyl compound) and the other with low probability. An additional study to estimate the ratio of complexed photochromic molecules at a concentration suitable for practical applications was performed using computer simulations.

5.1 Materials and methods

2,6-Diaminopyridine (referred to herein as compound B) was purchased from Sigma-Aldrich and purified by cold recrystallization from CH_2Cl_2. This involved preparation of a saturated solution at room temperature in CH_2Cl_2, followed by a slow partial distillation of the solvent at room temperature under reduced pressure. The resulting white crystals were filtered and used immediately. The photochromic compound 2,3-bis(2,4,5-trimethyl-3-thienyl)maleimide (MW=345.48 g/mol) was purchased from TCI America and 2,6-bis-(acetamido)pyridine (2,6-BAP, MW=193.21 g/mol) from Sigma-Aldrich (from the collection of rare chemicals) and used without any additional purification. NMR experiments were performed in $CDCl_3$ using at either 300 or 500 MHz for ^{1}H or 75 MHz for ^{13}C on Varian NMR spectrometers. High resolution mass spectrometry (HRMS) analysis was performed in the Department of Chemistry, University of Florida, Gainesville, FL.

5.1.1 Synthesis of precursor: 2-(4-(2-(9,9-bis(2-(2-methoxyethoxy)ethyl)-2-isothiocyanato-fluoren-7-yl)vinyl)phenyl)benzothiazole

Compound A (MW=662.86 g/mol) was prepared in a similar procedure as described in the literature.[1] 9,9-Bis(2-(2-methoxyethoxy)ethyl)-7-(4-(benzothiazol-2-yl)styryl)-9H-fluoren-2-amine (0.28 g, 0.45 mmol) was dissolved in $CHCl_3$ (10 mL) to which aq. $CaCO_3$ (0.15 g, 2.88 mmol) was added. Thiophosgene (0.054 mL, 0.76 mmol) was added dropwise at 0 °C with vigorous stirring. After 2.5 h the starting material was completely consumed and 10% HCl (7 mL) was added until no gas generation was observed. The reaction mixture was poured into H_2O, extracted with CH_2Cl_2, dried over $MgSO_4$, and upon filtration and concentration, resulted in orange oil. The crude product was purified by column chromatography on silica gel eluting with hexane/ethyl acetate (3:2), affording 0.24 g of a yellow solid (85 % yield, mp 106-107 °C). ^{1}H NMR (500 MHz, $CDCl_3$) δ: 8.12, (m, 3H), 7.92 (d, 1H), 7.62 (q, 4H), 7.51 (t, 2H), 7,39 (t, 2H), 7.28 (m, 4H), 3.29 (m, 10H, OCH_3, OCH_2), 3.13 (m, 4H, OCH_2), 2.86 (m, 4H, OCH_2), 2.48 (m, 4H, CH_2). ^{13}C NMR (125 MHz, $CDCl_3$) δ: 167.59 (Ar-C=N), 154.23, 151.02, 149.80, 139.90, 139.29, 139.22, 136.83 (N=C=S), 135.24, 135.04, 132.71, 130.20, 130.02, 128.06, 127.97, 127.02, 126.80, 125.19, 125.16, 123.18, 121.62, 121.15, 120.64, 120.41, 71.72, 69.98, 66.89, 59.01, 51.52, 39.68. HRMS-EI theoretical m/z $[M]^+$= 663.24, found 663.23.

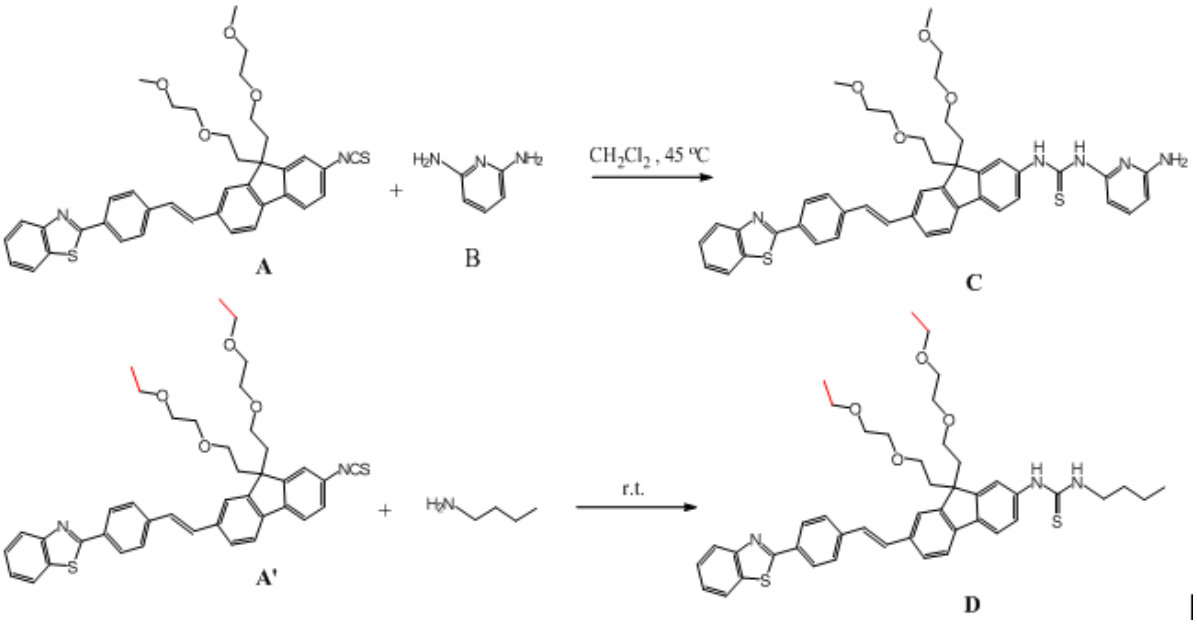

Figure 21. Preparation of model (D) and triple hydrogen bonding compound (C).

5.1.2 Synthesis of hydrogen bonding compound: 1-(6-aminopyridin-2-yl)-3-(7-(4-(benzothiazol-2-yl)styryl)-9,9-bis(2-(2-methoxyethoxy)ethyl)-fluoren-2-yl)thiourea.

Compound C (MW=771.99 g/mol) was prepared from A in reaction with 2,6-diaminopyridine (see Figure 21). Aliquots of a solution (0.5 mL) of compound B (80 mg, 0.12 mmol) in CH_2Cl_2 was added dropwise to a solution (2 mL) of compound A (132 mg, 1.2 mmol) in CH_2Cl_2, with gentle stirring. The resulting mixture was placed to react for 1 h at 45 °C, after which the mixture was passed through a silica gel chromatography column (15 cm length, 2.5 cm diameter) eluted with ethyl acetate-hexane mixture (3:1 ratio). Fractions containing the product were visualized by thin layer chromatography. The FRETention factor of the product in the above eluent is R_f=0.5. Fractions containing the product were combined and the solvent was distilled at reduced pressure (50 °C, 260 mbar). The resulting product (82 mg, 88% yield) was isolated as yellow crystals with m.p. 178.4-178.7 ˚C. ^{1}H NMR (500 MHz, $CDCl_3$) δ: 13.50 (s, 1H), 8.63 (s, 1H), 8.12 (d, 2H), 8.09 (d, 1H), 7.91 (d, 1H), 7.76 (s,

1H), 7.69 (s, 1H), 7.68 (m, 5H), 7.52 (m, 2H), 7.41 (m, 2H), 7.29 (d, 1H), 7.22 (d, 1H), 6.20 (d, 1H), 6.16 (d, 1H), 4.72 (s, 2H), 3.30 (m, 14H), 2.90 (m, 4H), 2.46 (m, 4H). Complete peak assignment and COSY spectrum are given in Appendix A . ^{13}C NMR (75 MHz, $CDCl_3$) δ: 178.9 (N-CS-N), 167.9 (S-C=N), 156.2, 154.5, 152.0, 150.1, 150.0, 140.8, 140.3, 138.6, 138.2, 136.3, 135.3, 132.7, 130.8, 128.2, 127.9, 127.6, 127.3, 126.9, 126.6, 125.4, 124.4, 123.3, 121.8, 121.3, 120.3, 120.1, 102.4, 101.2, 72.0, 70.2, 67.3, 60.7, 59.2, 51.7, 39.9. HRMS-ESI theoretical m/z $[M+H]^+$ = 772.2986, found 772.2990; theoretical m/z $[M+Na]^+$ = 794.2805, found 794.2802.

5.1.3 Synthesis of model compound: 1-(7-(4-(benzothiazol-2-yl)styryl)-9,9-bis(2-(2-ethoxyetoxy)ethyl)-9H-fluoren-2-yl)-3-butylthiourea

Model compound D (MW=764.05 g/mol) was prepared according to the procedure described in the literature.[1] The purity of the compound was verified by ^1H NMR (see Appendix A).

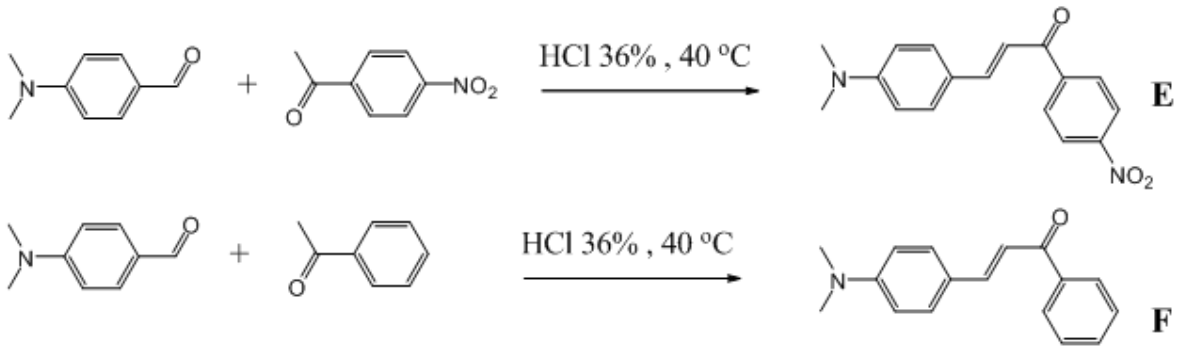

Figure 22. Synthesis of a non-fluorescent chalcone (E) and fluorescent chalcone (F).

5.1.4 Synthesis of (E)-3-(4-(dimethylamino)-phenyl)-1-(4-nitrophenyl)prop-2-en-1-one.

Nitrochalcone E (MW=296.32 g/mol), see Figure 22. A mixture of p-(dimethylamino)-benzaldehyde (1.49 g, 0.01 mol) and p-(nitro)-acetophenone (1.65 g, 0.01 mol) have been dissolved in ~10 mL HCl (37%). The reaction was carried out at 50 °C for 1 h. The reaction mixture was neutralized with $NaHCO_3$. The product was filtered and washed with ethanol, resulting in red needles, m.p. 215-216 °C. ^{1}H NMR (300 MHz, $CDCl_3$) δ: 8.35 (d, 2H), 8.13 (d, 2H), 7.83 (d, 1H), 7.58 (d, 2H), 7.27 (d, 1H), 6.71 (d, 2H), 3.08 (s, 6H).

5.1.5 Synthesis of (E)-3-(4-(dimethylamino)-phenyl)-1-(4-phenyl)prop-2-en-1-one

Fluorescent chalcone F (MW=251.3 g/mol) was synthesized following a procedure described previously.[4] Purity have been checked by ^{1}H NMR (300 MHz, $CDCl_3$) δ: 8.03 (d, 2H), 7.80 (d, 1H), 7.5 (m, 5H), 7.35 (d, 2H), 6.72 (d, 2H), 3.05 (s, 6H). See Appendix A.

5.1.6 Optical properties of compounds studied

Fluorescence quantum yields (QY_x) for the compounds studied were measured by a relative fluorescent method,[2] calculated with the following equation:

$$QY_x = QY_{st} \cdot \frac{A_{st}}{A_x} \cdot \frac{I_x}{I_{st}} \cdot \left(\frac{n_x}{n_{st}}\right)^2$$

Equation 3. Fluorescence quantum yield by relative method

9,10-Diphenylanthracene (9,10-DPA) in cyclohexane was used (QY_{st}=0.95). A_{st} and A_x are the optical densities at the wavelength of excitation (373 nm) for standard and sample and did not exceed 0.13. I_{st} and I_x – integral emission of the standard and sample, n_{st} and n_x are refractive indices of the used solvents. All photophysical data were obtained in

spectroscopic grade chloroform and DCM at room temperature. Absorption spectra were measured with an Agilent 8453 UV-visible spectrophotometer. The fluorescence spectra were obtained with a PTI QuantaMaster spectrofluorimeter in 10 mm spectrofluorometric quartz cuvettes with $C \sim 1\text{-}2 \cdot 10^{-6}$ M. All fluorescence spectra were corrected for the spectral responsivity of the PTI detection system (monochromator and PMT).

Table 5. Fluorescence quantum yields of compounds used in the study

Solvent	Model compound (D)	THB compound (C)	Photochrome	Nitrochalcone
$CHCl_3$	0.79 ± 0.05	0.59 ± 0.05	<0.01	0
CH_2Cl_2	0.95 ± 0.05	0.70 ± 0.05	<0.01	0

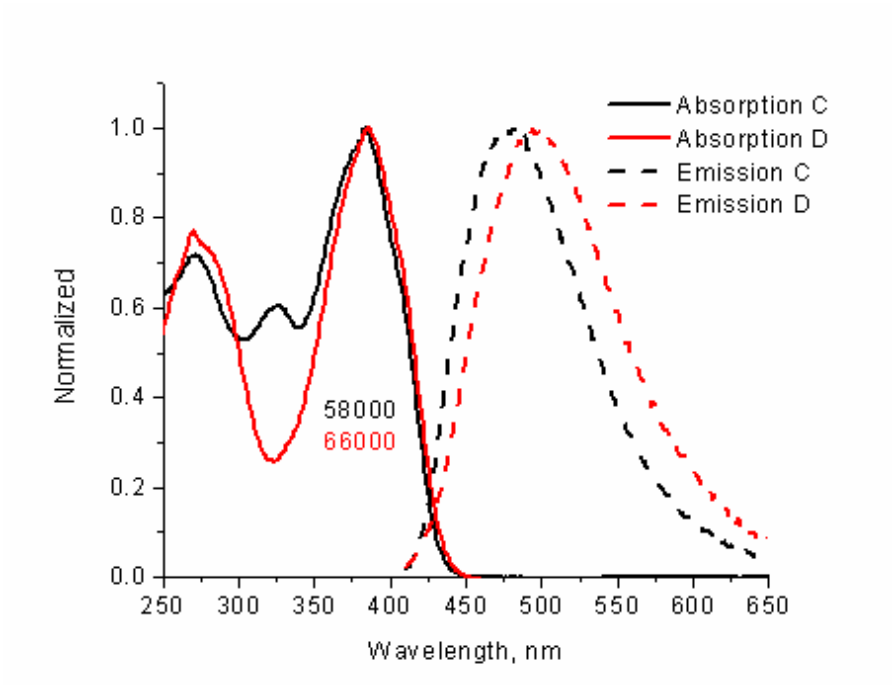

Figure 23. Absorption and emission spectra of model (D) and triple hydrogen bonding (C) compounds in $CHCl_3$. Numbers indicate extinction coefficients at λ=385 nm.

Table 6. Extinction coefficients for model and THB compound at selected wavelengths, M^{-1} cm^{-1}

Model compound (D)	ε_{385}=66000	ε_{405}=49200
THB compound (C)	ε_{385}=58000	ε_{405}=40000

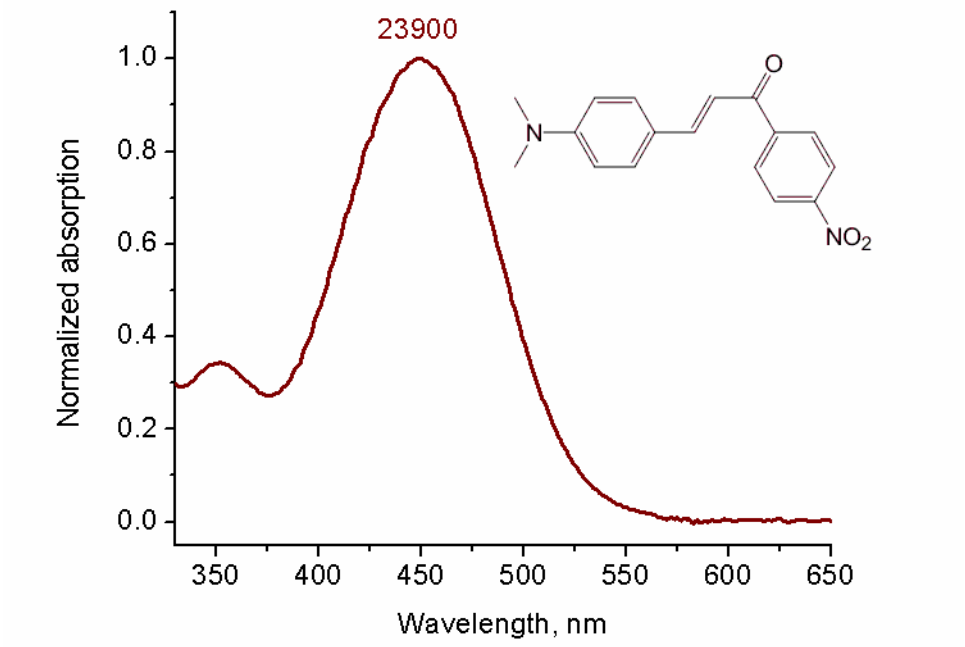

Figure 24. Absorption spectrum of nitrochalcone in chloroform. Number indicate extinction coefficient at λ=450 nm.

Table 7. Nitrochalcone extinction coefficients at selected wavelengths, M^{-1} cm^{-1}

Nitro-chalcone	ε_{450}=23900	ε_{405}=13100	ε_{542}=880

5.1.7 Preparation of solutions for study of RET to closed form

A solution of C was prepared by dissolving compound C (48 mg, 62.3 micromol) in 10 mL of $CHCl_3$, followed by dilution of 1 mL of this solution to 25 mL. This yielded a stock solution used for research with the concentration 0.25 mmol/L of compound C. This solution was used to prepare all the other solutions. 7.8 mg (22.5 micromol) of the photochrome was dissolved in a few droplets (approximately 0.2 mL) of $CHCl_3$, and uniformly irradiated for 1 h with a 405 nm laser at 100 mW optical output. The above concentrated solution of photochrome was diluted to 5 mL with a stock solution of compound C. This yielded the first working solution, with the concentration of the compound C close to 0.25 mmol/L and concentration of the photochrome 4.5 mmol/L. Other solutions in the Table 3 were prepared by consequent dilution of first working solution, as follows: 2.5 mL of solution was removed and used for study, the other 2.5 mL was diluted to 5 mL with the primary solution containing compound C. By repeating this procedure three more times all other solutions were prepared. At every repetition the concentration of the photochrome halves, while the concentration of compound C remains the same.

5.1.8 Study of energy transfer from 2PA dye to the closed form of photochrome

Energy transfer was investigated by changes in fluorescence lifetimes and changes in fluorescence spectra of the 2PA dye. Both types of measurements were performed on the same sample, at room temperature. First, the emission spectrum was recorded, then

fluorescence lifetimes were determined. Two-photon excitation of the sample, in a 10 mm path length quartz cuvette, was performed at 800 nm (290 mW of laser power). The beam (linearly polarized and oriented by the magic angle) was focused toward the edge of the cuvette (detector side) to minimize possible fluorescence reabsorption. The excitation source was a tunable Ti:sapphire laser system (Coherent Verdi-V10 and MIRA 900, pulse duration ~200 fs/pulse (FWHM), repetition rate 76 MHz). Fluorescence spectra were recorded using a PTI spectrofluorimeter; as detector a photomultiplier tube was used, all data was corrected for its wavelength response function. For lifetime measurements, fluorescence from the sample was collected into a multi-mode fiber and delivered to an avalanche photodiode detector (APD, PicoQuant GmbH, LSM_SPAD). A broad band-pass filter (D500/200m) was placed in front of the avalanche photodiode. Data acquisition was accomplished with a PicoQuant time-correlated single photon counting system, PicoHarp300. All experimental decay curves have shown to be fitted with a single exponential decay function. Lifetime data in Table 3 represents an average of 3 measurements. The relative percent error of about 4% was estimated from 10 measurements of the same sample.

5.1.9 FRET to OF measurements by absorption method

Solutions for FRET measurements were prepared in the following manner: 6.1 mg of photochrome was dissolved in 5.88 mL of $CHCl_3$ to yield the working solution of $3*10^{-3}$ mol/L. This solution (1 mL) was added to vials containing $3*10^{-6}$ mol of compound C and the model compound D.

Solutions were placed in 1 mm path length quartz cuvettes and were uniformly irradiated at 405 nm with a laser diode in its far field. The intensity of the laser irradiance

was reduced with a neutral density filter to 28 mW/cm^2 (measured with a BeamStar powermeter). After every 10 s, an absorption spectrum was recorded. For precise time control, a ThorLabs electronic shutter with shutter controller (SC10) was used to interrupt laser beam.

5.1.10 Monte Carlo method for calculation of FRET efficiency in solution

The Monte Carlo method is a powerful tool, applicable in situations where no other method is suitable. Normally used to model complex natural phenomena. FRET in solution is such a phenomenon. FRET has a simple mathematical apparatus in the case of covalently linked donor and acceptor pairs. In the case of multiple donors and acceptors randomly moving in solution the situation changes. The complexity of FRET in solution arises mainly from the need to take into account the distance distribution between donors and acceptors. Also different efficiencies of FRET from acceptors to donors and acceptors to acceptors further complicates the situation. All this makes mathematical calculations challenging. A significantly easier solution is to employ computer simulation.

Here, a simulation was performed with a simplified model of molecule distribution using a single processor computer. The following assumptions, conditions, and limitations were used in the model:

1. All molecules are uniformly and randomly distributed in the solution.

2. The unit volume is contained in a cube with a side of 50 nm. This gives a volume of 125000 nm^3 to run the simulation on.

3. The concentration used for simulation was $3*10^{-3}$ mol/L (see part 5.2 for more details).

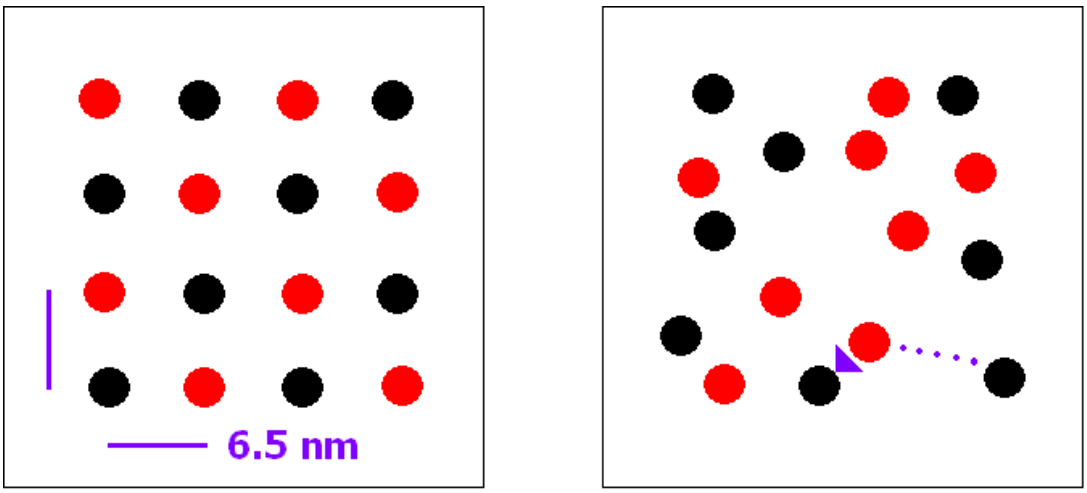

Figure 25. Molecule distribution: arranged (on left) and random as in solution. Red circles represent donor molecules, black – acceptors. In both cases the concentration is the same, but FRET efficiency is different. The average distance of 6.5 nm corresponds to the between molecules for the concentration used in the study (see part 5.2).

4. For the above concentration in the unit volume, the number of donor and acceptor molecules is calculated to be 225.8 each; this number has been rounded to an integer value – N=226 molecules for donor and N=226 molecules for acceptor.

5. Each molecule received random coordinates in the unit volume with a discrete step of 0.5 nm. This gives a 100 possible coordinate values for each axis (50 nm side/0.5 nm step).

6. For each donor molecule FRET is assumed to occur to the closest neighbor only, regardless of relative molecular dipole orientations.

7. The model is static, molecules do not change their coordinates in time.

For each donor molecule (i=1,2,3..N) the distance (r) to every acceptor (j=1,2,3..N) in the unit volume is calculated according to the formula:

$$r_i = \sqrt{(x1_i - x2_j)^2 + (y1_i - y2_j)^2 + (z1_i - z2_j)^2}$$

In the above expression, $x1_i$, $y1_i$, $z1_i$ are three-dimensional coordinates of the donor (i) and $x2_j$, $y2_j$, $z2_j$ are the coordinates of the acceptor (j).

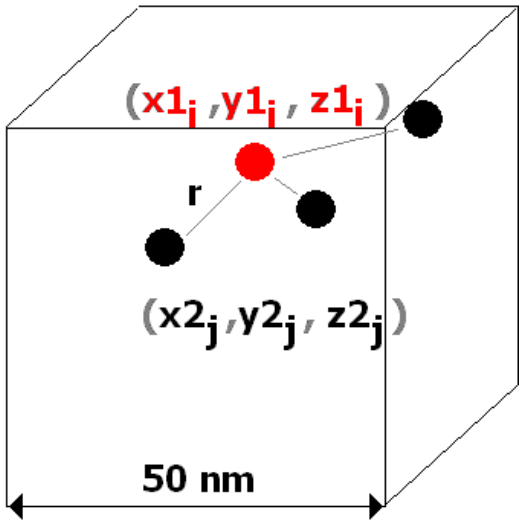

Figure 26. Modeling is performed on a small volume of solution - 125000 nm^3. Distance (r) from a donor to all acceptors is calculated (shown here 3 acceptors only) based on their coordinates in 3-dimensional space. Minimum distance is recorded and used to compute the efficiency of FRET.

For every donor molecule a total of N distances are calculated and the minimal distance ($r_{i,\,min}$) is being used to compute FRET efficiency (E_i) according to the equation:[2]

$$E_i = \frac{R_0^6}{R_0^6 + r_{i,min}^6}$$

R_0 is the Förster distance, computed from spectral data of the donor and acceptor. The average FRET efficiency (E) in the unit volume is simply the average value of individual FRET efficiencies (E_i):

$$E = \frac{\sum_{i=1}^{N} E_i}{N}$$

Since the FRET efficiency may slightly vary in different unit volumes (molecule distribution are different), the overall FRET efficiency in solution is be calculated as the average of several (10 to 100) FRET efficiencies in unit volumes.

The concentration used for simulation was $3*10^{-3}$ mol/l. The average distance between a donor and an acceptor in homogeneous solution is calculated as:

$$\bar{r}(nm) = \sqrt[3]{\frac{0.83}{C(mol/l)}}$$

Equation 4. Average distance between a donor and an acceptor in homogeneous solution.

This gives the average distance between a donor and an acceptor r=6.5 nm for $C=3*10^{-3}$ mol/l. The simulated results for minimal distance distribution are presented in Figure 27 and explain some of the difficulties associated with analytical calculation of FRET efficiencies in solutions. The majority of donor molecules are located closer to an acceptor than the average computed distance. Taking R_0 as 25 angstroms, it can be noted from Figure 27 that a significant fraction of donors are located at distances smaller than R_0 from the acceptors (where FRET efficiency is very high).

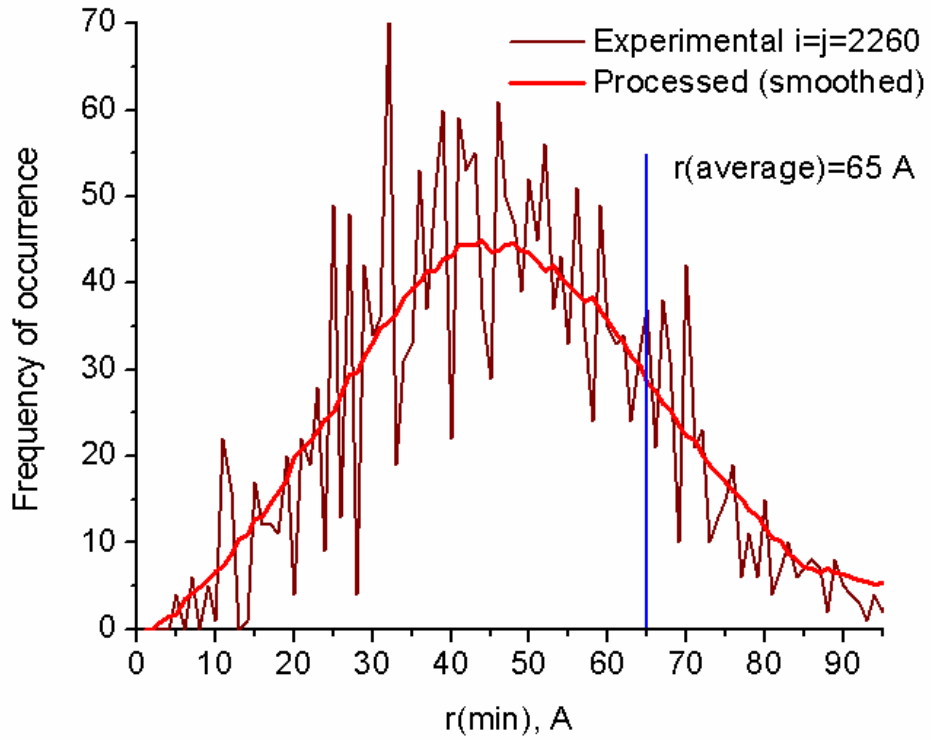

Figure 27. Minimal distance distribution between donors and acceptors in solution (10 modeled unit volumes). The majority of donors find an acceptor at smaller distance than computed average distance. The spikes in modeled spectrum are a result of discrete (0.5 nm step) coordinate assignment.

An additional factor that has been taken into account in the Monte Carlo algorithm is the possibility of a donor to serve as an acceptor for a different donor molecule[3]. This additional effect decreases the FRET efficiency to pure acceptors (photochrome molecules in this study). Though it has been implemented in the computer software for comparison, the results are not very accurate due to the following additional assumptions:

1. A donor molecule (which served as an acceptor) is assumed to become FRET inactive (will not re-donate the photon energy). Though this is not a real case, this assumption was needed to keep the computational algorithm simple.

2. FRET efficiency from a donor to an acceptor is taken to be the same as from a donor to a donor. For this particular analysis this assumption is acceptable, since the spectral overlap of donor-donor and donor-acceptor pairs are of the same order of magnitude, which in turn gives yields small difference in R_0. In general, the differences in R_0 will have an impact on results.

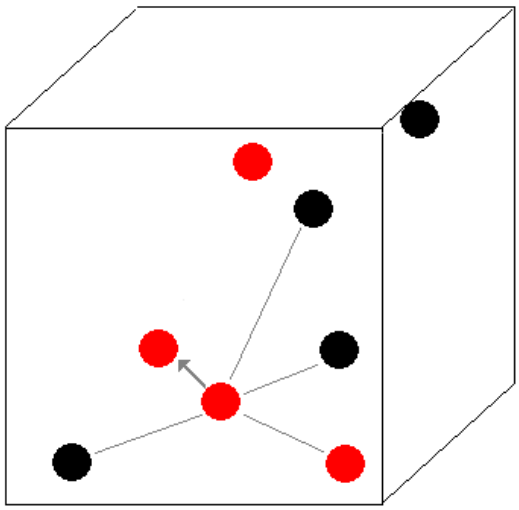

Figure 28. The complexity of RET in solution. Not only it's important to consider the minimal distance from a donor to acceptor, but also from a donor to a donor. In some cases RET from a donor to a donor (which can serve as an acceptor) can not be ignored.

5.2 General considerations for choosing the concentration of study

Since this research is partially application-oriented (3D optical data storage), it is important to estimate the range of concentrations suitable for practical application and elucidate concentration related effects that might possibly interfere with the operation of the data storage device.

Some of the important technological parameters that depend on the concentration of the substances in the polymer disk are listed below.

1. Optical quality of the data storage medium. At high concentrations phase separation may occur, typically at of 5-10 weight percent. For a supramolecular complex with MW=1117 g/mol in PMMA (density=1.18 g/cm^3) this would limit the maximum concentration to ~ $5*10^{-2}$ mol/l.

2. The cost the chemicals used in the disk. Currently the production cost of the photochromes suitable for optical data storage is relatively high, at the order of $1000 per gram. Even for a 1 gram disk, 5% by weight of the photochrome translates into $50 dollars in price. For comparison, the production cost of a DVD, currently is less than 15 cents. To be competitive on the market, the concentration of expensive substances (photochrome and 2PA dye) should be kept minimal, less than 10^{-2} mol/l.

3. Level of the fluorescence signal and signal to noise ratio. This has a direct impact on the selection of the detector suitable for signal detection and laser excitation source and therefore on the final cost of the device. Unfortunately, the dependence of the fluorescence signal upon the dye concentration (and in mixture with photochrome) under 2PA is a very complex function. This is a result of several competing effects. With the increase of concentration the nonlinear absorption coefficient of the material increases (bulk cross section) $\beta \sim \delta_{2PA} * C$, and a higher concentration of molecules in exited state is present. At the same time, the fluorescent quantum yield typically tends to decrease with the increase of the dye concentration. Also at high dye concentrations, the overall fluorescent signal is reduced by reabsorption.

An example of the dependence of fluorescence signal upon concentration is presented in Figure 29. In this example, 3-(4-(dimethylamino)-phenyl)-1-(4-phenyl)prop-2-en-1-one was used as a fluorescent substance (further in the text referred to as “fluorescent chalcone”), because of its simple and cheap preparation in quantities.

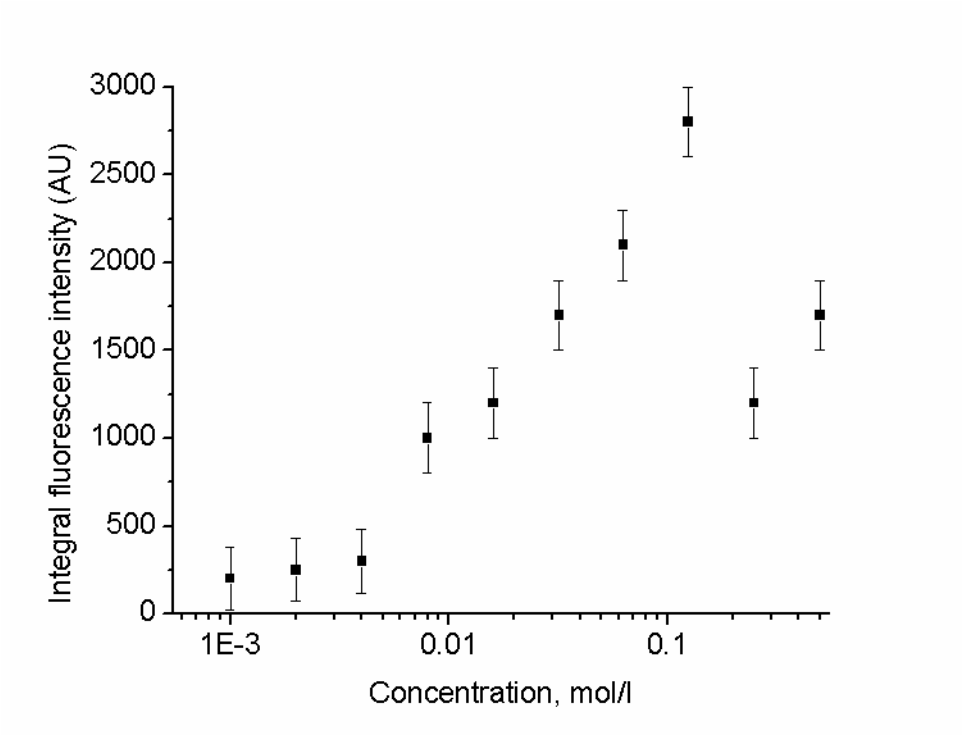

Figure 29. An example of fluorescence signal dependence under 2PA on concentration of a dye (fluorescent chalcone F).

The experiment was performed with an 808 nm laser diode (CW mode) at 850 mW. The highest concentration used was 0.5 mol/L (1.25 g of chalcone dissolved in 10 mL of acetone). All other concentrations were prepared by dilution of the initial solution. Solutions were placed in a square 10 mm path length quartz cuvette. The laser beam was focused into the central part of the cuvette (5 mm from each side). Fluorescence spectra were recorded using a PTI spectrofluorimeter with a PMT detector. To prove that the emission signal is 2PA

upconverted fluorescence, a quadratic dependence check for the fluorescence intensity on the laser power was demonstrated (Figure 30).

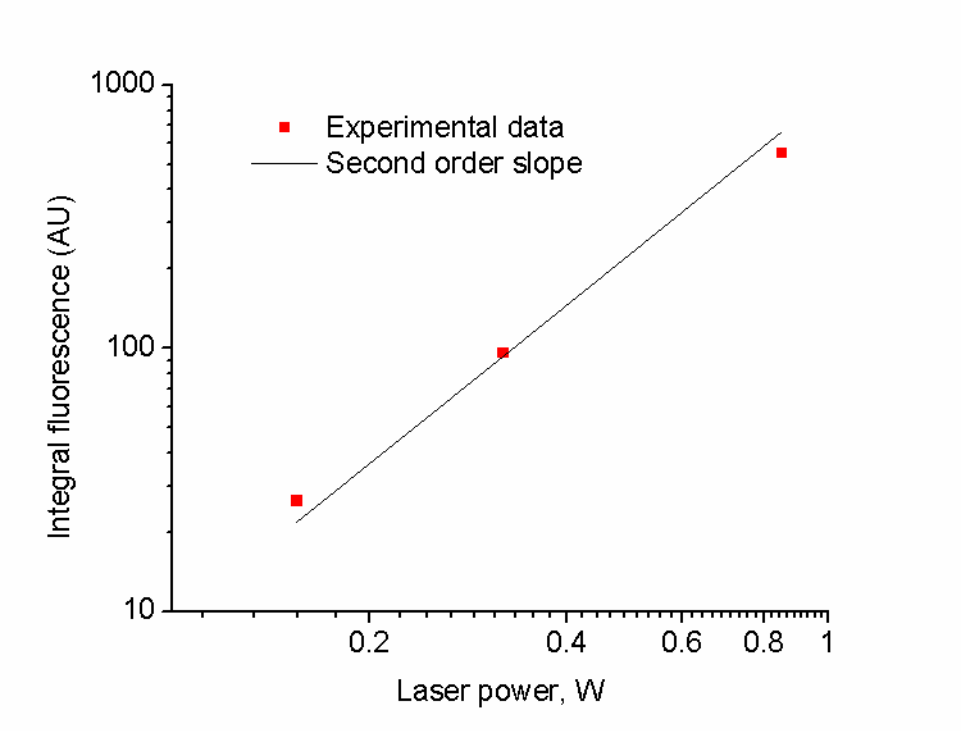

Figure 30. Fluorescence intensity quadratic dependence check on the laser power.

Note: for different excitation geometries and different cuvette path lengths the dependence shown in Figure 29 may be different due to a different experienced reabsorption levels. Absorption and emission data for the fluorescent chalcone is presented in Appendix F.

The experimental data presented in Figure 29 demonstrates that there exists an optimal concentration for a maximum fluorescence signal. For different substances this concentration should be different. However at relatively low concentrations the trend should be the same: the higher the concentration, the higher the fluorescence signal upon 2PA.

In the case of the FRET-based photochromic system, for efficient FRET a large spectral overlap between of the photochrome CF and the fluorescent dye is required. This

results in large levels of reabsorption and limits the maximum concentration of the substances to 10^{-3} – 10^{-2} mol/L. Taking into account all the above factors, a practically reasonable concentration is $3*10^{-3}$ mol/L.

5.3 Results and discussion

In the previous chapter it was shown that the selected photochrome can undergo hydrogen bonding with 2,6-BAP. One may expect that other compounds containing the same hydrogen bonding site as in 2,6-BAP will form similar complexes. Compound C was synthesized to contain a diaminopyridine residue, which has nearly identical hydrogen bonding properties as in 2,6-BAP. Compound C has relatively high fluorescence quantum yields in polar media (solvents or polymers) and therefore can serve as a FRET donor. Assuming that the dye forms hydrogen bonding in the same way as 2,6-BAP (has the same bonding site), the distance between the two chromophores in the supramolecular structure can be estimated. This is the distance between fluorene and the photochrome, since the pyridine ring is not in conjugation with the rest of the dye molecule. For exact distance calculations, one needs to know the values and space transition dipole orientations of the photochrome and dye molecule, which is not essential for our study. For different conformations of the 2PA dye molecules, this distance ranges from ca. 1.5 nm to less than 0.5 nm (Figure 31). In the worst case it does not exceed 2 nm. In all cases, the distance is favorable to facilitate FRET.

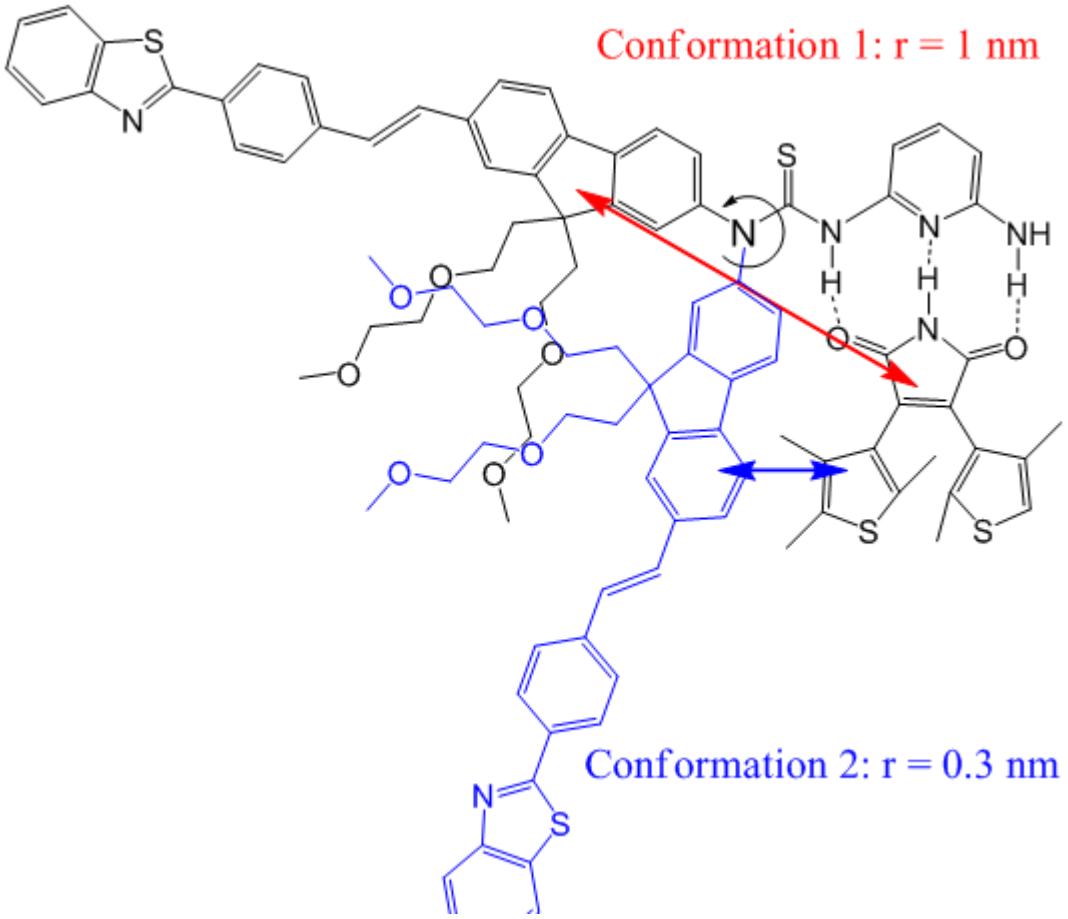

Figure 31. Different conformations of the 2PA fluorescent dye are possible, due to the free rotation along the C-N σ-bond. As a result, the distance between chromophores vary from about 1 nm to nearly contact distance. Short arrow corresponds to 0.3 nm, long arrow – 1 nm. Regardless of conformation, for Förster distance R_0>2 nm, the efficiency of FRET is expected to be close to unity.

5.3.1 FRET to both forms of the photochrome

The emission spectrum of compound C (THB), as shown in Figure 34, is localized between 400 nm and 650 nm, which entirely lies in the absorption region of the closed form of the photochrome compound, and partially (400-500 nm) in the absorption region of the open form of the photochrome. At the photostationary state both forms are present and FRET

to both forms is possible. It is essential to note that the concentration of the closed form at the photostationary state is lower than the concentration of the open form (Table 3). Nevertheless, the presence of the closed isomer in solution is expected to reduce the fluorescence of the donor dye by a measurable value. This is due to a better spectral overlap with the donor dye, and, therefore, a higher FRET efficiency to the closed form of the photochrome.

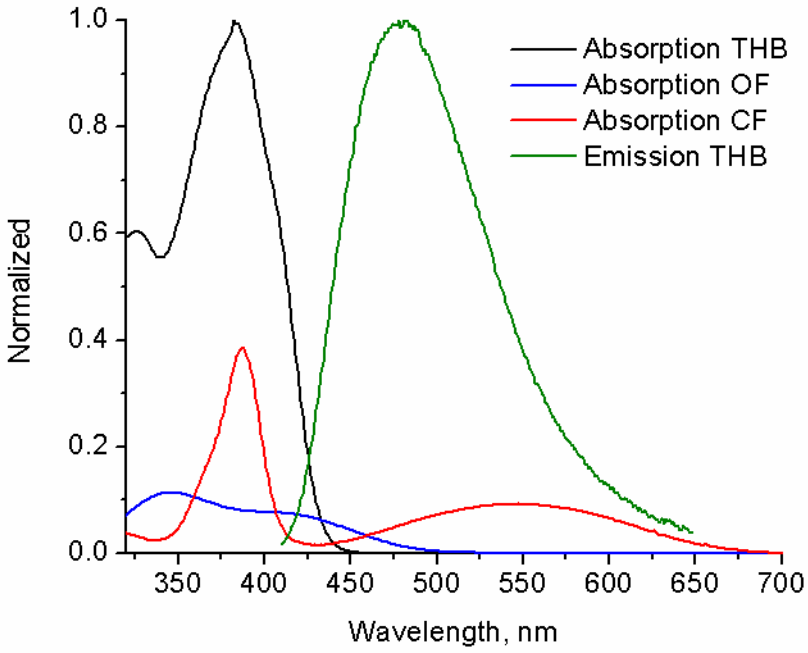

Figure 32. Comparative spectral overlap (normalized to concentration). Extinction coefficient ratio in the maximum of THB, photochrome in closed form (CF) and photochrome in open form is 1 : 0.39 : 0.11.

Calculation of Förster distances gives a value of R_0=2.6 nm for the open form of the photochrome –THB dye pair and R_0=3.6 nm for the closed form – THB dye pair.

Table 8. Calculated overlap integral J, R_0 values and FRET efficiency (E_{RET}) by Monte Carlo method from photochrome to dye C (THB compound). Concentration of both photochrome and dye is C=3*10^{-3} M

	J, M^{-1} cm^3	R_0, nm	E_{RET}
Open form	3.58*10^{-15}	2.6	0.15
Closed form	2.53*10^{-14}	3.6	0.32

The calculated FRET efficiency from spectral data for both open and closed form by a Monte Carlo method is presented in Table 8. Though this data is not accurate, as the simulation model does not consider partial molecular complexation, it still provides a good estimate of the closed form input to total fluorescence quenching level. At the photostationary state, the total FRET efficiency to the mixture of isomers is approximated to:

$$E_{total} = E_{open} \cdot (1 - \eta) + E_{closed} \cdot \eta$$

In the above expression, conversion at photostationary state to the closed form is η=0.077, giving a value for E_{total}=0.163, which in comparison with E_{open}=0.15 is about 9% higher.

Experimental observation of energy transfer can be concluded from changes in fluorescence lifetime and emission quantum yield of the donor molecule. Compound C has a similar conjugated part of the molecule as its precursor A**,** which has been used for 2PA imaging.[1] By keeping the concentration of the dye C the same in all experiments, and by varying the concentration of the photochrome (at photostationary state), a decrease in fluorescent lifetimes (Table 9) and intensity of the fluorescence signals of the dye with increase of photochrome concentrations was observed (Figure 33).

Table 9. Fluorescence lifetime as function of photochrome concentration (at PSS). A higher photochrome concentration translates into higher concentration of the supramolecular species in solution and lower fluorescence lifetime. The relative error of lifetime measurement is 4%.

Conc. of 2PA dye C *10000, mol/L	Conc. of photochrome C *10000, mol/L	Average lifetime, ns
2.5	45.2	1.05
2.5	22.6	1.15
2.5	11.3	1.20
2.5	5.6	1.25
2.5	2.8	1.26
2.5	0	1.27

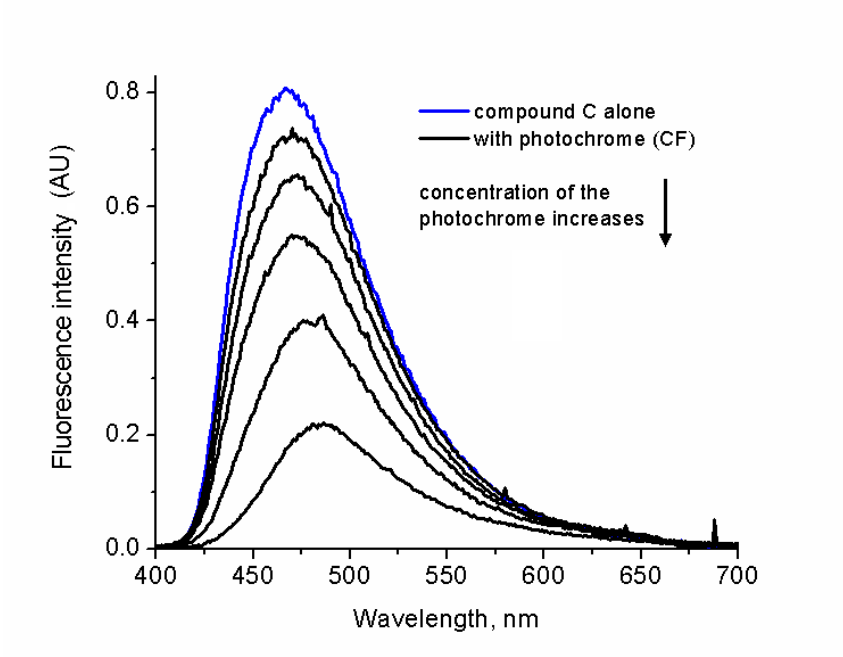

Figure 33. Decrease in fluorescence intensity (quantum yield) of compound C, under 2PA, with an increase in photochrome concentration. Concentrations of the photochrome in solution are given in Table 9, the photochrome is at the photostationary state.

Performing quantitative fluorescence measurements with concentrated solutions is a difficult task, as several effects may alter the results. The most severe input comes from the inner filter effect and reabsorption. The first effect was completely eliminated by performing the experiments under two-photon excitation at 800 nm. However, the reabsorption effect (especially by the closed form of the photochrome) could not be eliminated. The concentrations of photochrome and donor dye used for study were relatively small, on the order 10^{-4} M. Lower concentrations could not be used, as the FRET efficiency for very dilute solutions is expected to be small, which is difficult to measure. Though excitation occurred at the edge of the cuvette (less than 1 mm away), the absorbance of the solution is still relatively high. For example, the highest concentration of photochrome used was $4.5*10^{-3}$ mol/L, the optical density of the solution at 1 mm from the cuvette edge at 542 nm (absorption maximum of closed form) was calculated to be 0.19 and about 0.35 at 475 nm

(close to emission maximum of 2PA dye). Experimentally, reabsorption yields a spectral shift in emission (see Figure 34).

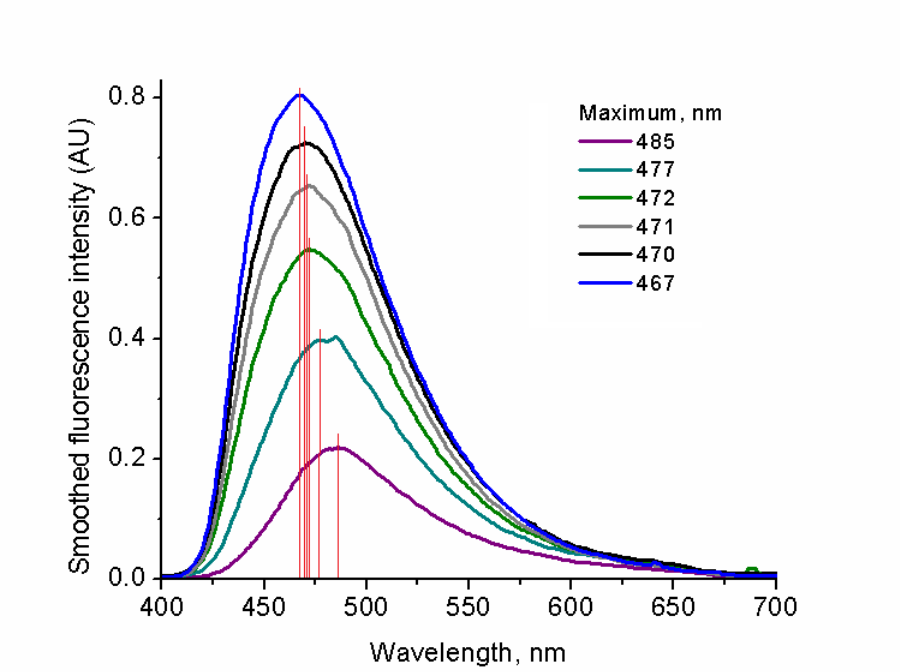

Figure 34. Fluorescence maximum shift (compound C) due to reabsorption.

Fluorescent methods are suitable to study FRET in dilute solutions. However, performing quantitative fluorescence measurements with concentrated solutions is a difficult task, because of the described effects (inner filter effect and reabsorption). Nevertheless, in the case of photochromes, a clean experiment to extract FRET information is possible using an absorption method described below. To simplify the experiment and required calculations, FRET efficiency to the open form of the photochrome was investigated. With this information in hand, FRET efficiency to the closed form can be theoretically estimated.

5.3.2 FRET to the open form of the photochrome

For experimental demonstration of FRET to the open form of the photochome, a comparative study was performed. For comparison, several compounds were synthesized and used. One compound (D) with similar optical properties to compound C was prepared (see Figure 21). The key difference between the two compounds is their ability to form supramolecular structures with the photochrome via hydrogen bonding. Dye D lacks the diaminopyridine residue and, therefore, has fewer possibilities to form supramolecular structures with the photochrome (e.g., fewer H-bonding sites and steric hindrance from the adjacent PEG chains). Still one such possibility is depicted in Figure 35.

Heretofore compound C will be referred to as THB (triple hydrogen bonding) and compound D will be referred to as model compound. A third compound (for reference) used in this study was a nitrochalcone. This compound is non-fluorescent and therefore FRET to the photochrome is not possible.

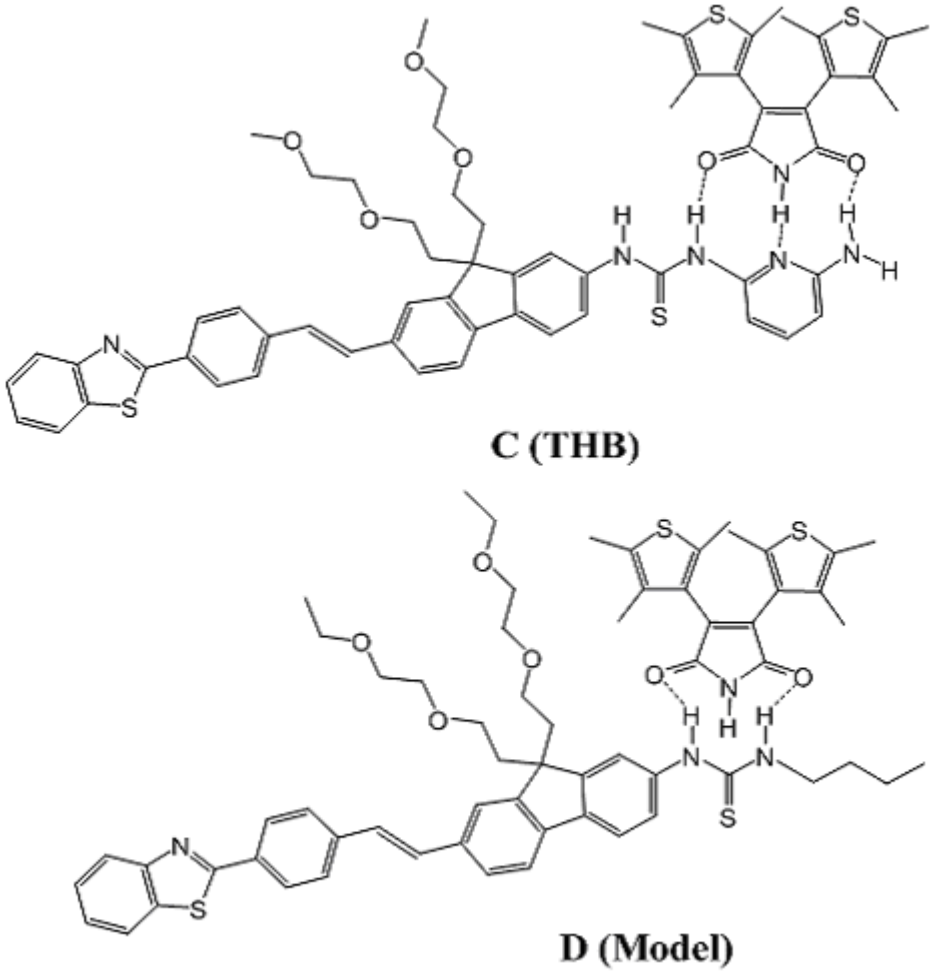

Figure 35. Possible supramolecular structures of photochrome molecule with the fluorenyl dyes.

Two equimolar solutions, each containing $3*10^{-3}$ M of photochrome (open form) and $3*10^{-3}$ M of dye, were prepared. One solution contained THB as the fluorescent dye, the other solution contained the model compound as dye. Both solutions in 1 mm cuvettes were uniformly irradiated in nearly identical conditions with the output from a 405 nm laser. At equal time intervals (10 s) an absorption spectrum was recorded. Experimental results are presented in Figures 36 and 37.

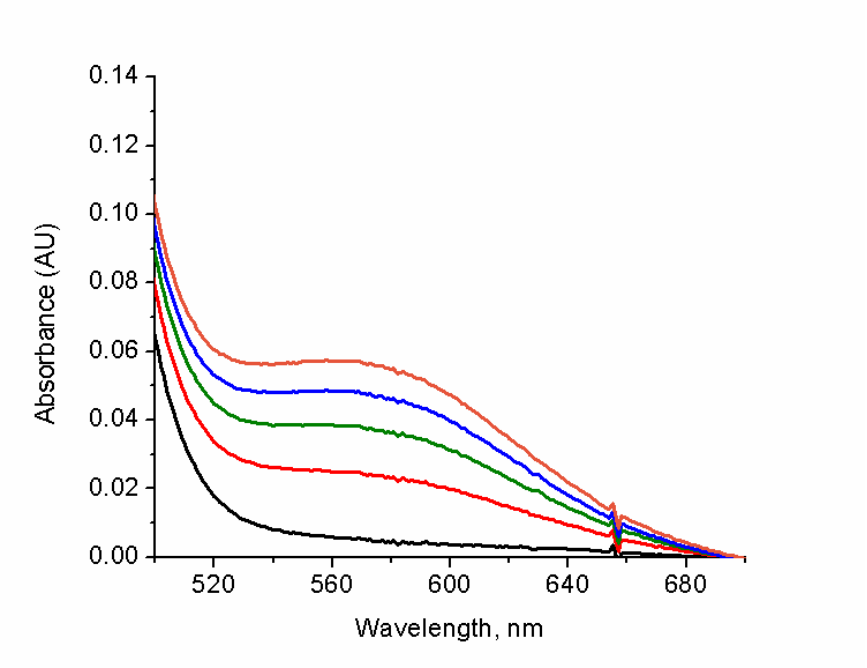

Figure 36. Photochromic changes in absorption in the presence of THB compound (C). Black spectrum – before irradiation, with colors after every 10 seconds of irradiation at 405 nm.

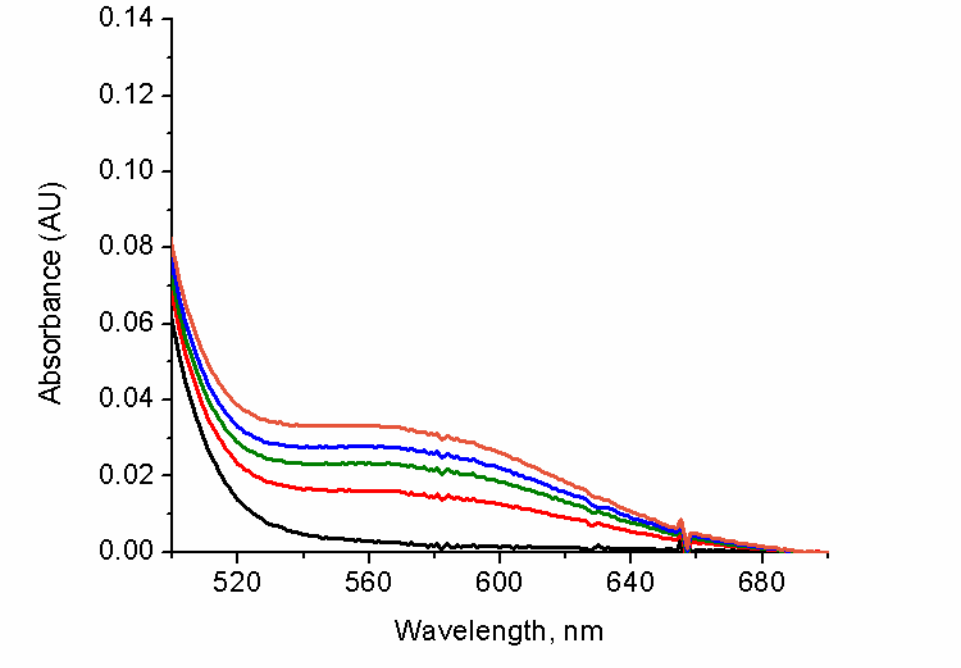

Figure 37. Photochromic changes in absorption in the presence of model compound (D). Black spectrum – before irradiation, with colors after every 10 seconds of irradiation at 405 nm.

For reference, a third solution containing $3*10^{-3}$ M of photochrome and $1.13*10^{-2}$ M of nitrochalcone was used for the same measurements (Figure 38). A $1.13*10^{-2}$ M solution of nitrochalcone has the same optical density at 405 nm as $3*10^{-3}$ M of model compound (A=14.76 in 1 mm cuvette). At such high optical density, it is possible to consider that essentially all photons (28 mW/cm^2) that fall on the sample are being absorbed. The numbers of absorbed photons by the dye (N_{dye}) and the photochrome (N_p) are proportional to the values of their extinction coefficients (ε_{dye} and ε_p):

$$\frac{N_{dye}}{N_p} = \frac{\varepsilon_{dye}}{\varepsilon_p}$$

Assuming there is no excited state absorption (the laser power was low), the number of molecules in excited state (N^*) will be equal to the number of absorbed photons (N). It is therefore possible to express the number of dye molecules in excited state (N^*_{dye}) as function of the number of photochrome molecules in the excited state (N^*_p) and their extinction coefficients:

$$N^*_{dye} = N^*_p \cdot \frac{\varepsilon_{dye}}{\varepsilon_p}$$

Equation 5. Correlation between the number of excited state molecules of dye and photochrome

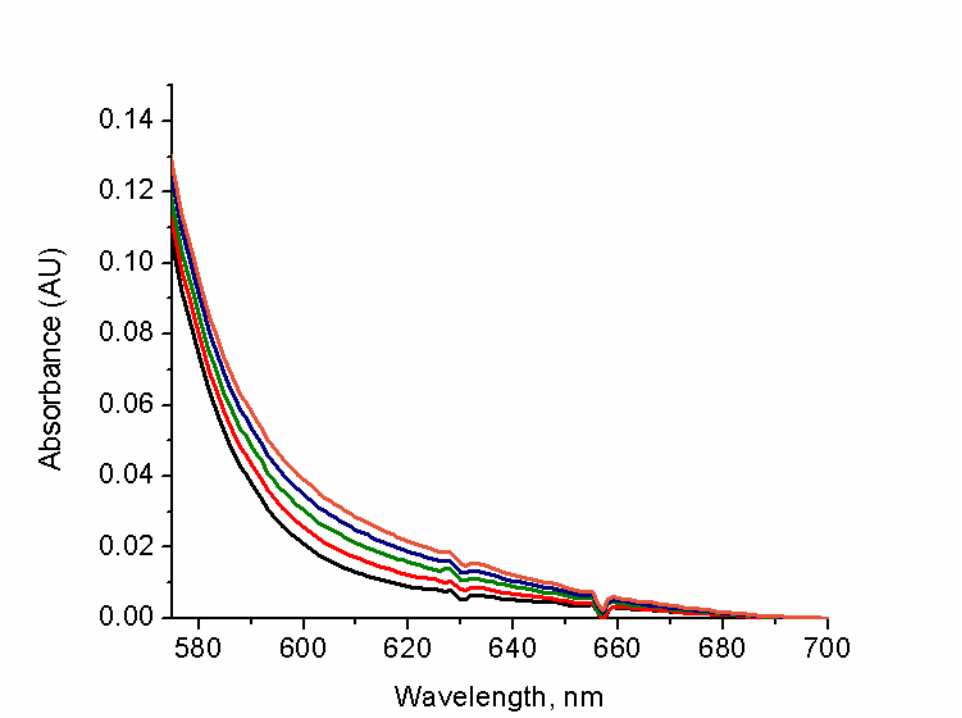

Figure 38. Photochromic changes in absorption in the presence of non-fluorescent nitrochalcone (E). Black spectrum – before irradiation, with colors after every 10 seconds of irradiation at 405 nm. The absorption tale of nitrochalcone overlaps with the absorption of the closed form of the photochrome; to keep the same absorbance scale in all 3 graphs, all absorption data below 575 nm has been cut.

When the photochrome is mixed with non-fluorescent nitrochalcone, the change in absorption upon irradiation ($\Delta D_p^{chalcone}$) is proportional to the number of photochromic molecules in the excited state:

$$\Delta D_p^{chalcone} = N_p^* \cdot \Phi_{O \to C} \cdot k$$

In the above expression, Φ is the photoisomerization quantum yield (open form to closed form) and k is a proportionality constant (see appendix D for details).

In the case when a fluorescent dye (model or THB compound) is present in solution, the number of photochromic molecules in the excited state (N*) will be higher, due to an additional energy transfer (φ) from the fluorescent dye. For the model compound:

$$N^* = N_p^* + N_{model}^* \cdot \varphi \cdot QY$$

In the above expression, N^*_{model} is the number of molecules of model compound in excited state, QY is the fluorescence quantum yield for model compound, and φ is the additional energy transfer due to all possible mechanisms (FRET in complex, FRET for non-complexed molecules, fluorescence reabsorption):

$$\varphi = E_{RET}^{complex} + E_{RET} + E_{reabsorption}$$

Equation 6. Energy transfer from a donor to acceptor

In this case (when the photochrome is mixed with a fluorescent dye – model compound), the change in absorption upon irradiation (ΔD_p^{model}) is also proportional to the number of photochrome molecules in the excited state, but at this time the number is larger:

$$\Delta D_p^{model} = (N_p^* + N_{model}^* \cdot \varphi \cdot QY) \cdot \Phi_{O \to C} \cdot k$$

Expressing N^*_{model} as a function of N^*_p and after expanding the above equation yields:

$$\Delta D_p^{model} = N_p^* \cdot \Phi_{O \to C} \cdot k + N_p^* \cdot \frac{\varepsilon_{dye}}{\varepsilon_p} \cdot \varphi \cdot QY \cdot \Phi_{O \to C} \cdot k$$

Since

$$\Delta D_p^{chalcone} = N_p^* \cdot \Phi_{O \to C} \cdot k$$

and the optical density of nitrochalcone solution is equal to that of model compound, combining the above equations:

$$\Delta D_p^{model} = \Delta D_p^{chalcone} + \Delta D_p^{chalcone} \cdot \frac{\varepsilon_{model}}{\varepsilon_p} \cdot \varphi \cdot QY$$

where the energy transfer from the fluorescent dye (φ) can be expressed as:

$$\varphi = \frac{\Delta D_p^{model} - \Delta D_p^{chalcone}}{\Delta D_p^{chalcone} \cdot QY} \cdot \frac{\varepsilon_p}{\varepsilon_{model}}$$

Equation 7. Energy transfer efficiency

Equation 7 is valid with several assumptions.

Assumption 1. The extinction coefficient of the photochrome does not change significantly in the presence of the fluorescent dye or nitrochalcone. It was shown in the previous section that in the presence of hydrogen-bonding compound 2,6-BAP, at very high concentrations of photochrome and 2,6-BAP, the extinction coefficients for both photochrome isomers increased. To estimate the level of this change for $3*10^{-3}$ M solutions, the photochrome absorption spectra were recorded with and without 2,6-BAP (see Figure 39). A slightly lower solution concentration was used to remain in the linear range of instrument's detector. The result shows, that for the concentration used, this change is small (less then 2%) and constitutes an insignificant source of error.

Assumption 2. Photoisomerization quantum yields (Φ) for photochrome have the same value in the presence of nitrochalcone and fluorescent dyes. In the previous section, it was shown that a decrease of about 20% in photoisomerization quantum yield was observed in the presence of a hydrogen-bonding compound. Though how the presence of nitrochalcone affects the photoisomerization quantum yield of photochrome is not known, for the purpose of comparison (and to provide and range of possible φ values) the following corrected equation will be considered:

$$\varphi = \frac{\Delta D_p^{model} - w \cdot \Delta D_p^{chalcone}}{w \cdot \Delta D_p^{chalcone} \cdot QY} \cdot \frac{\varepsilon_p}{\varepsilon_{model}}$$

Equation 8. Corrected equation for energy transfer efficiency

In the above equation,

$$w = \frac{\Phi_p^{model}}{\Phi_p^{chalcone}}$$

is the ratio of photoisomerization quantum yields of photochrome in the presence of model compound and nitrochalcone. This value can range anywhere from 1 down to 0.8 (according to data from previous chapter).

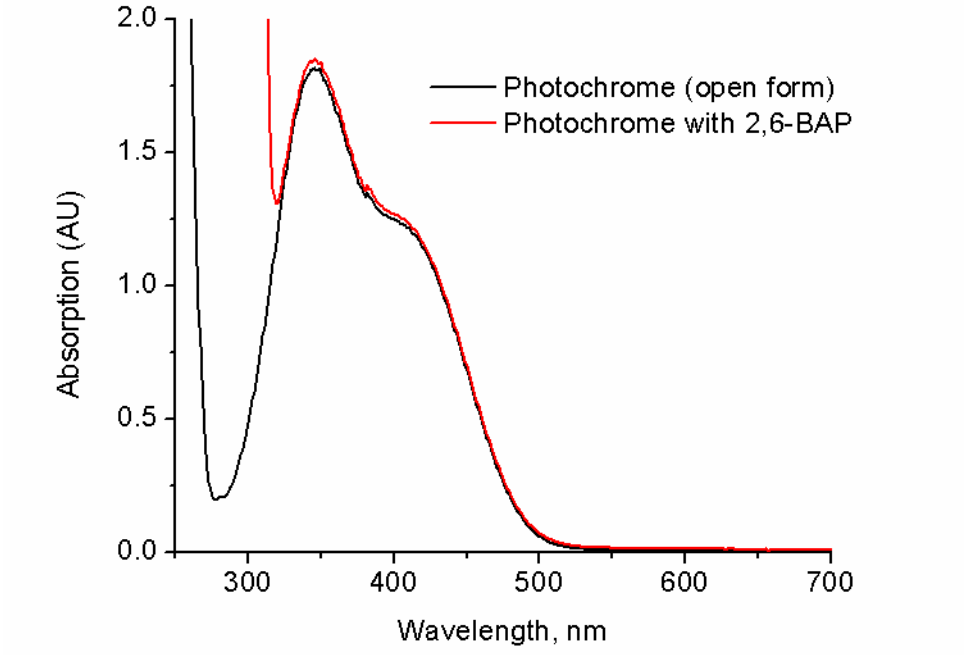

Figure 39. Changes in extinction coefficient of open form of photochrome in the presence of 2,6-BAP. Both substances have the concentration ≈2.7*10^{-3} M. After 400 nm (away from the absorption tail of 2,6-BAP) this change constitutes less than 2%.

Assumption 3. No reverse photoisomerization reaction occurs during the time of measurement. In general, this assumption is not valid, since the closed form of the photochrome also absorbs at 405 nm and the reverse reaction takes place. However, the concentration of the closed form present at the beginning of irradiation (first few seconds) is small relative to the concentration of the open form (less than 1%). Hence, an insignificant amount of the formed closed isomer undergoes the reverse photoisomerization reaction. Overall, the absorption changes in the absorption spectrum at the beginning of solution

irradiation can be considered to be nearly entirely due to the open-to-closed photoisomerization process. For this reason, only the spectra after 10 s of irradiation (spectra shown in red color in Figure 36, Figure 37 and Figure 38) shall be considered suitable for quantitative calculations of FRET efficiency. Changes in absorption, after 10 s of irradiation are presented in Table 10.

In the case of THB, compound D, same equation (Equation 7 or Equation 8) with a minor correction was used to calculate energy transfer efficiency to the open form of the photochrome. Equation 7 was derived with the condition that the optical density of the fluorescent dye solution was equal to the optical density of nitrochalcone solution. Experimentally this condition was met for the model compound, but not for THB. The extinction coefficient of THB is about 20% smaller at 405 nm than the extinction coefficient of the model compound. Therefore a less concentrated solution ($9.19*10^{-3}$ M) of nitrochalcone was necessary (to have same optical density as $3*10^{-3}$ M solution of THB). As an alternative to the experimental data (to avoid additional experimental errors), the resulting absorption change of the mixture of photochrome ($3*10^{-3}$ M) and nitrochalcone ($9.19*10^{-3}$ M) upon irradiation can be easily calculated in an analytical way. This absorption change is higher then for the solution mixture of photochrome ($3*10^{-3}$ M)– nitrochalcone ($1.13*10^{-2}$ M) by a factor (f):

$$f = \frac{\varepsilon_p + \varepsilon_{model}}{\varepsilon_p + \varepsilon_{THB}}$$

In the above expression ε_{THB} is the extinction coefficient of THB. A complete derivation is presented in Appendix E.

The calculated energy transfer efficiencies (φ) for THB and model compounds are presented in Table 10. As expected, for both compounds, this value was higher than

calculated FRET efficiency for the solution by the Monte Carlo method (E_{FRET}^{sol}). The input of the FRET for the complex was calculated as:

$$E_{RET}^{complex} = \varphi - (E_{RET}^{sol} + E_{reabsorption})$$

An accurate value for energy transfer due to the reabsorption effect is likely not possible. However, an estimate can be performed in the following manner. Fluorescence reabsorption by the fluorescent dye and the by the open form of the photochrome are approximately equal (spectral integrals have similar values). Reabsorption by the fluorescent dye can be estimated from its spectral data. Assuming all the photons with the wavelength contained in the spectral overlap (absorption with emission) are being absorbed, this represents only about 5% from the number of all emitted photons. For the open form of the photochrome, spectral overlap extends over a broader wavelengths range, but at the same time its extinction coefficient has a very low value in the range of those values. A few other factors that suggest a smaller reabsorption value are the quantum yield less than a unity and geometrical factor – only part of the photons are emitted into the solution. As a total estimate, 4% in reabsorption will be taken for calculation of FRET of the complex input.

Considering that FRET efficiency of the complex is close to 100% (due to small distances between donor and acceptor), the calculated value for $E_{FRET}^{complex}$ shows the fraction of photochrome molecules (Y_k) that are complexed with fluorescent dye molecules.

FRET efficiency in solution was calculated by the Monte Carlo method taking into account FRET from the fluorescent dye to itself.

Table 10. Comparative changes in absorption of photochrome with different compounds, calculated efficiency of energy transfer (φ) from experimental data according to Equation 7 (and in parentheses according to Equation 8, for w=0.8), spectral integral (J), Förster distance (R), FRET efficiency in homogeneous solution calculated with Monte Carlo method, input of FRET in the complex and percentage of complexed photochrome molecules (Y_k)

Additive	Model	THB
ΔD_p at λ=600 nm	0.0112	0.0162
$\Delta D_p^{chalcone}$ at λ=600 nm	0.0048	0.0058
φ	0.15 (0.22) ± 2	0.34 (0.47) ± 3
$J_{dye\text{-}photochrome,}$ M^{-1} cm^3	$2.51*10^{-15}$	$3.58*10^{-15}$
R_0, nm	2.5	2.6
E_{RET}^{sol}	0.12	0.13
$E_{reabsorption}$	0.04 ± 0.02	0.04 ± 0.02
$E_{RET}^{complex}$	0 (0.06) ± 0.02	0.17(0.3) ± 0.03
Y_k, %	0-2 (4-8)	14-20 (27-33)

For a strict proof of FRET, a six order dependence of energy transfer efficiency on the distance between chromophores has to be shown. In the case of supramolecular complex formation in solution, the distance between the two types of molecules cannot be precisely calculated from their concentrations. The solution will represent a mixtrure of complexed and unbound molecules. At the same time, the comparative study has shown a clear difference in photochromic transformations for THB and the model compound. It is reasonable that the primary mechanism that results in such changes arsies from FRET within the complex.

The opposite process, energy transfer from the photochrome to the 2PA dye by a Forster mechanism, is not possible (the photochrome is not fluorescent), and this leads to a

cumulative effect. Photon energy can be acquired by the photochrome molecules in two ways: (a) directly and (b) received from the 2PA dye by FRET. The contribution from (b) acts as a virtual enhancement of the effective 2PA cross section of photochrome molecules. It is also expected that the direct 2PA cross section of photochrome compound may change upon formation of supramolecular structure, however this effect is expected to be insignificant relative to the contribution from FRET.

References

[1] Morales, A. R.; Schafer-Hales, K. J.; Marcus, A. I.; Belfield, K. D. *Bioconjugate Chem.* **2008**, *19*, 2559-2567.

[2] Joseph R. Lakowicz. *Principles of fluorescence spectroscopy*, Springer Science: New York, **2006**

[3] Lunz, M.; Bradley, A. L.; Gerard, V. A.; Byrne, S. J.; Gun'ko, Y. K.; Lesnyak, V.; Gaponik, N. *Phys. Rev. B* **2011**, *83*, 115423

[4] Zubarovskii, V. M.; Bricks, J. L. *Ukr. Khim. Zh.* **1982**, *48*, 761.

CHAPTER 6. NONLINEAR ABSORPTION EXPERIMENTS

This chapter finalizes all pre-application research from the previous chapters and demonstrates some practical results in data recording and readout under 2PA for all photochromic systems used in this research, as well as two-photon absorption (2PA) cross section data for the compounds employed. Also in this chapter is disclosed a procedure to calculate the 2PA cross section in an analytical way from experimental Z-Scan curves. Additionally, a new method for 2PA cross section measurements suitable for photochromic compounds is presented.

6.1 Materials and methods

6.1.1 Two-photon absorption cross section measurements by Z-Scan

Z-Scan measurements were performed in the open aperture configuration, using femtosecond pulses with 1 kHz repletion rate. Experimental setup is presented in Figure 40. The output of the OPA tuned over the range 540-1400 nm, pulse duration ≈ 100 fs (FWHM), and pulse energies ≤ 100 nJ were used. For measurements, solutions were placed in a 1 mm path length cuvette or, in case of photochromic compounds, in a flow cell (same path length). Concentrations of all solution were prepared to be ~ 10^{-2} M.

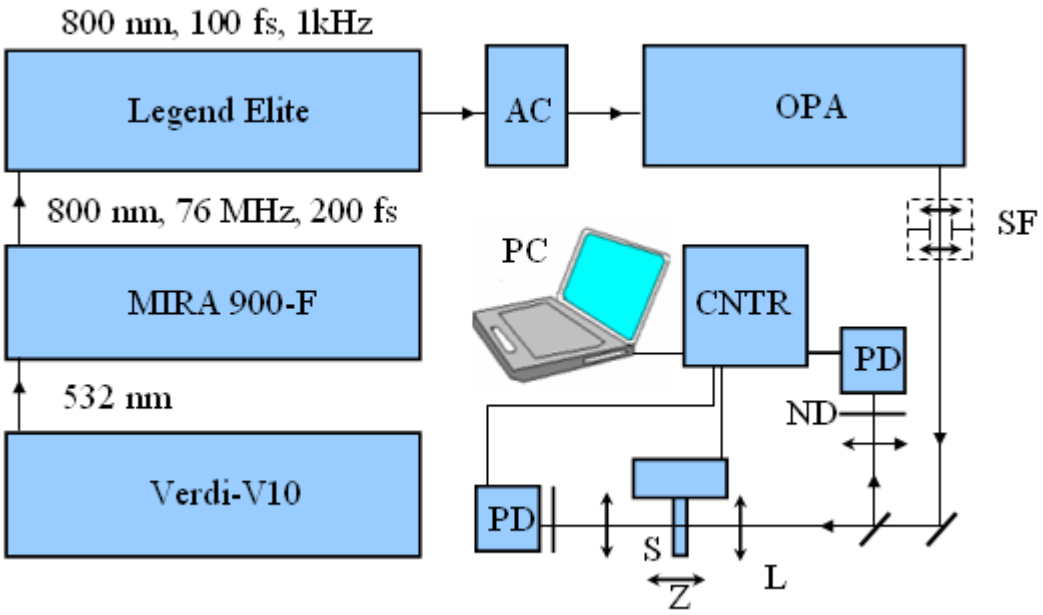

Figure 40. Z-Scan experimental setup. Starting from bottom left corner, clockwise: 532 nm pump laser (Verdi-V10), femtosecond 76 MHz laser, regenerative amplifier (Legend Elite), auto correlator (AC), optical parametric amplifier (OPerA Solo, OPA), space filters (SF), 100% reflection mirrors, translation stage (Z), sample holder (S), focusing lenses (L), neutral density filters (ND) in front of Si photodetectors (PD). Data acquisition electronics and translation stage controllers (CNTR) are linked to a PC with a custom made software.

Currently, there is no commercial Z-Scan instrument available. Therefore, all the equipment has to be custom made or assembled from different commercial modules (stepper motor and shutter controllers, data acquisition boards and software). The format of the dissertation does not allow a full description of the equipment due to its oversized documentation. For example the Z-Scan software alone – named Alice, in its latest version 5.0 has over 5000 code lines (over 200 pages of text, in dissertation format), its add-on for 3D object design and recording (for 3D optical data storage and microfabrication) – over 2000 lines of code; the electronics is built around 18 microcomputers (for parallel multi-tasking and multiple Z-Scan measurements) each with a separate firmware, totaling over

1000 lines of code. Some methods implemented in the Z-Scan equipment that have scientific value are presented below.

6.1.2 Analytical calculation of 2PA cross section and beam waist from experimental Z-Scan data

All reported cross sections from Z-Scan experimental data in this dissertation have been calculated by Alice 5.0 software in semi-automatic mode. Below, the mathematical apparatus and the algorithm for computing the nonlinear coefficient β and beam waist ω_0 is disclosed.

Nonlinear transmission T(z) of the sample can be written[1] as a sum of an infinite number (m) of terms S_m. Practically, for m>5, in most cases, the terms S_m are extremely small and can be ignored.

$$T(z) = \sum_{m=0}^{\infty} \frac{(-q(z))^m}{(m+1)^{3/2}} = \sum_{m=0}^{\infty} S_m(z) \qquad \text{(K1)}$$

In which:

$$q(z) = \frac{\beta \cdot I_0(0) \cdot L_{eff}}{1 + \left(\frac{z}{z_0}\right)^2} \qquad \text{(K2)}$$

Figure 41 shows the sum of 3 terms S_1, S_2, S_3 with first term S_0=1 and a Z-Scan curve as a sum of first 6 terms: $T=1+S_1+S_2+S_3+S_4+S_5$.

In the above expression (K2), β is the 2PA coefficient, z is the longitudinal space coordinate,

$$z_0 = \frac{\pi \cdot \omega_0^2}{\lambda} \qquad \text{(K3)}$$

λ is the laser wavelength, L_{eff} is the effective length of the sample

$$I_0(z) = \frac{2 \cdot E}{\pi\sqrt{\pi} \cdot \tau \cdot \omega_{(z)}^2} \quad \text{(K4)}$$

where $\omega(z)$ is the transverse size of the beam, τ – laser pulse width (HW1/e^2M), E – energy per laser pulse (average),

$\omega_{(z=0)}^2 = \omega_0^2$ (beam waist)

$$\omega(z) = \omega_0\sqrt{1 + \frac{z^2}{z_0^2}} \quad \text{(K5)}$$

From K4 and K5:

$$I_0(0) = \frac{2 \cdot E}{\pi\sqrt{\pi} \cdot \tau \cdot \omega_0^2} \quad \text{(K6)}$$

$$q(z) = \frac{\beta \cdot 2 \cdot E \cdot L_{eff}}{\pi\sqrt{\pi} \cdot \tau \cdot \omega_0^2 \left[1 + \left(\frac{z \cdot \lambda}{\omega_0^2 \cdot \pi}\right)^2\right]} = \frac{\beta \cdot A}{\omega_0^2 \left[1 + \frac{z^2 \cdot B}{\omega_0^4}\right]} = \frac{\beta \cdot A}{\omega_0^2 + \frac{z^2 \cdot B}{\omega_0^2}} \quad \text{(K7)}$$

In the above equation, A and B represent the following expressions:

$$A = \frac{2 \cdot E \cdot L_{eff}}{\pi\sqrt{\pi} \cdot \tau} \quad \text{(K8)}$$

$$B = \frac{\lambda^2}{\pi^2} \quad \text{(K9)}$$

Deriving an analytical expression for calculation of nonlinear coefficient β and beam waist ω_0 directly from K1 is an extremely difficult task (if possible). This is the reason, subsequent guessing of different values β and ω_0 is used by researchers until the T(z) curve "fits" the experimental curve. This process can be time consuming and, most important, boring. An easier solution exists.

Let us examine the position of $1+S_1$ curve. On the graph, it is always below the experimental (and theoretical) Z-Scan curve. For $1+S_1$, the "shift" down will be marked as $u_1(z)$, which is a complex function of its own. Practically, for every z-position it is the ratio between the sum of first two terms (m=0, 1) and the sum of all terms (m=0, 1, 2, 3, 4, 5 …): $u_1(z)=(1+S_1(z))/T(z)$. For different experimental conditions, the value of $u_1(z)$ is different, which complicates the task (making a database, for example). Let us assume, for now, that this value $u_1(z)$ is known for every z – point (later an algorithm to calculate this value will be presented). If so, $S_1(z)$ or in general case $S_m(z)$ can be calculated from the Z-Scan curve:

$$S^z_{m>0} = u_m(z) \cdot T^z - 1 \qquad \text{(K10)}$$

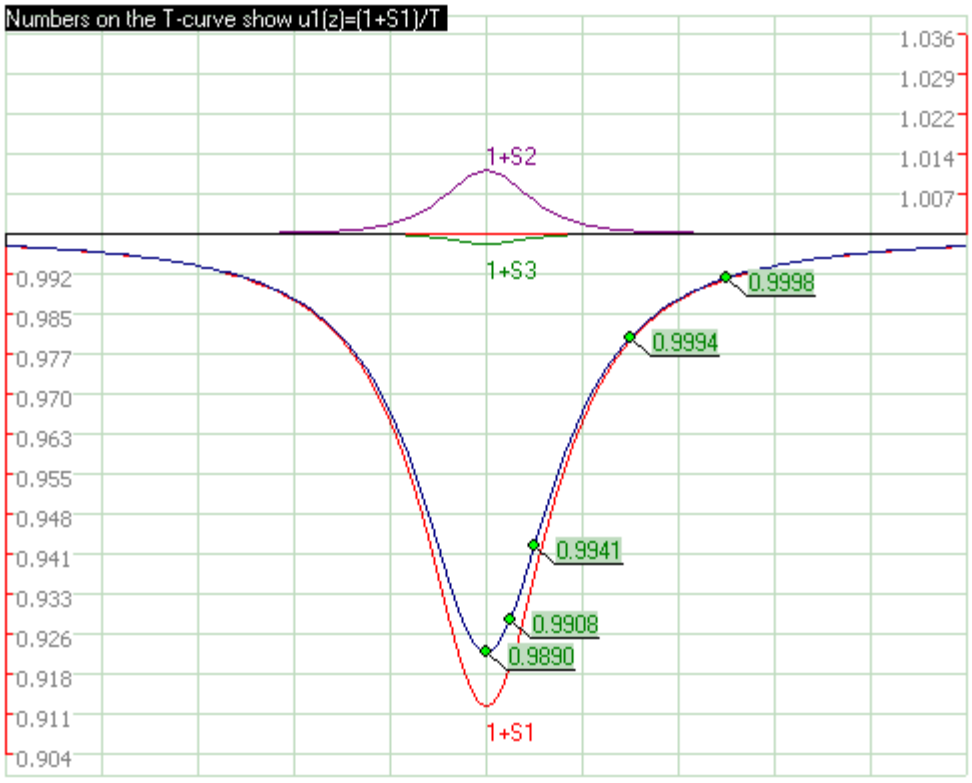

Figure 41. An example of a theoretical Z-Scan curve (in blue) and first three sum terms of the Z-Scan curve in other colors (screenshot from Alice 5.0 software). Numbers in green indicate the calculated $u_1(z)$ values for five z-positions.

Any equation $S_m(z)$, can be shown to have a single solution of ω_0 and β.

In terms of A and B (see K8 and K9), the sum term $S_m(z)$ can be written as:

$$S_m(z) = \frac{(-q(z))^m}{(m+1)^{3/2}} = \left(\frac{-\beta \cdot A}{\omega_0^2 + \frac{z^2 \cdot B}{\omega_0^2}}\right)^m \cdot \frac{1}{(m+1)^{3/2}} \qquad \text{(K11)}$$

Next, the terms are separated; one containing coefficient β to the left, and beam waist ω_0 to the right side:

$$\frac{(-\beta \cdot A)^m}{(m+1)^{3/2}} = S_m(z) \cdot \left(\omega_0^2 + \frac{z^2 \cdot B}{\omega_0^2}\right)^m \qquad \text{(K12)}$$

The above equation is valid for any point on $(1+S_m)$ Scan curve, therefore for two selected points on the $(1+S_m)$ curve with coordinates $(z_1, 1+S_m^{z1})$ and $(z_2, 1+S_m^{z2})$ one can write:

$$S_m^{z_1} \cdot \left(\omega_0^2 + \frac{z_1^2 \cdot B}{\omega_0^2}\right)^m = S_m^{z_2} \cdot \left(\omega_0^2 + \frac{z_2^2 \cdot B}{\omega_0^2}\right)^m \qquad \text{(K13)}$$

From (K13) ω_0 can be expressed as:

$$\omega_0 = \pm \sqrt[4]{\frac{\varsigma \cdot z_1^2 \cdot B - z_2^2 \cdot B}{1-\varsigma}} \qquad \text{(K14)}$$

The above expression (K14) shows that one (S_m+1) scan curve has only one value of ω_0 as solution (mathematically calculated negative solution has no physical meaning). Note:

$$\varsigma = \sqrt[m]{\frac{S_m^{z_1}}{S_m^{z_2}}} \qquad \text{(K15)}$$

If ω_0 is known, from K11, 2PA coefficient β is found as a unique solution from a single z-point with coordinates $(z_1, 1+S_m(z_1))$:

$$\beta = \frac{1}{A} \cdot \left(\omega_0^2 + \frac{z^2 \cdot B}{\omega_0^2}\right) \cdot \left| \sqrt[m]{S_m^{z_1} \cdot (m+1)^{3/2}} \right| \qquad \text{(K16)}$$

2PA cross section (δ) is calculated as:

$$\delta = \frac{\beta \cdot h \cdot \nu}{C} \qquad \text{(K17)}$$

$h\nu$ is the photon energy and C is the molecular concentration in the sample.

Above calculations can be performed if $u_1(z)$ is known (and therefore $S_1(z)$ can be computed from T(z) curve). If $u_1(z)$ is not known (real case), then a self correction algorithm can be used to calculate the values for $u_1(z)$. It is sufficient to find these values for only 2 selected z-points.

Step 1. Some initial values for $u_1(z_1)$ and $u_1(z_2)$ are given. In the simplest case, assignments are $u_1(z_1)=1$ and $u_1(z_2)=1$.

Step 2. For each point, values for $S_1(z)$ are calculated from K10.

Step 3. Next, ω_0 and β are calculated (K14, K16).

Step 4. Using equation K1 values for T(z) are calculated (can be plotted).

Step 5. New values for $u_1(z)$ are calculated: $u_1(z)= (1+S_1(z))/ T(z)$

Step 6. Go to step 2 and repeat this procedure m times (4 repetitions is sufficient).

A graphical representation of algorithm results is presented in Figure 42.

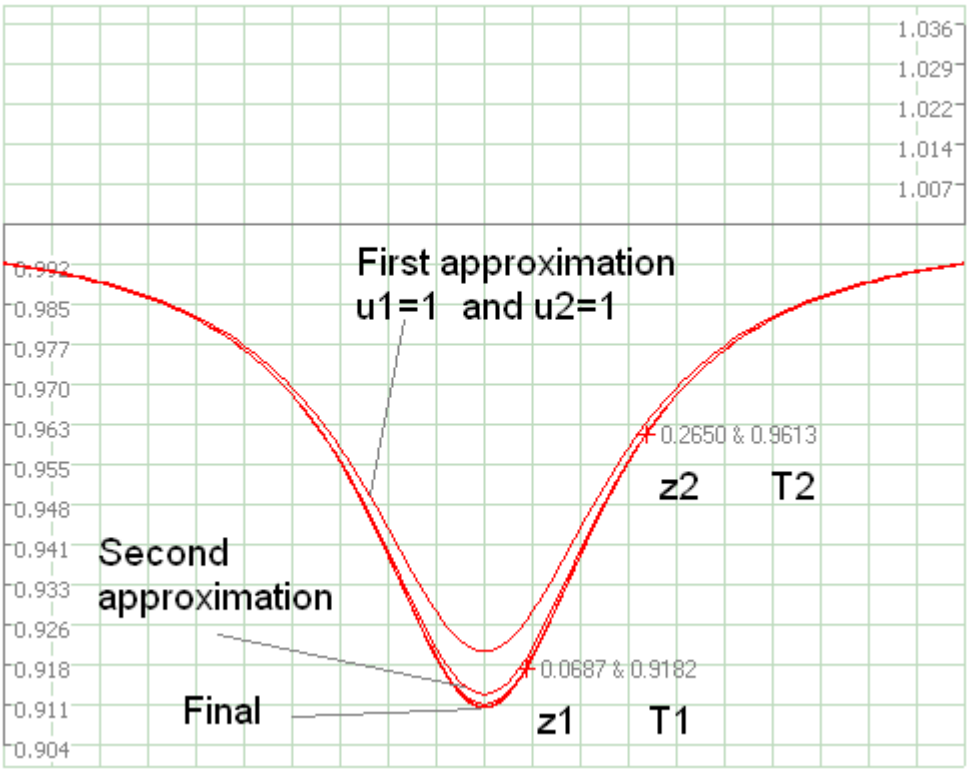

Figure 42. Drawing the theoretical Z-Scan curve trough two randomly selected points on the screen. Points, marked with red crosses, have coordinates (z_1, $T(z_1)$) and (z_2, $T(z_2)$). In the first approximation, the software takes "wrong" values for $u_1(z_1)=1$ and $u_1(z_2)=1$ and "misses" the target points. However, from the "wrong" curve it computes $u_1(z_1)'=(1+S_1(z_1))/ T(z_1)$ and $u_1(z_2)'=(1+S_1(z_2))/ T(z_2)$ and uses these values for its second approximation. Repeating this procedure m times, it positions the final curve precisely on the selected points (screenshot from Alice 5.0 software, normally only the final curve is displayed).

Practically, for the software to compute the 2PA cross section from the Z-Scan curve, two more data points are needed: the position of the baseline (where the transmittance is considered to be unity) and the position of the symmetry line. Relative to these lines, the coordinates of the two selected points on the screen can be computed. Some experiments done to position these lines in fully automatic mode (by software vision) have given, on average, worse results than positioning these lines in manual mode (by an operator with human vision). For this reason, choosing the location of the baseline, symmetry line and the

two points that best represent the expected theoretical Z-Scan curve was left to the human operator (a few clicks with a mouse button). A relatively rare example is presented in Figure 43, when the symmetry line does not correspond to the minimum on experimental data plot (due to noise or some issues in the optical alignment), and it is the experience of the researcher that is required to aid the software.

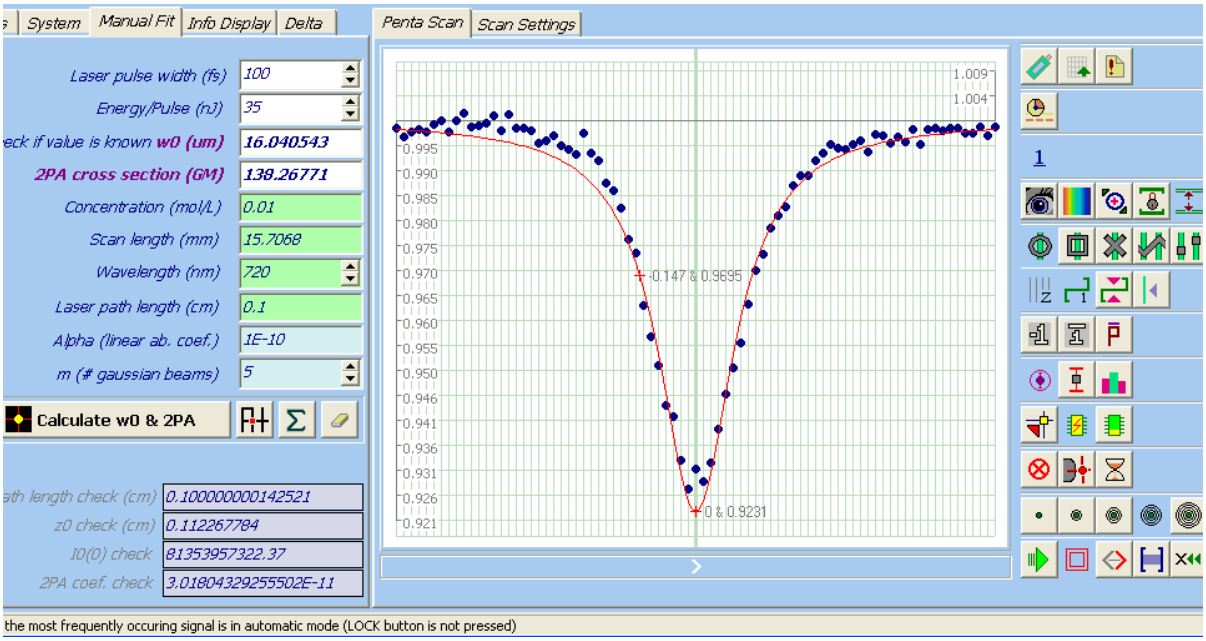

Figure 43. Implementation of the algorithm into the software. Example of calculated Z-Scan curve (red) trough two selected points (red crosses, numbers show coordinates z and T). On the left side of the screenshot – calculated ω_0 and δ, on the right side – operator's controls. In the center blue circles represent experimental data.

6.1.3 Method for 2PA cross section measurements of photochromic compounds

Z-Scan is considered to be a very powerful general method for 2PA cross section determination of the vast majority of compounds (fluorescent and nonfluorescent). Nevertheless, Z-Scan method has some limitations that make it difficult to be used in cases of

photo-non-stable substances. A way to overcome this problem is to use a flow cell, through which fresh solution is being constantly pumped, during 2PA measurements. If a very small quantity of substance is available, instead the use of a flow cell, low repletion rate of laser pulses can be used (an additional shutter can also be used to interrupt laser beam). This procedure is necessary to allow the substance (photo-decomposed or photo-isomerized) from the focal volume of the laser to diffuse into the other parts of solution. Other limitations of Z-Scan arise from the fact that it is an absolute method: the need to know all optical parameters, not applicable to complex optical absorption geometries and non-Gaussian beam profiles. Small changes in the experimental setup or some errors in calculations of optical parameters often cause the method to yield less than reproducible results across different research groups.

Below a relative method that may be more suitable for 2PA measurements of photochromic compounds is described. The method does not require long exposure of the substance to the laser, the 2PA cross section can be computed from just a few transmitted laser pulses. The theoretical basis is described below.

For a square-shape laser pulse, the transmitted light intensity through a sample with two photon absorption is given by the equation:

$$I = \frac{I_0}{1 + \beta \cdot C \cdot k \cdot x \cdot I_0} \qquad \text{(J1)}$$

In this equation, β is the 2PA cross section of molecular species of the concentration C, I_0 is the laser intensity in the optical path cross section x and k is an additional conversion factor present in case of molecular 2PA cross section (if taken k=1, β is 2PA non linear coefficient). Since there is no direct method to measure the laser focal volume and light intensity distribution inside the focal volume, values for both x and I_0 cannot be determined with

required accuracy. To make a method reliable, values of x and I_0 have to be eliminated from calculations.

In the most general case, for three substances with 2PA cross sections δ_1, δ_2, δ_3 and concentrations C_1, C_2, C_3 can be written:

$$I_1 = \frac{I_0}{1 + \beta_1 \cdot C_1 \cdot k \cdot x \cdot I_0} \quad \text{(J2)}$$

$$I_2 = \frac{I_0}{1 + \beta_2 \cdot C_2 \cdot k \cdot x \cdot I_0} \quad \text{(J3)}$$

$$I_3 = \frac{I_0}{1 + \beta_3 \cdot C_3 \cdot k \cdot x \cdot I_0} \quad \text{(J4)}$$

Assuming that it would be possible to maintain for 3 measurements same x and I_0 then, then one can calculate the following ratio by dividing expression (J2) by (J3):

$$a = \frac{I_1}{I_2} = \frac{1 + \beta_2 \cdot C_2 \cdot k \cdot x \cdot I_0}{1 + \beta_1 \cdot C_1 \cdot k \cdot x \cdot I_0} \quad \text{(J5)}$$

and dividing expression (J2) by (J4):

$$b = \frac{I_1}{I_3} = \frac{1 + \beta_3 \cdot C_3 \cdot k \cdot x \cdot I_0}{1 + \beta_1 \cdot C_1 \cdot k \cdot x \cdot I_0} \quad \text{(J6)}$$

From (J5) one can express x k I_0 :

$$k \cdot x \cdot I_0 = \frac{1 - a}{a \cdot \beta_1 \cdot C_1 - \beta_2 \cdot C_2} \quad \text{(J7)}$$

From (J6) x k I_0 is expressed as:

$$k \cdot x \cdot I_0 = \frac{1 - b}{b \cdot \beta_1 \cdot C_1 - \beta_3 \cdot C_3} \quad \text{(J8)}$$

Since in all cases x, k, I_0 are the same, right sides of expressions (J7) and (J8) are also equal:

$$\frac{1 - a}{a \cdot \beta_1 \cdot C_1 - \beta_2 \cdot C_2} = \frac{1 - b}{b \cdot \beta_1 \cdot C_1 - \beta_3 \cdot C_3} \quad \text{(J9)}$$

From (J9), one can express β_3 as a function of a, b, β_1, β_2, C_1, C_2, C_3:

$$\beta_3 = \frac{b \cdot \beta_1 \cdot C_1 - (1-b)(a \cdot \beta_1 \cdot C_1 - \beta_2 \cdot C_2)}{(1-a)C_3} \qquad \text{(J10)}$$

For the simplicity it is possible to take $\beta_1=\beta_2$, but $C_1 \neq C_2$, and this yields the expression to calculate the 2PA cross section of an unknown substance β_x:

$$\beta_x = \beta_1 \cdot \frac{b \cdot C_1 - (1-b)(a \cdot C_1 - C_2)}{(1-a)C_3} = \beta_1 \cdot M \qquad \text{(J11)}$$

Equation 9. Relative 2PA cross section by three point method (Delta method)

M - is the relative multiplicator, it the value that shows how much bigger or smaller the 2PA cross section is relative to the standard (β_1).

A major source of errors comes from solution preparation, and cannot be avoided in any method. To estimate the error of the method, same substance in all three measurements is used (at three different concentrations). In the case of a perfect setup and flawless work one can expect:

β_x (calculated) = β_1 or M=1

In a real case, the relative error can simply be calculated as:

$$Error = \frac{|\beta_x - \beta_1|}{\beta_1} = \frac{|M(calculated) - 1|}{1} \qquad \text{(J12)}$$

Though equation J11 was derived for a square laser pulse, it is easy to show that it is valid for any other pulse shape (see Appendix E).

The experimental setup for this method, named 3-point method (or simply Delta), is identical to the Z-Scan experimental setup, and can be used to reinforce it. Although Delta method as described does not look attractive because of the need to do measurements on 3 samples, the computerized approach may change the situation. The method described above

normally involves the use of a standard or a substance for reference in the first two measurements. It has to be noted, that in the case when experimental conditions do not change, it is sufficient to do this procedure only once. For the best results, a computer program could create a large data base, which will include values of transmission for the standard at different incident laser intensities. With the completion of the database the method becomes significantly more attractive for practical use. To measure the 2PA cross section of a new sample, it is sufficient to measure a few values (to average) of the transmitted power of the sample. All the other information will be taken from the database. The software will use the values of the standard that were recorded at the same laser power (or energy per pulse) as of the sample, for the same solvent. The required time for measurements of 2PA cross sections in this case is limited only by the speed of sample replacement in the cuvette. The method is not suitable for substance that exhibit 1PA at the wavelength of measurement (same as Z-Scan).

6.1.4 Data recording and readout under 2PA with the researched photochromic systems

Two-photon recording and readout were performed on a modified Olympus Fluoview FV300 laser scanning confocal microscopy system equipped with a broad-band, tunable Coherent Mira Ti:sapphire laser (200 fs pulse width, 76 MHz repetition rate), pumped by a 10 W Coherent Verdi frequency-doubled Nd:YAG laser. The FV300 was coupled to an Olympus IX-70 microscope. In two-photon writing, exposure time and position were controlled by means of an electronic shutter and electronic (XYZ) stage, respectively, both from Thor Laboratories, that was in turn controlled by means a customized equipment and program. Two-photon optical recording was achieved by inducing conversion OF to CF.

Readout was performed by inducing the upconverted fluorescence of the fluorescent dye.

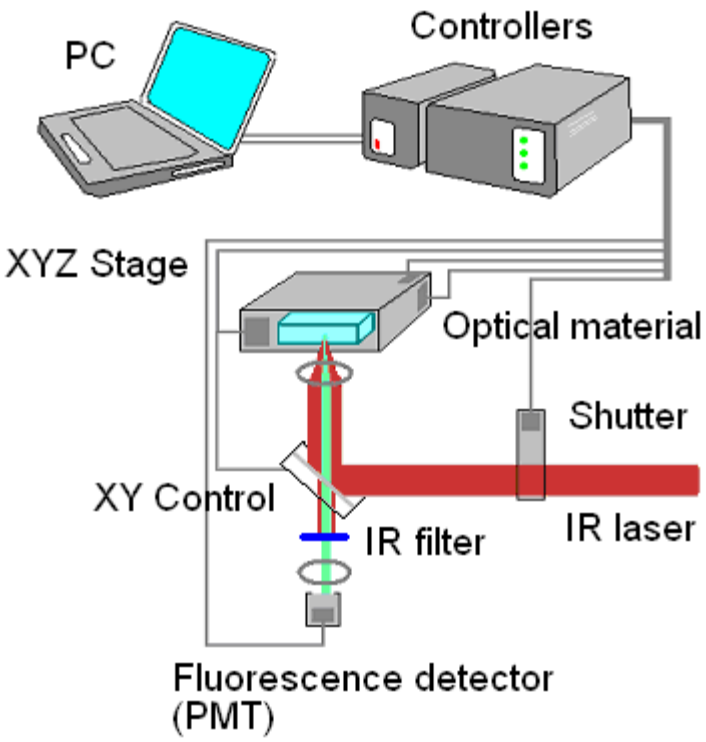

Figure 44. Schematic experimental setup for data recording by 2PA. Recording in XY place was performed by moving the stage, while readout was performed with a scanning XY mirror system (XY Control). Fluorescence was detected by a PMT detector. A shortpass filter was used to block the reflected IR laser radiation.

The customized program (see Figure 45) is a CAD (computer aided design) type software with a built-in hardware controlling feature. It allows recording information in both analog (images, see example in Figure 45) and digital, as discrete exposed and unexposed dots (zeros and ones).

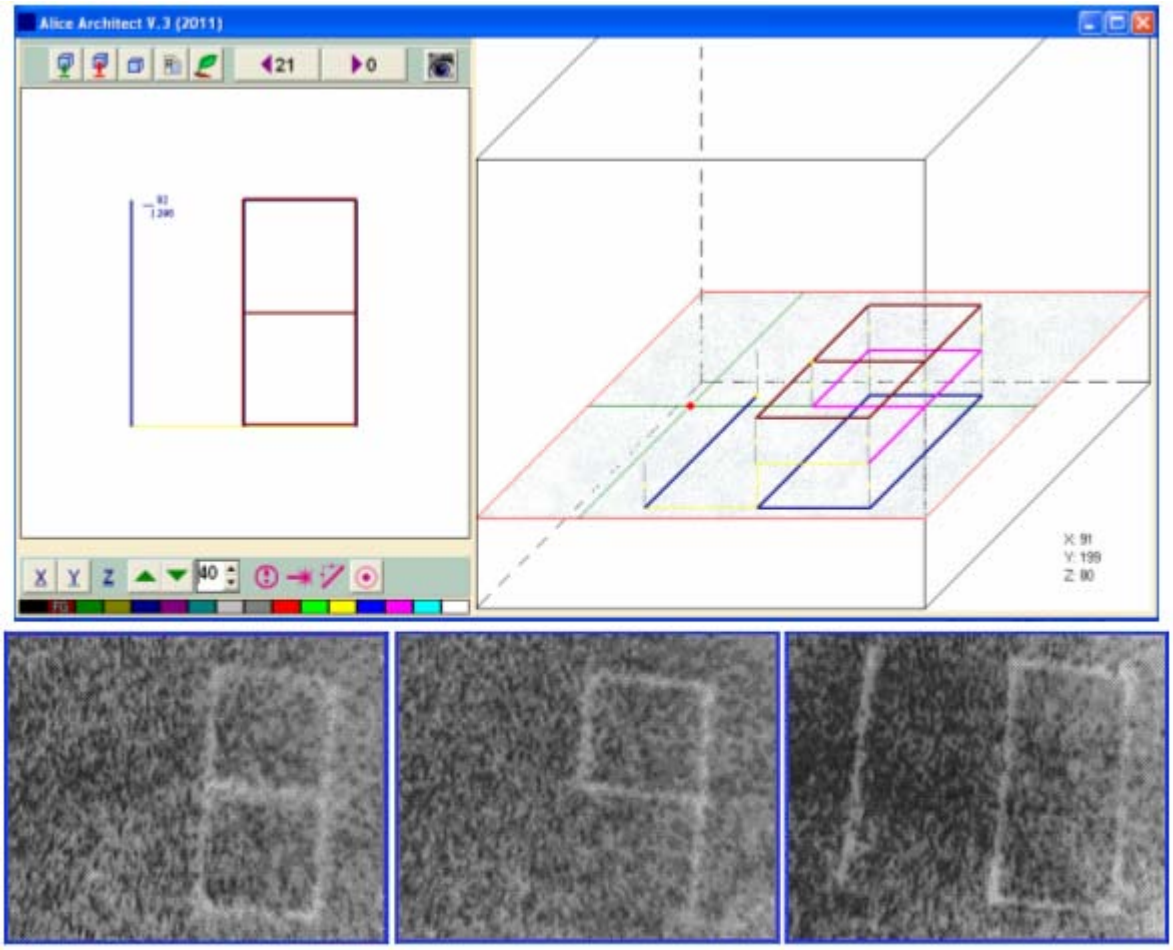

Figure 45. Top image: screenshot from Alice Architect, a CAD type software developed for 3D data recording and 3D micro-fabrication. In this example 8, 9, and 10 numeral are prepared to be recorded. Bottom image: example of recorded images (by photobleaching method) in three different layers. Recording medium (for testing purposes): PMMA film with fluorescent dimethylamino-chalcone. White lines – non fluorescent (photobleached) areas, darker background – fluorescent.

All photosensitive polymer films were prepared from mixing the corresponding dyes with PMMA polymer (average molecular weight = 5,000 g/mol) and solution-casted (from CH_2Cl_2) onto 2.5 x 2 .5 cm microscope glass coverslips.

6.2 Results and discussions

To compute the efficiency of 2PA cross section enhancement in the proposed methods, 2PA spectra were experimentally obtained. This data also allows selecting a proper wavelength for recording and readout under 2PA.

6.2.1 2PA spectra of 1

To assess the two-photon absorptivity and sensitivity of diarylethene **1**, the degenerate 2PA spectra of the OF and CF were obtained over a broad spectral range by an open aperture femtosecond Z-scan method with data presented in Figure 46. The values of the OF 2PA cross sections were relatively low (δ_{2PA} ~ 50-70 GM) with a well-defined maximum in the range $\lambda_{2PA}/2$ ≈ 380-420 nm (curve 1) that closely overlapped with the corresponding linear (one-photon allowed) absorption band at ≈ 400 nm (curve 3). The nature of this 2PA maximum, which is electronically forbidden in symmetric molecules can be explained by strong vibronic interactions playing an important role in their nonlinear optical properties.[2,3] It should be noted that OF 2PA spectrum is similar to that of a separate fluorene compound with NO_2 substituents in the 2-position[4] and related diarylethene derivatives.[5] This suggests that the OF of **1** possesses a restricted π-conjugation length, resulting in relatively small transition dipoles. A strong enhancement of 2PA efficiency (up to one order of magnitude) with δ_{2PA} ~ 450-600 GM was observed after photocyclization of **1** in DCM (curve 2) to produce the CF. Apparently, this enhancement reflects a drastic increase in π-conjugation length upon cyclization. In contrast to the OF, the 2PA spectrum of

the CF exhibited a long wavelength maximum at $\lambda_{2PA}/2 \approx 500$ nm that did not overlap with the main one-photon allowed absorption band of CF.

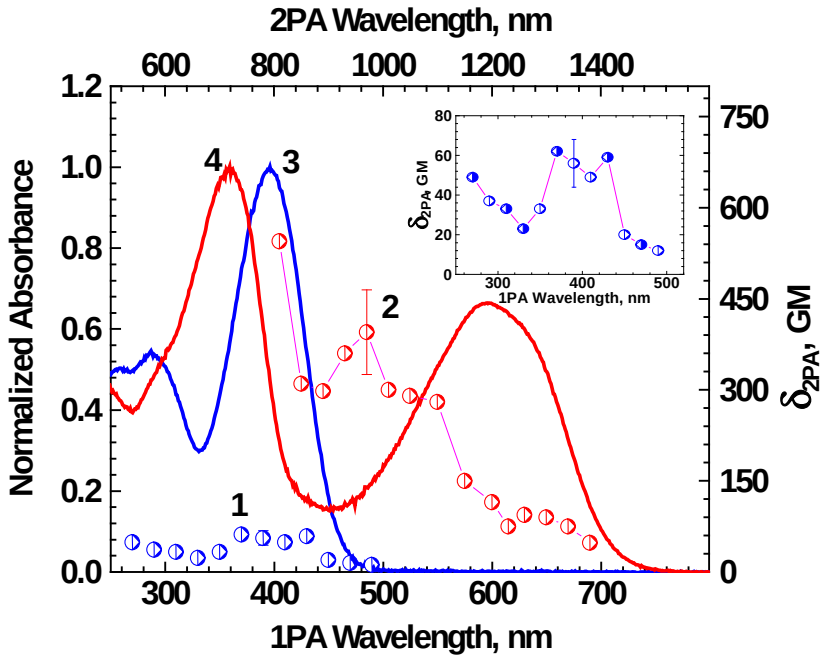

Figure 46. 2PA spectra of the OF (1) and CF (2) with corresponding linear one-photon absorption spectra of the OF (3) and CF (4) of 1 in DCM. The inset is a scaled 2PA contour of the OF (curve 1).

6.2.2 2PA data of the compounds used in FRET study

For the THB compound, 2PA cross section data was measured by the Z-Scan method for several wavelengths (see Figure 47). For the case of an unsymmetrical compound, the shape of the 2PA spectrum was similar to the shape of the 1PA spectrum.

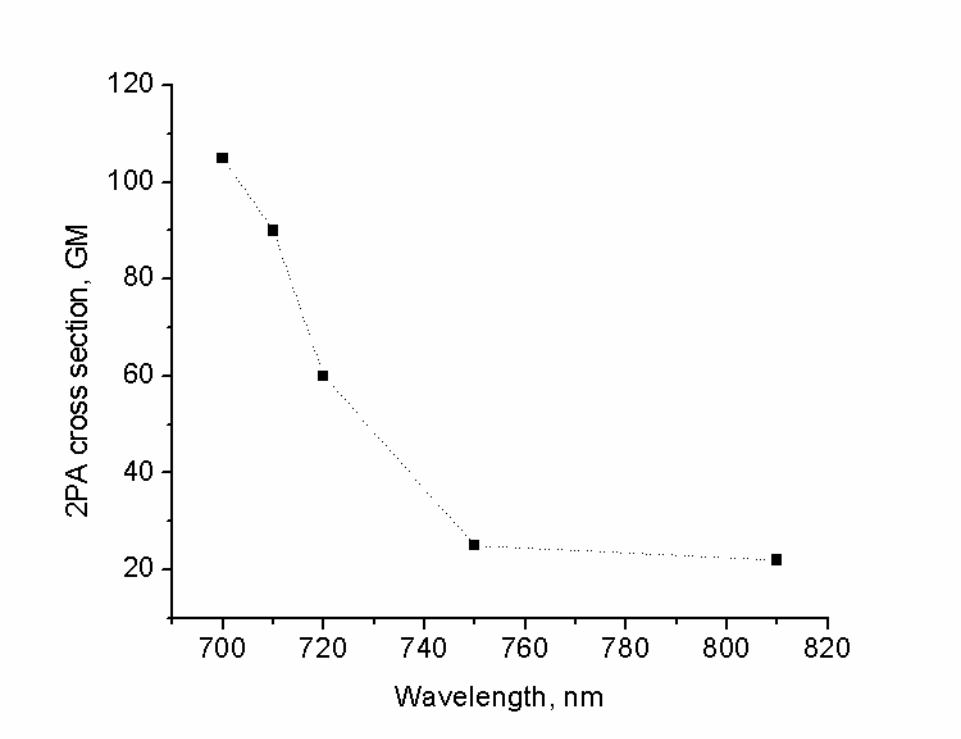

Figure 47. Two photon absorption cross section of THB compound (C). Relative error of the measurement ~ 20%

The 2PA spectral data suggest that 700 nm was the best choice for recording and readout. However, problems in mode-locking the laser at this wavelength have been experienced. For data recording and readout application 710 nm was selected. For this wavelength, the 2PA cross section of the model compound and of the photochrome OF, were measured via Z-Scan. The data are presented in Table 11.

Table 11. Two-photon absorption cross sections values by open aperture Z-Scan method for the compounds in the study.

λ, nm	δ_{THB}, GM	δ_{model}, GM	$\delta_{p\text{-}OF}$, GM
700	105±21		
710	90±18	120±24	10±2
720	60±12		
750	25±5		
810	22±4		

At 710 nm, a relative 2PA cross section value for model compound C, relative to THB compound D, was obtained by fluorescent method. For the same excitation geometry, same laser power, and same concentration of substances (in the same solvent), the relative 2PA cross section of model compound D was calculated as:

$$R = \frac{\delta_D}{\delta_C} = \frac{S_D \cdot QY_C}{S_C \cdot QY_D} = 1.3$$

where S_D is the integral fluorescence signal of compound D under 2PA, S_C – integral fluorescence signal of compound C, and QY_C and QY_D are fluorescent quantum yields of compounds of study. Relative integral fluorescence signals are shown in Figure 48. The ratio of 2PA cross sections by the fluorescent method (1.3) matches the ratio obtained via Z-Scan (120/90=1.33). A quadratic dependence check was performed in order to ensure that the observed fluorescence is induced by 2PA (Figure 49).

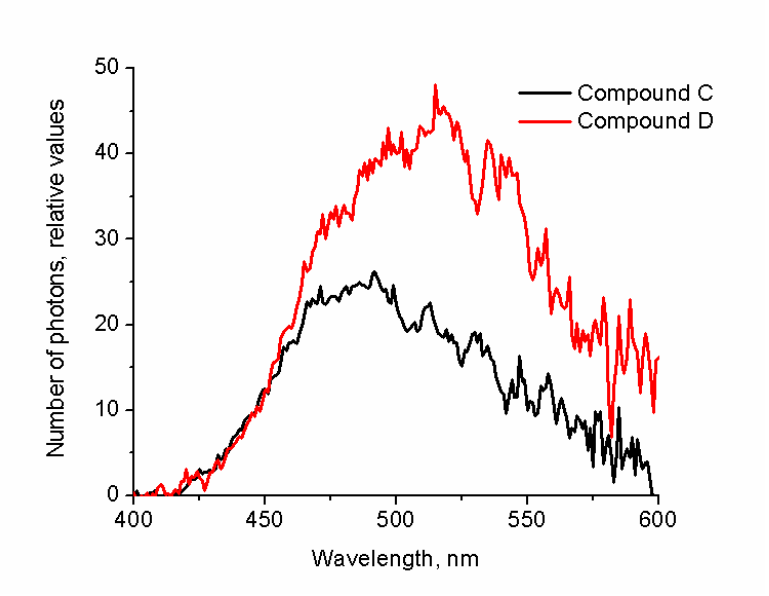

Figure 48. Fluorescence spectra for compounds C and D, under 2PA at 710 nm (40 mW, MIRA 80 Mhz). Concentration of both dyes was on the order 10^{-6} mol/L. Integral signals: $S_D = 1.9 * S_C$.

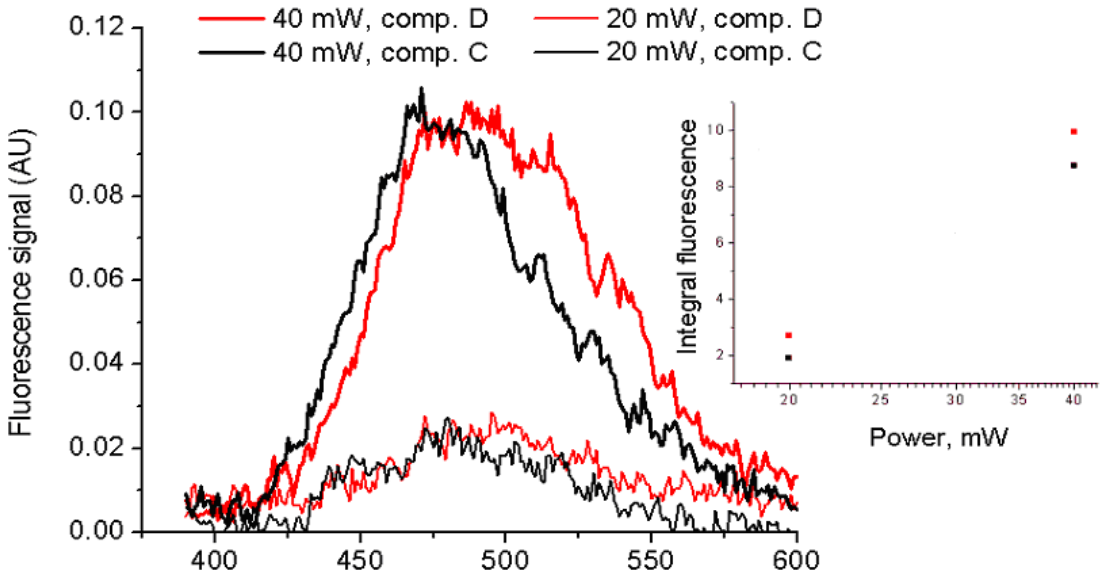

Figure 49. Quadratic dependence check of fluorescence for two laser powers (20 and 40 mW).

In case of the photochromic compound, the δ_{2PA} of the open is very low, which resulted in high level of noise in experimental data (see Figure 50). An additional obstacle in

measuring δ_{2PA} of the open form is the linear absorption of the closed form for this wavelength (710 nm). As soon as some closed form is produced upon two-photon excitation in the focal volume, the experimental 2PA data becomes uncertain. To minimize this effect, the exposure in the focal volume has been reduced to minimum by performing a fast Z-Scan in a flow cell.

For the purpose of comparison, the 2PA cross section of the open form has been measured by Delta method, which gave a 2PA cross section of 0.12 ± 0.05 relative to Rhodamine B at 710 nm. Assuming the cross section of Rhodamine B at 710 was measured correctly (95 GM), slightly different from the reported value,[6] the Delta method afforded 7 to 16 GM. The higher range of values given by Delta method is a result of low signal to noise ratio – noise reaches 40% from the signal for the scan above. In this particular case of noisy experimental data, the Z-Scan method has an advantage, as it extracts the 2PA cross section from multiple experimental points.

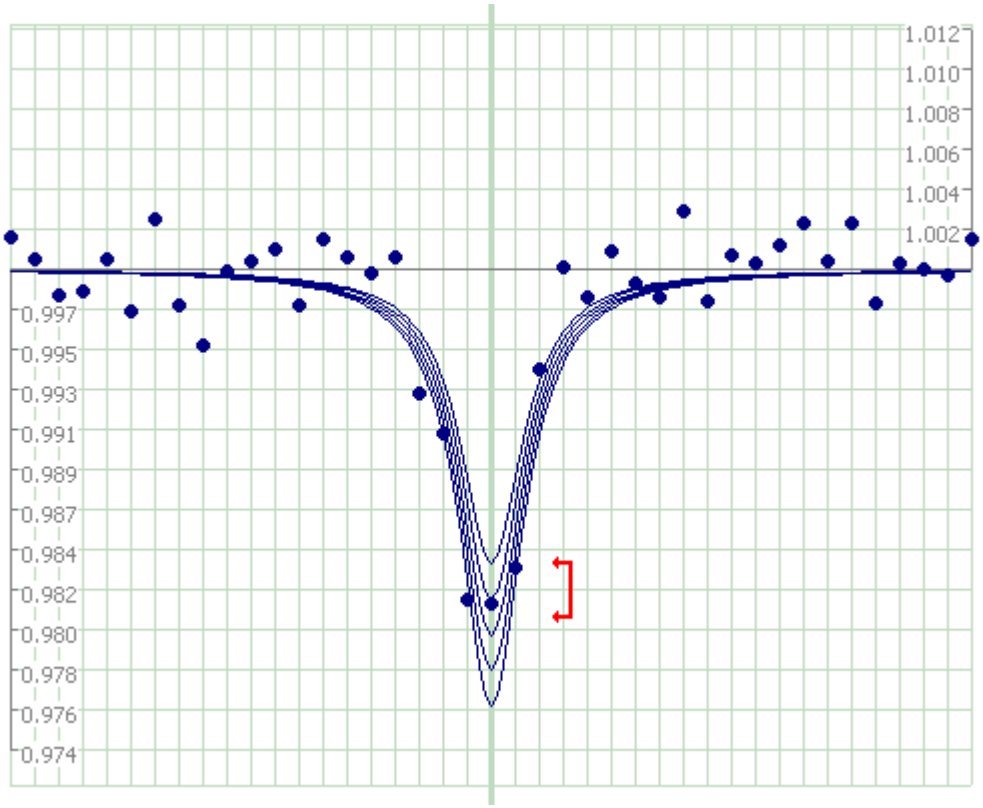

Figure 50. Z-Scan experimental data for photochrome at 710 nm (z=25.84 mm, ω_0=15 µm, C=0.01 mol/L, FWHM=100 fs, E=100 nJ, L=0.1 cm). Theoretical fit curves – solid lines correspond to 8, 9, 10, 11, and 12 GM. Red arrow indicate the points used to calculate 2PA cross section by Delta method, which gives 0.12 ± 0.05 relative to Rhodamine B 2PA at 710 nm.

The δ_{2PA} value for the open form of the photochrome at 710 nm is several times smaller than that of the dyes that were employed. Combined with THB, the photochrome would experience an additional energy transfer φ of 30-40% from the dye. The result is equivalent to a virtual increase of its own cross section by 300% at 710 nm (10 GM + φ* 90 GM).

6.2.3. Optical data recording and readout by 2PA

The potential utility of **1** in optical data storage was demonstrated in a system consisting of PMMA doped with **1** ($5.3 \cdot 10^{-3}$ M) and Rhodamine 6G ($1.0 \cdot 10^{-3}$ M). In this

system, voxels representing data were registered ("written") inducing the photoisomerization of **1** from the OF to the CF by 2PA at 750 nm). Once the film of the photoreactive media was placed on the microscope stage and immobilized, the stage was "parked" at a specific location and exposed for 2 ms (≈ 130 mW of laser power, 40X objective). The voxels were "readout" by recording the fluorescence of Rhodamine 6G induced by 2PA (750 nm; 130 mW; 40x). This indirect readout methodology was employed to avoid direct interrogation of the CF of **1**, providing a relatively destructive readout. The fluorescence of Rhodamine 6G overlaps with absorption of the CF. Thus, the intensity of the Rhodamine 6G fluorence is a measure of the relative amount of CF vs. OF (hence data recording).[7,8] In the areas where the materials had been exposed little to no fluorescence was observed due to the reabsorption of the Rhodamine 6G fluorescence by the CF of compound **1** that had been previously generated in the writing process, as well as FRET from Rhodamine 6G to CF of compound **1**. Once the fluorescence had been recorded, the image was imported to SlideBook 4.2, where a Gaussian filter was employed in order to reduce noise. The channels were inverted resulting in fluorescent pixels showing minimum to no intensity and non-fluorescent pixels showing the highest intensities. A signal intensity versus distance plot (Figure 51a) was traced along the red line shown in the inverted fluorescence micrograph (Figure 51b) to illustrate how clearly the data can be readout, enabling a binary data optical data storage.

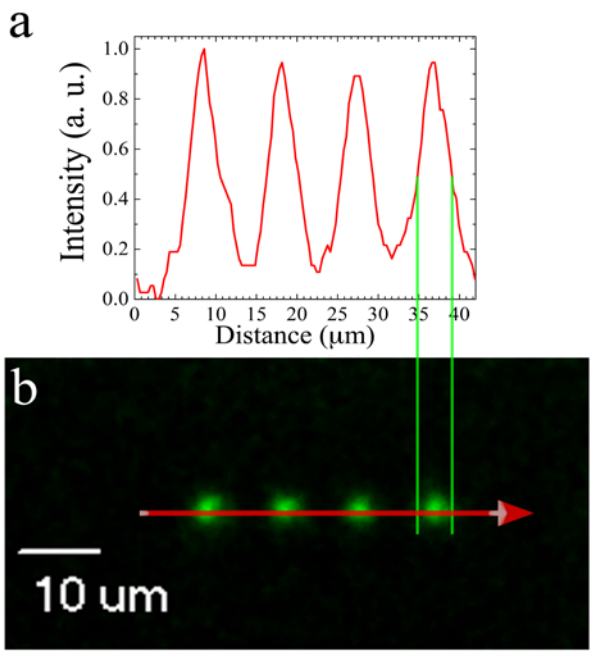

Figure 51. Inverted signal intensity versus distance (μm) (a) along pixels traced by red arrow (b). Voxels recorded in photoreactive material consisting (b) of 1 and Rhodamine 6G in PMMA. Two-photon recording by inducing conversion OF to CF. Fluorescence of Rhodamine 6G was interrogated for two-photon fluorescence readout. After channel inversion, green pixels show the area within the material where fluorescence intensity was a minimum.

As a control, a film containing only Rhodamine 6G ($1.0 \cdot 10^{-3}$ M) in PMMA was prepared and exposed under the same conditions as described above for data recording. No changes were observed, which supports that data recording is modulated by the photochrome's photoisomerization and not photobleaching of Rhodamine 6G.

For the case of FRET-based photochromic systems, a comparative recording and readout under 2PA has been performed. Two photochromic media were prepared and cast on the same microscope slide, separated by a thin tungsten wire (80 μm in diameter). To keep both media on the same field of view (and the wire), a 10X objective was used. Both photochromic systems were prepared in PMMA, doped with photochrome (2,3-bis(2,4,5-

trimethyl-3-thienyl)maleimide, $3*10^{-3}$ M) and a fluorescent dye ($3*10^{-3}$ M); model compound D or THB compound C. Figure 52 shows the fluorescence signal of both media under two photon excitation.

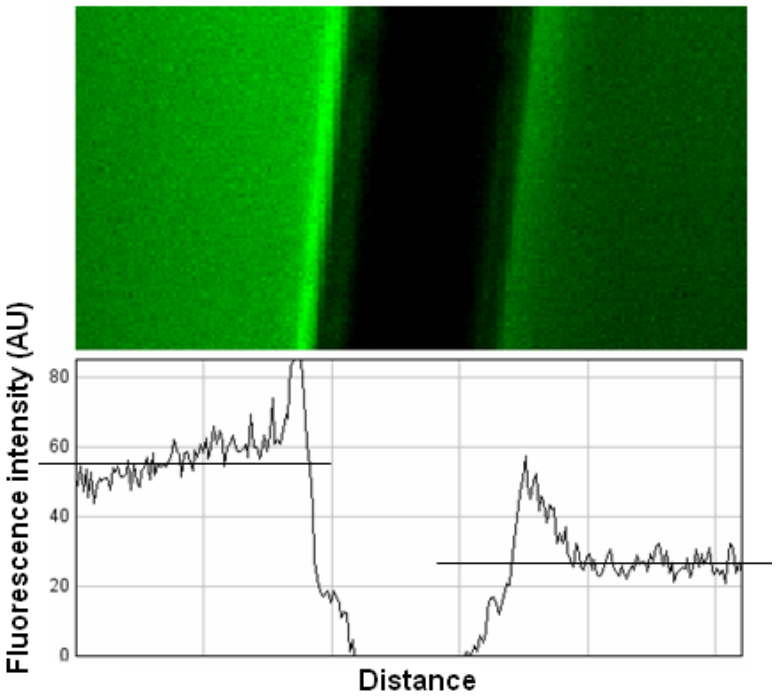

Figure 52. Background fluorescence signal under 2PA (710 nm) of the photochromic systems used in the FRET study. Left side – photochrome with model compound. Right side photochrome with THB. Middle – 80 µm diameter tungsten wire.

The observed relative fluorescence signal level correlates well with the theoretical signal ratio, calculated using data from Table 10 and Table 11. The fluorescence signal level for a fluorescent dye under two photon excitation is given by the following expression:

$$Signal = p \cdot \delta_{2PA} \cdot QY \cdot (1 - E_{RET}^{sol} - E_{RET}^{complex})$$

Here, δ_{2PA} is the 2PA cross section of the dye, QY – fluorescent quantum yield, E – efficiency of FRET to the photochrome, p – a proportionality coefficient (includes parameters of equal value for both systems: dye concentration, detector response at the fluorescence wavelength etc). Calculation of signal level for model compound gives a value

of Signal(model)=100*p, and for THB, Signal(THB)=44*p. This gives a theoretical signal ratio of 2.27, which is close to the observed signal ratio (57/26=2.2) from Figure 52.

Voxels representing data were registered inducing the photoisomerization of the photochrome from the OF to the CF by 2PA at 710 nm. Exposed time per voxel was 10 ms at ≈ 200 mW of laser power. Once the fluorescence was recorded, the image was imported to ImageJ 1.44, where intensity profiles were obtained. Results are presented in Figure 53, no filters or channel inversion was used.

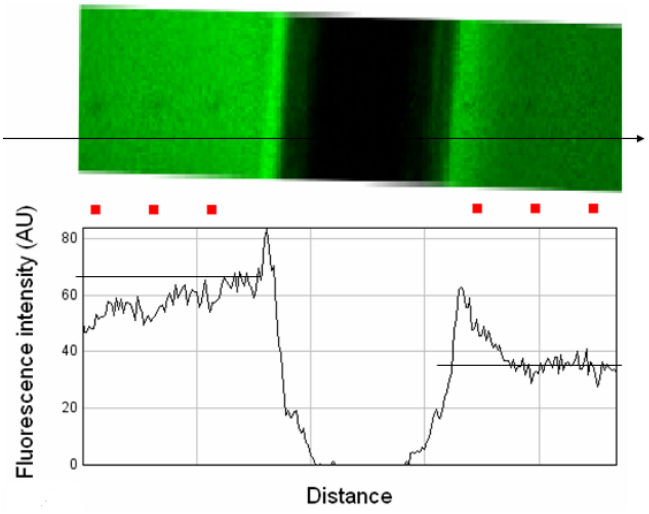

Figure 53. Comparative data recording by 2PA. Left side – photochrome with model compound. Right side - photochrome with THB compound. Middle – tungsten wire (80 µm in diameter). Darkening of the spots is mainly due to FRET to closed form of the photochrome. The process is almost entirely reversible upon irradiation at 532 nm.

Here the signal to noise ratio is significantly worse (less than 10% of signal level from background fluorescence), however this result validates the theoretical rationale from previous chapter, where the cause of a low expected signal was discussed.

As a control, films containing only fluorescent dyes ($3 \cdot 10^{-3}$ M) in PMMA were prepared and exposed under the same conditions as described above for data recording. For the experimental conditions employed (exposure time and laser intensity), no discernable

change in recording systems was observed. At significantly higher laser powers (~450 mW) and exposure time intervals (~400 ms), photobleaching of the fluorescent dyes occur, which results in a irreversible data recording (see Figure 56).

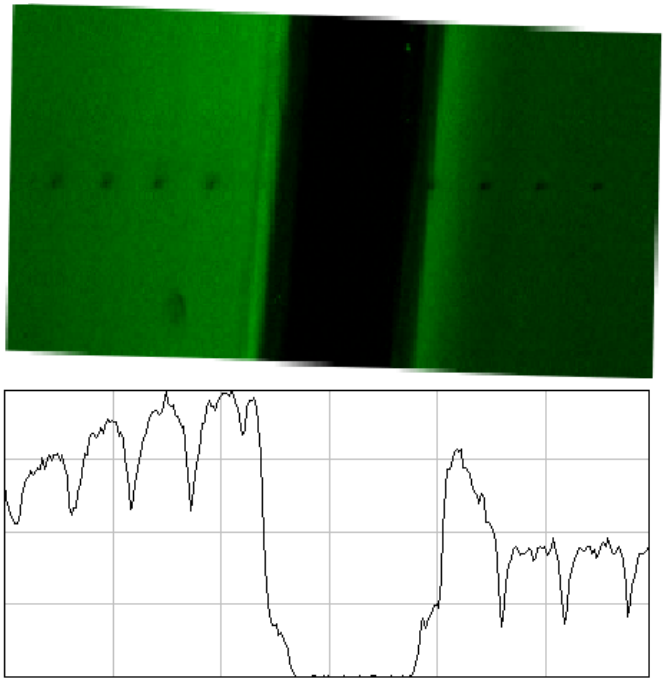

Figure 54. Irreversible data recording by 2PA (overexposure), darkening of the spots is primarily due to the photobleaching of the fluorescent dyes. The bottom plot shows fluorescence intensity profile along recording line. Experimental conditions: 450 mW laser power (at 710 nm) and 400 ms of exposure per voxel.

Photoisomerization is a significantly more efficient process compared to photobleaching. In this particular example, the quantum yield of photoisomerisation was $2*10^{-2}$, while typical values for photodecomposition quantum yields are in the range of 10^{-4} – 10^{-6}. In general, lower exposure times and lower laser powers are required to induce photoisomerisation relative to photobleaching. This is a significant advantage of photochrome-based optical data storage. In case of photochrome 1, it exhibited efficient (quantum yield of photoisomerisation OF→ CF is close to unity) photoswitching via 2PA in

the spectral range 800-980 nm, and for the reason described above, it can find an application in a WORM-type (write-once, read many) optical data storage.[9,10]

References

[1] Sheik-Bahae, M.; Said, A.A.; Wei, T. H.; Hagan, D. J.; Van Stryland, E. W. *IEEE J. Quantum Electron.* **1990**, *26*, 760

[2] Belfield, K. D.; Bondar, M. V.; Hernandez, F. E.; Przhonska, O. V.; Yao, S. *J. Phys. Chem. B* **2007**, *111*, 12723

[3] Terenziani, F.; Painelli, A.; Katan, C.; Charlot, M.; Blanchard-Desce, M. *J. Amer. Chem. Soc.* **2006**, *128*, 15742.

[4] Belfield, K. D.; Bondar, M. V.; Hernandez, F. E.; Masunov, A. E.; Mikhailov, I. A.; Morales, A. R.; Przhonska, O. V.; Yao, S. *J. Phys. Chem. C* **2009**, *113*, 4706.

[5] Corredor, C. C.; Belfield, K. D.; Bondar, M. V.; Przhonska, O. V.; Hernandez, F. E.; Kachkovsky, O. D. *J. Photochem. Photobiol. A Chem.* **2006**, *184*, 177.

[6] Makarov, N.; Drobizhev, M.; Rebane, A. *Optics express*, **2008**, *16*, 4029

[7] Corredor, C. C.; Huang, Z. L.; Belfield, K. D.; Morales, A. R.; Bondar, M. V. *Chem. Mater.* **2007**, *19*, 5165

[8] Corredor, C. C.; Huang, Z.-L.; Belfield, K. D. *Adv. Mater.* **2006**, *18*, 2910

[9] Belfield, K. D.; Schafer, K. J. *Chem. Mater.* **2002**, *14*, 3656

[10] Yanez, C. O.; Andrade, C. D.; Yao, S.; Luchita, G.; Bondar, M. V.; Belfield, K. D. ACS Appl. Mater. Interfaces **2009**, *1*, 2219

CHAPTER 7. CONCLUSIONS

Two-photon absorption cross section enhancement of photochromic compounds was investigated by two methods. In the first method, a new diarylethene-fluorenyl derivative (1) was synthesized and photophysically characterized by means of the steady-state spectroscopy and nonlinear optical techniques. Cyclization and cycloreversion processes of 1 were investigated at room temperature in hexane, cyclohexane and DCM. A very high quantum yield of nearly 1.0 was observed for the direct photochromic transformation of 1 in nonpolar medium. Degenerate 2PA spectra of 1 were obtained over a broad spectral range 560-980 nm (OF) and 810-1380 nm (CF) by an open aperture Z-scan method using 1 kHz femtosecond excitation. A drastic increase in the 2PA cross section from δ_{2PA} ~ 50-70 GM for the OF up to δ_{2PA} ~ 450-600 GM for the CF was observed, ascribed to the pronounced extension of its π-conjugation length upon photocyclization. An example of photochromic medium for two-photon optical recording based on PMMA doped films containing a new diarylethene-fluorene compound 1 was presented with preliminary two-photon data recording and readout. At the same time, a decrease in photoswitching quantum yield and low photoconversion to open form of 1 was observed, suggesting 1 may be suitable for a WORM-type data storage, demonstrated in Chapter 6. By considering these results, along with that of others around the world, extending the conjugation may not be the best solution for developing two-photon photochromic systems.

A new method of two-photon absorption cross section enhancement of photochromic compounds was proposed. The method did not involve alteration of photochrome's

molecular structure and, therefore, photochromic properties are almost entirely preserved. The enhancement of the 2PA cross section results from FRET in, presumably, a supramolecular complex with an efficient 2PA dye. A commercially available photochromic compound, 2,3-bis(2,4,5-trimethyl-3-thienyl)maleimide, was shown by H^1 NMR to form a 1:1 hydrogen bonded complex with 2,6-bis-(acetamido)pyridine. The resulting interaction altered the photophysical and photoisomerization properties of the photochromic compound, as seen from the photoisomerization studies, including ^1H NMR studies of the isomer conversion, extinction coefficients (molar absorptivity), and photoisomerization quantum yields. For some prospective practical applications, such as data storage, a decrease of the maximum conversion of the photochrome to closed form, decrease in quantum yield, and photoisomerization reaction rate may not be entirely desirable. However, the magnitude of this decrease (less than 20%) with the formation of a supramolecular structure is not significant and should not serve as an obstacle in applications. One advantange that cannot be efficiently achieved by other methods, may be the opportunity to increase the effective 2PA cross section of the photochromes. This may be possible by carefully choosing the photochrome-2PA dye pair, according to their photophysical and chemical properties, to form a supramolecular complex. An example for design and synthesisis of a complexing dye, starting from a precursor that was used in 2PA upconverted fluorescence imaging. It has the same triple hydrogen bonding motif as the model compound, 2,6-bis-(acetamido)pyridine. Therefore, it was expected to form a similar supramolecular structure, with similar optical property changes of the photochrome. Theoretical considerations suggest that this dye has high efficiency of energy transfer to the selected photochrome compound. Experimental data provided support to this expectation. At the same time, a compound with similar optical

properties, but with fewer hydrogen bonding sites, revealed a smaller degree of energy transfer to the photochrome.

Resonance energy transfer from a 2PA dye, can be used to virtually enhance the effective 2PA cross section of the photochrome molecules. The maximum level of this enhancement is limited only by the 2PA cross section of the fluorescent dye. Therefore, very high values of virtual 2PA cross sections of the photochromes in supramolecular compexes can be obtained. This approach may be a solution to some of the problems in photocrome-based 3D optical data storage technology.

APPENDIX A: STRUCTURES, ^{1}H and ^{13}C NMR SPECTRA OF COMPOUNDS USED

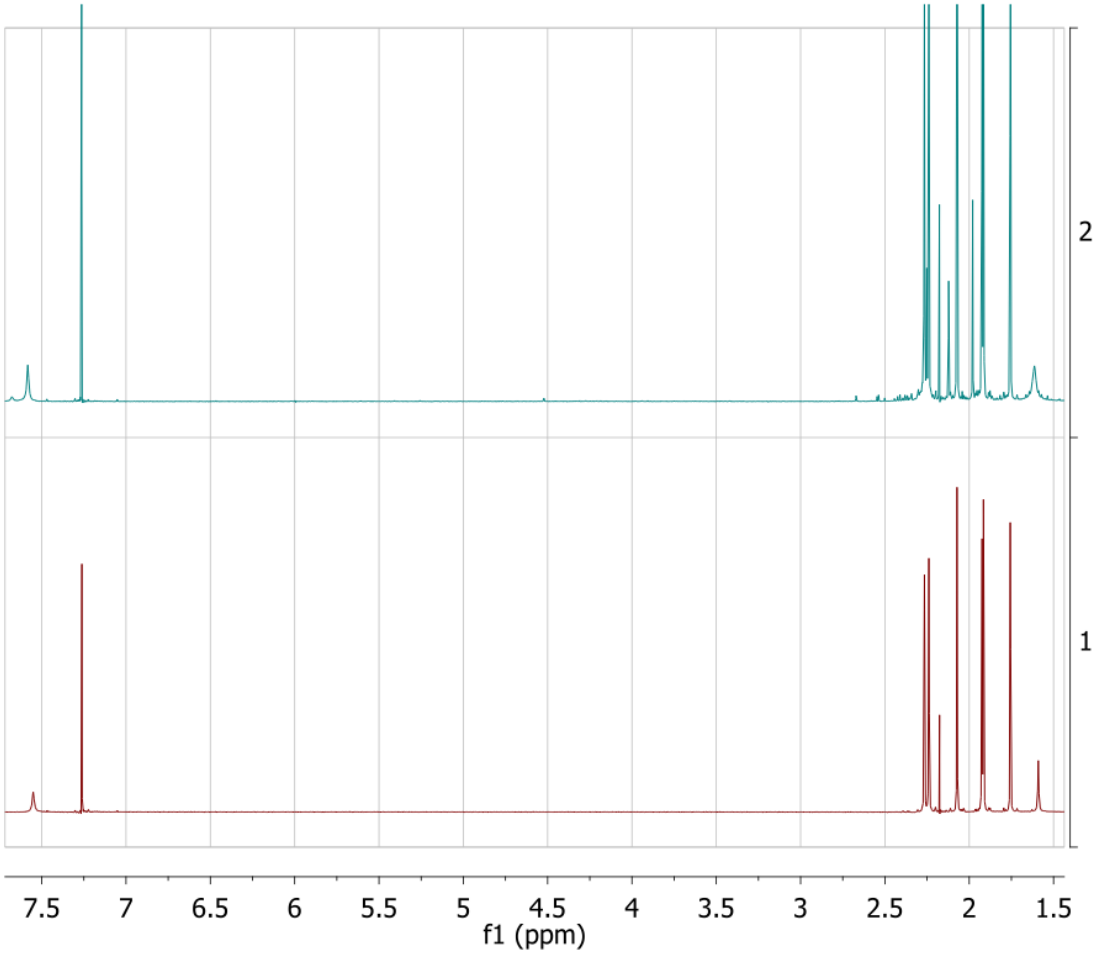

Figure A1. ^{1}H NMR (300 MHz) stacked full spectra of photochrome in open form (spectrum 1, in red) and at photostationary state (spectrum 2, in cyan) in $CDCl_3$.

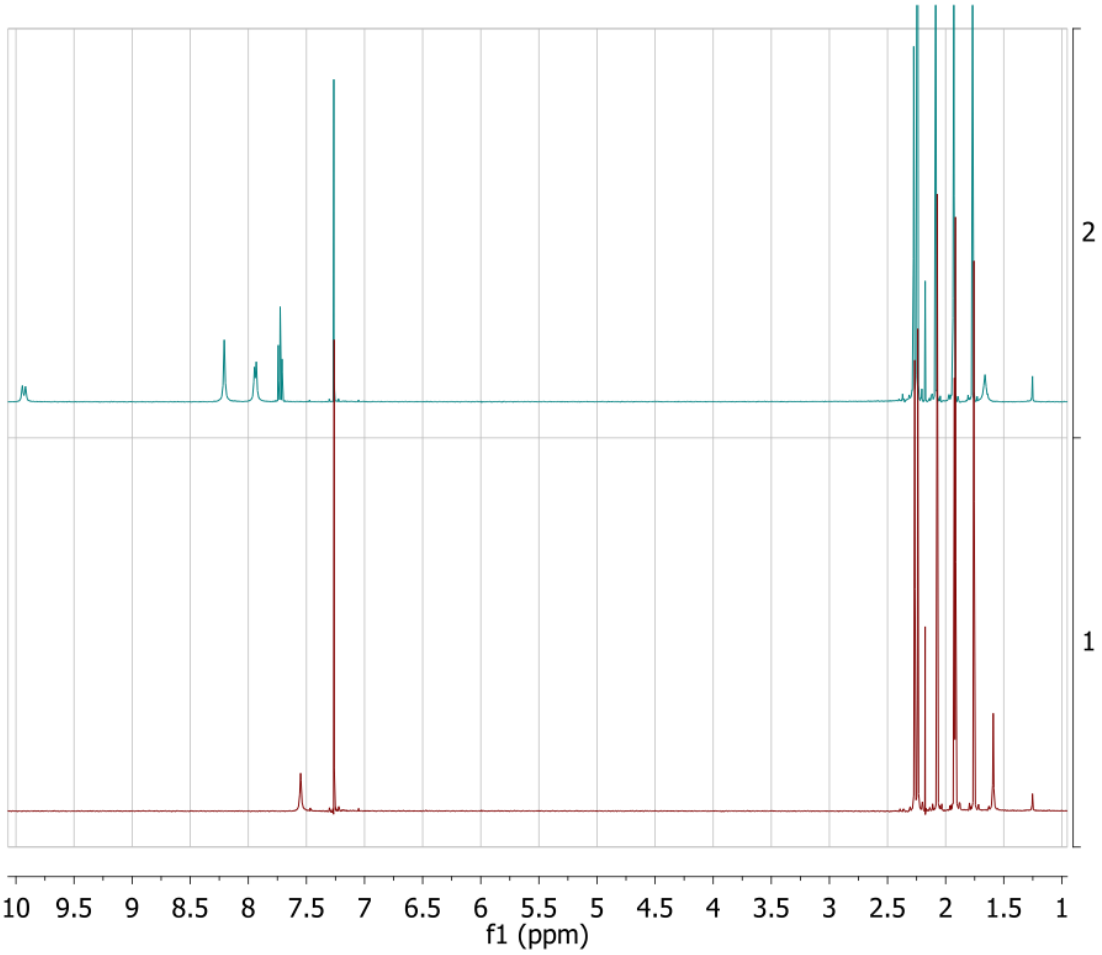

Figure A2. ^{1}H NMR (300 MHz) stacked full spectra of photochrome in open form (spectrum 1, in red) and the mixture of photochrome with 2,6-BAP (spectrum 2, in cyan) in $CDCl_3$.

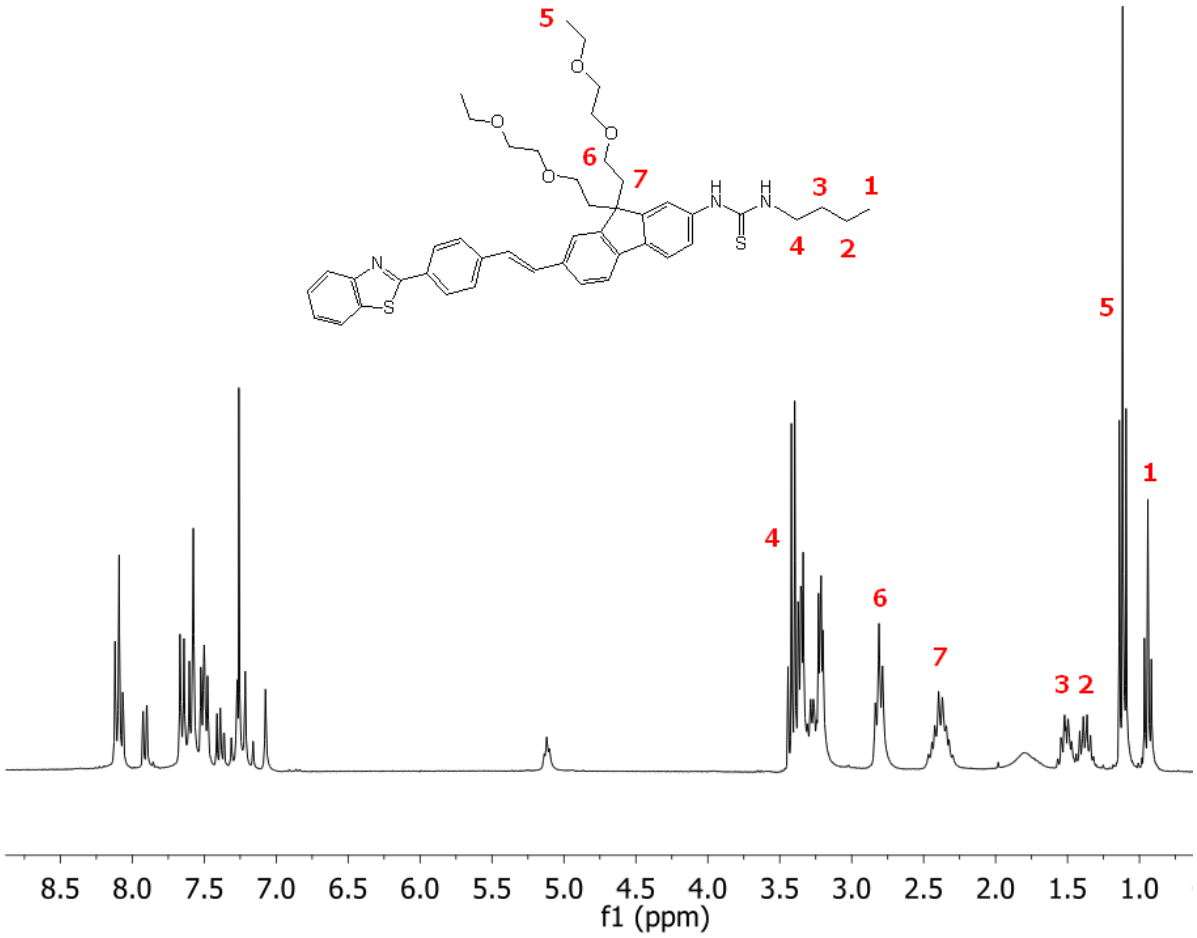

Figure A3. ^{1}H NMR (300 MHz) of model compound D in $CDCl_3$.

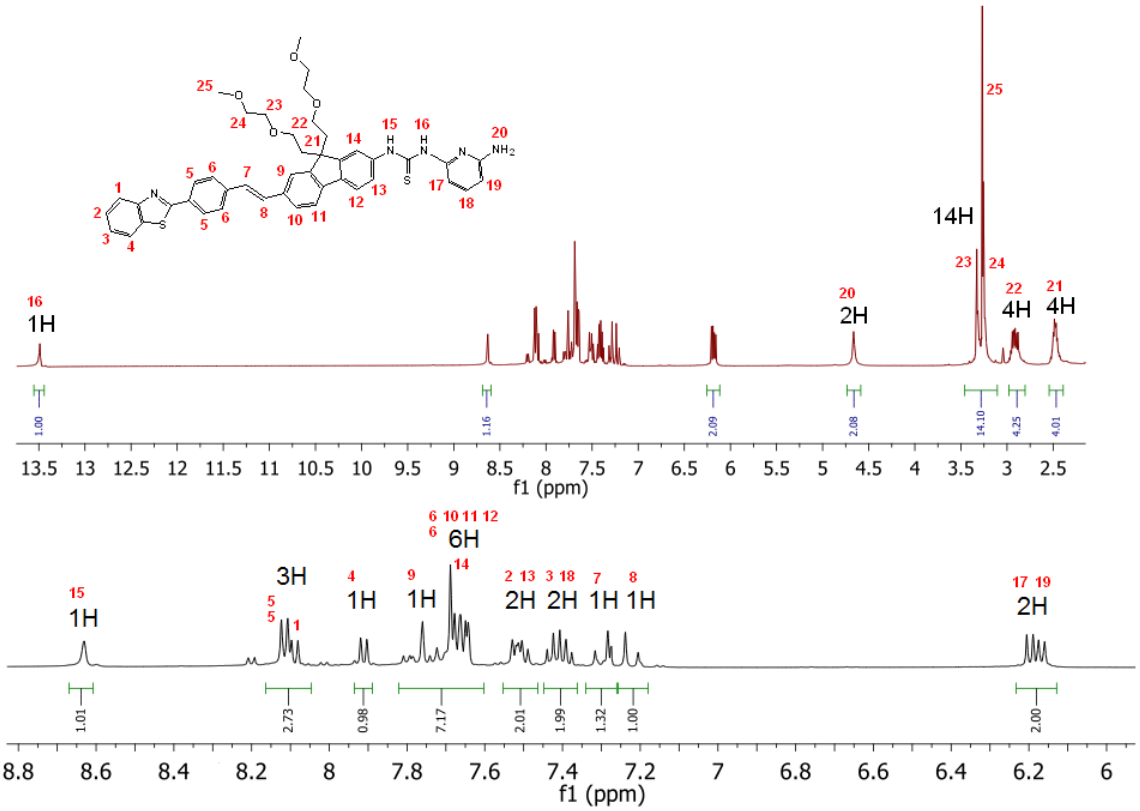

Figure A4. ^{1}H NMR (500 MHz) spectra and peak assignments for THB compound C in $CDCl_3$. Top - full spectrum, bottom – zoomed of the aromatic region.

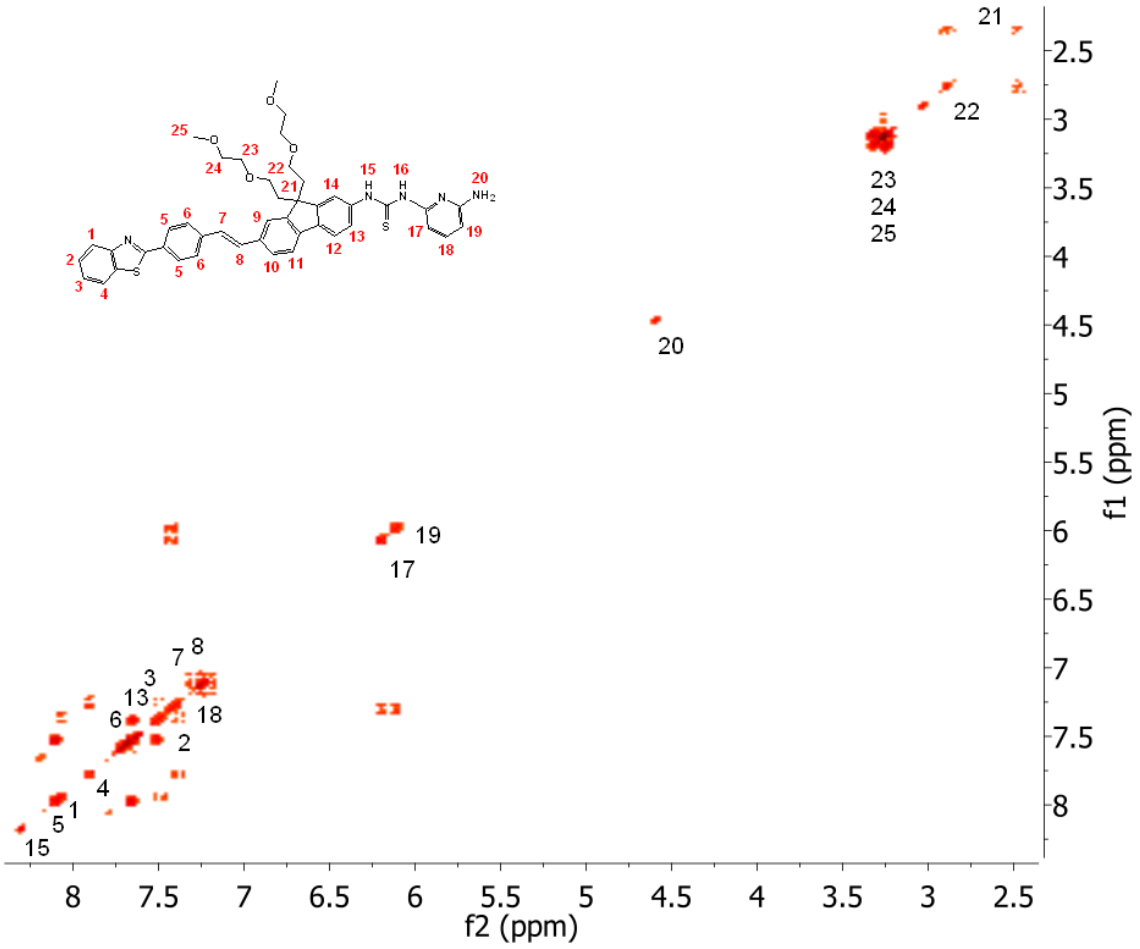

Figure A5. COSY spectrum and signal assignments for THB compound C in the region of 9 to 2 ppm. Solvent $CDCl_3$.

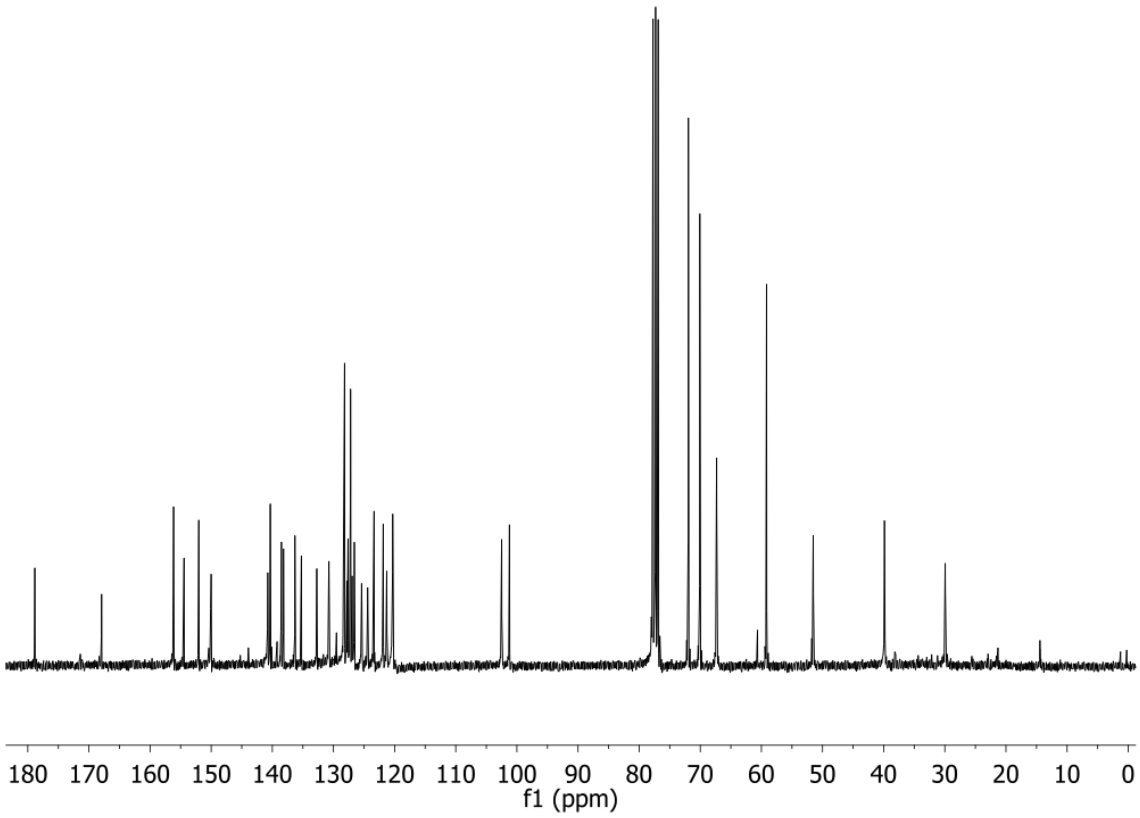

Figure A6. ^{13}C NMR (75 MHz) spectrum of THB compound C, solvent $CDCl_3$ (at 77 ppm).

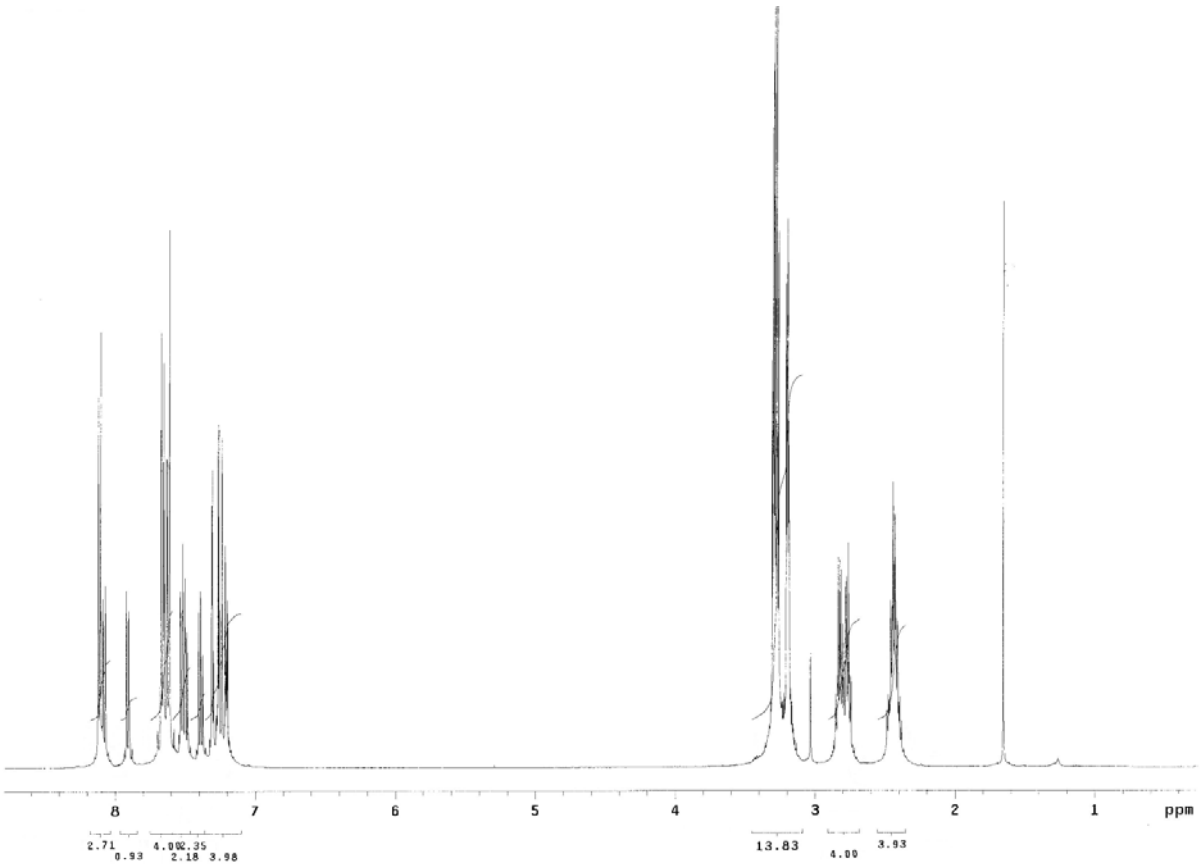

Figure A7. ^{1}H NMR (300 M Hz) spectrum of compound A in $CDCl_3$.

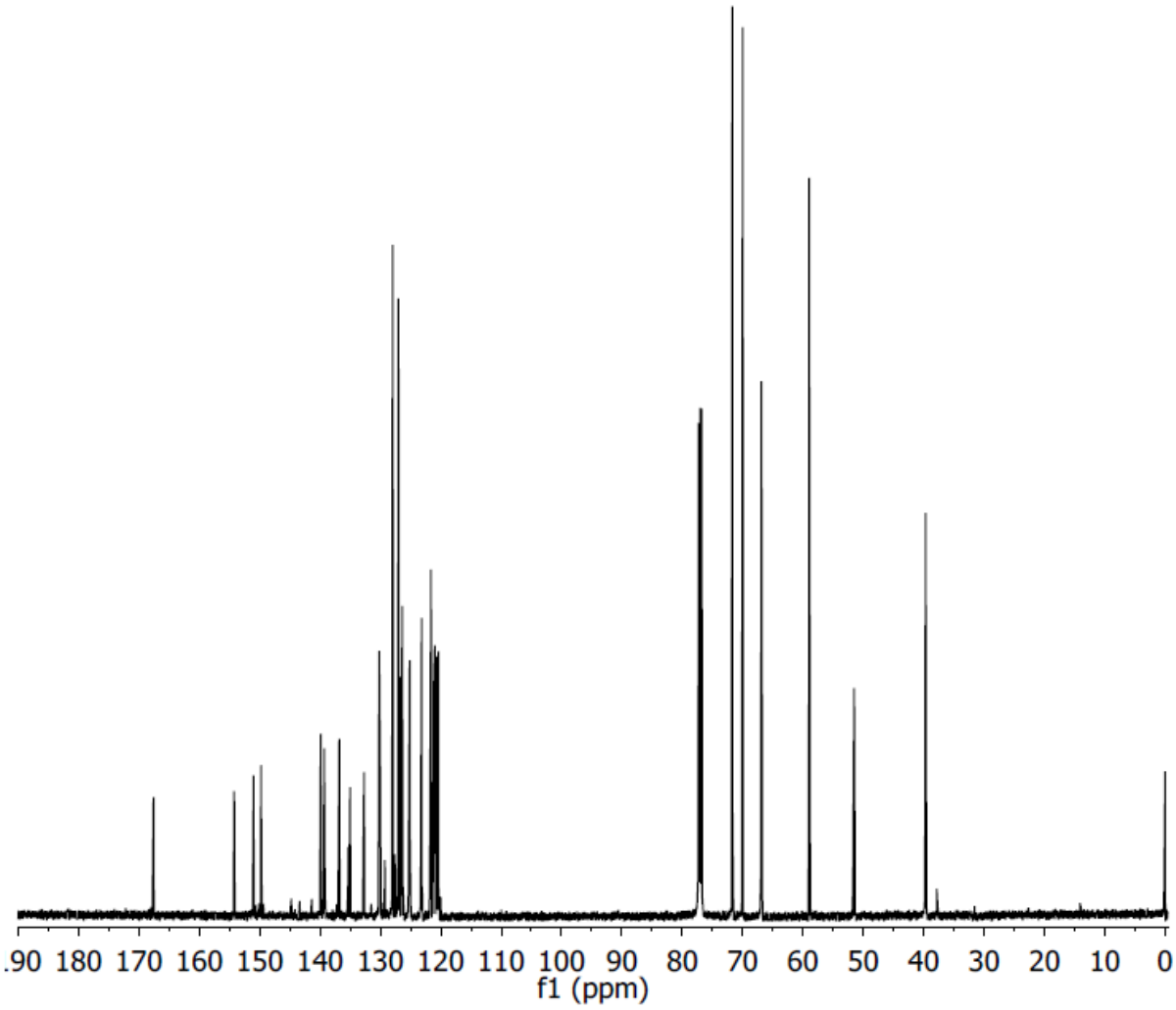

Figure A8. ^{13}C NMR (75 MHz) spectrum of compound A in $CDCl_3$.

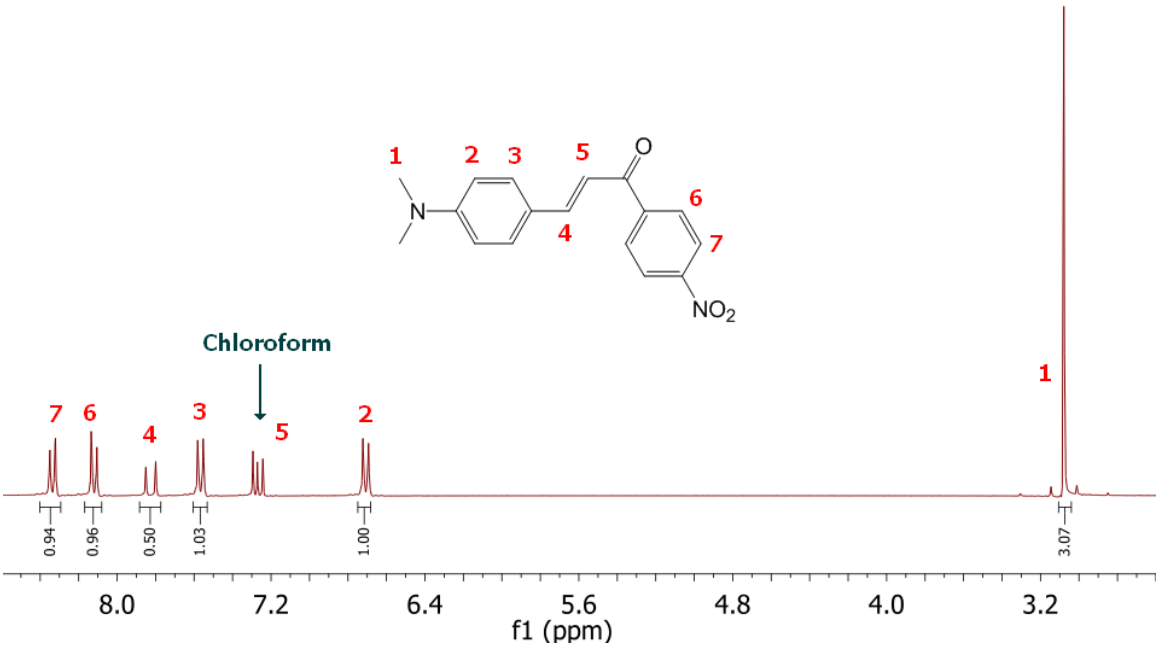

Figure A9. ^{1}H NMR (300 MHz) spectrum and peak assignment of nitro-chalcone in $CDCl_3$.

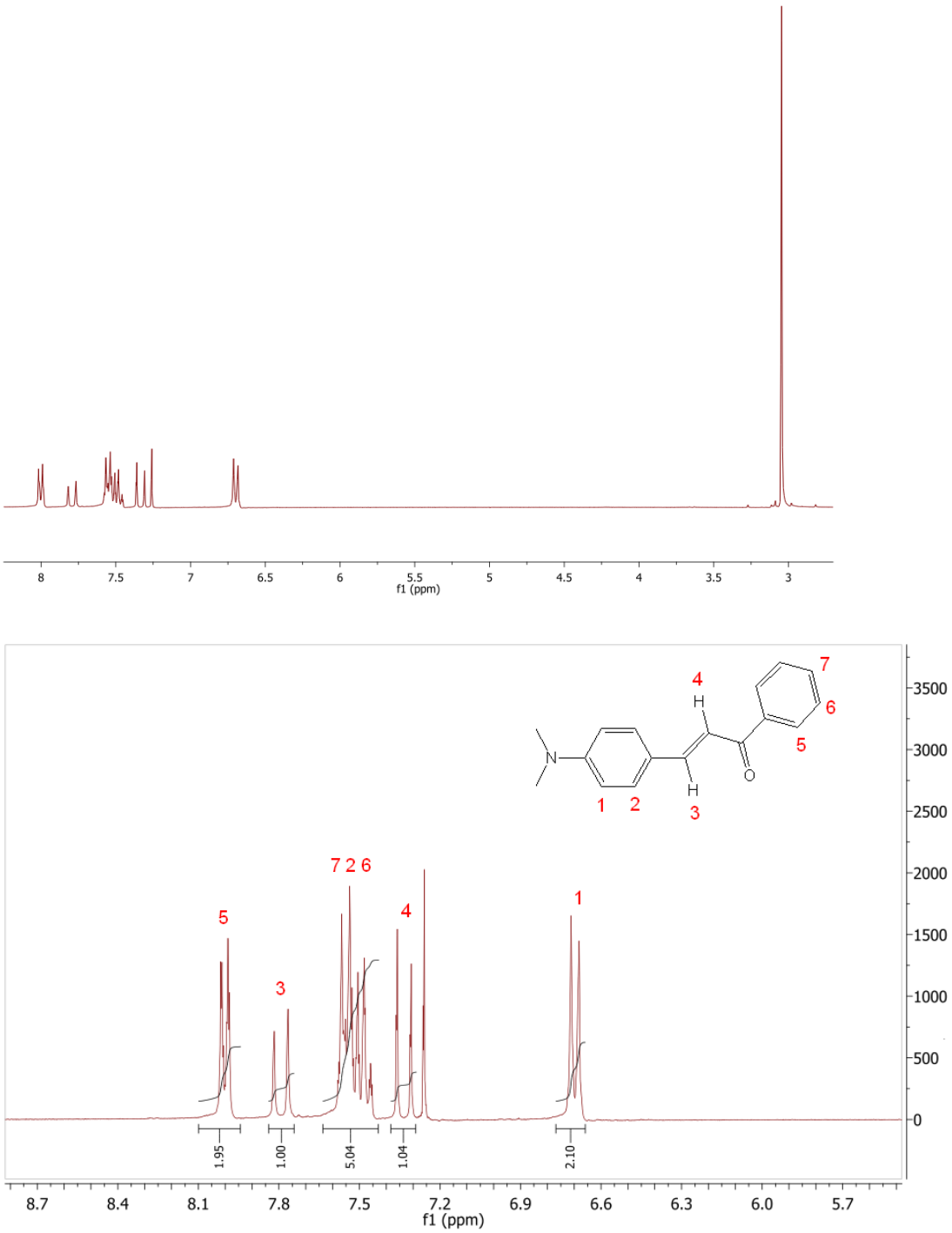

Figure A10. ^{1}H NMR (300 MHz) spectra and peak assignment of chalcone F in $CDCl_3$. Top – full spectrum, bottom – aromatic region.

APPENDIX B: MASS SPECTRUM OF THB COMPOUND C

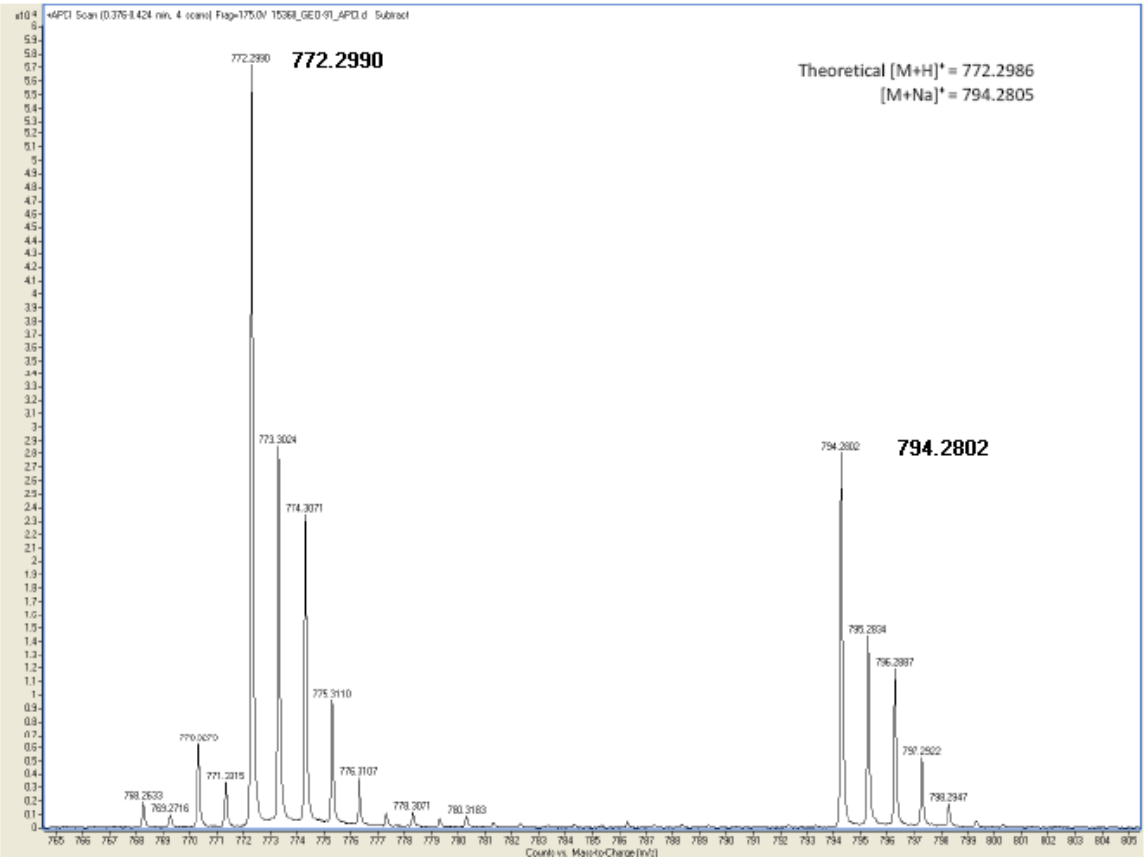

Figure B1. Mass spectrum of THB compound C.

APPENDIX C: MONTE CARLO ALGORITHM

[Compiler: Delphi]

```
VAR
  TabD: array [1..226,1..3] of integer; //donor coordinates
  TabA: array [1..226,1..3] of integer; //acceptor coordinates
  ETab,MinDistance: array [1..226] of double;
   x1,y1,z1,x2,y2,z2,i,j,k:integer;
  Min,D,R0:double;

BEGIN
R0:=2.6; //2.5 nm for THB and 2.6 nm for Model Compound
for i:=1 to 226 do  //Clear tables from old data
 for j:=1 to 3 do
    begin  TabD[i,j]:=0;   TabA[i,j]:=0; end;
 //Fill Donor and Acceptor table with random coordinates
  Randomize;   //Initialize random number generator
 for i:=1 to 226 do
  begin
   //get random numbers from 1 to 100, assign to X,Y,Z coordinates of Donor and //Acceptor
molecules
  TabD[i,1]:=Random(100)+1;   //x coordinate of Donor i molecule
  TabD[i,2]:=Random(100)+1;   //y >>
  TabD[i,3]:=Random(100)+1;   //z >>
```

```
TabA[i,1]:=Random(100)+1;   //x coordinate of Acceptor i (j) molecule
TabA[i,2]:=Random(100)+1;  //y >>
TabA[i,3]:=Random(100)+1;  //z >>
 end;
//Find the clossest acceptor from the donor and compute distance;
  for i:=1 to 226 do //go over all donor molecules coordinates
  begin
   //Get X, Y, Z coordinates of Donor I molecule
   x1:=TabD[i,1];    y1:=TabD[i,2];   z1:=TabD[i,3];
  Min:=50; //50 nm as starting number
       for j:=1 to 226 do  //go over all acceptor molecule coordinates
       begin
      x2:=TabA[j,1];    y2:=TabA[j,2];     z2:=TabA[j,3];
      D:=sqrt(sqr(x1-x2)+sqr(y1-y2)+sqr(z1-z2))*0.5;  // distance in nm
      if D<Min then Min:=D; //Update the minimum distance
       end;
     MinDistance[i]:=Min; //Write distance in memory to get their distribution
     ETab[i]:=Power(R0,6)/(Power(R0,6)+Power(Min,6)); //Record RET eff. of donor i
  //see if another donor is in the range  Donor-to-Donor transfer
       for j:=1 to 226 do  //go over all acceptor molecule coordinates
       if j<>i then  //exclude itself
       begin
       x2:=TabD[j,1];       y2:=TabD[j,2];      z2:=TabD[j,3];       //coordinates of donor j
```

```
        D:=sqrt(sqr(x1-x2)+sqr(y1-y2)+sqr(z1-z2))*0.5;  //calculate distance in nm
        if D<=Min then ETab[i]:=0;    //if closer that an acceptor, consider RET efficiency to
//acceptor  as zero
         end;
END;
```

APPENDIX D: DERIVATION OF EXPRESSION FOR CORRECTION FACTOR (f)

Transmitted light intensity at a distance x for an equimolar solution with concentration C, containing photochrome with extinction coefficient ε_p and a dye with extinction coefficient ε_m is given by the following expression:

$$I(x) = I_0 \cdot 10^{-x \cdot [\varepsilon_p + \varepsilon_m] \cdot C} \quad \text{(D1)}$$

Concentration of the closed form increases upon irradiation of the open form. Assuming that during the first seconds of irradiation, the concentration of the closed form is insignificant and no reverse photoreaction occurs (from closed to open), the change in concentration of the closed form can be approximated as:

$$\frac{dC_{CF}}{dt} = C_{OF} \cdot \delta_p \cdot \Phi_{OF \to CF} \cdot I(x) \quad \text{(D2)}$$

In this expression, C_{OF} is the concentration of the open form of the photochrome, δ_p its single photon cross section, Φ – photoisomerization quantum yield (open to closed form).

Note (N_A – Avogadro's number):

$$\delta_p = \frac{1000 \cdot \varepsilon_p \cdot ln10}{N_A} \quad \text{(D3)}$$

For a discrete time interval Δt, concentration change at a distance x from the cuvette edge:

$$\Delta C_{CF}(x) = C_{OF} \cdot \delta_p \cdot \Phi \cdot I(x) \cdot \Delta t \quad \text{(D4)}$$

The total change in concentration of the closed form in the cuvette is the integral over the length of the cuvette (L):

$$\Delta C_{CF} = \int_0^L C_{OF} \cdot \delta_p \cdot \Phi \cdot \Delta t \cdot I_0 \cdot 10^{-x \cdot [\varepsilon_p + \varepsilon_m] \cdot C} dx \quad \text{(D5)}$$

Removing outside integral the terms which are not function of distance:

$$\Delta C_{CF} = C_{OF} \cdot \delta_p \cdot \Phi \cdot \Delta t \cdot I_0 \int_0^L 10^{-x \cdot [\varepsilon_p + \varepsilon_m] \cdot C} dx \quad \text{(D6)}$$

or:

$$\Delta C_{CF} = \alpha \cdot \int_0^L 10^{-x \cdot [\varepsilon_p + \varepsilon_m] \cdot C} dx \quad \text{(D7)}$$

After integration:

$$\Delta C_{CF} = \alpha \left(\frac{10^{-L \cdot [\varepsilon_p + \varepsilon_m] \cdot C} - 1}{-[\varepsilon_p + \varepsilon_m] \cdot C \cdot ln10} \right) \quad \text{(D8)}$$

Since the extinction coefficients at 405 nm of the dyes used are >3*10^4 M^{-1} cm^{-1}, for the concentration of study 3*10^{-3} M and L=0.1 cm, the below term is extremely small:

$$10^{-L \cdot [\varepsilon_p + \varepsilon_m] \cdot C} \approx 0 \quad \text{(D9)}$$

Removing this term, yields the simplified expression for the increase in closed form concentration:

$$\Delta C_{CF} = \frac{\alpha}{[\varepsilon_p + \varepsilon_m] \cdot C \cdot ln10} \quad \text{(D10)}$$

For a different dye (reference) with extinction coefficient ε_m^R mixed with the photochrome, same expression applies:

$$\Delta C_{CF}^R = \frac{\alpha}{[\varepsilon_p + \varepsilon_m^R] \cdot C \cdot ln10} \quad \text{(D11)}$$

The change in absorption spectra is proportional to the concentration change ($\Delta D = L\ \varepsilon_p\ \Delta C$). For the two solutions (with 2 different dyes mixed with photochrome):

$$\frac{\Delta D_{CF}^R}{\Delta D_{CF}} = \frac{\Delta C_{CF}^R}{\Delta C_{CF}} = \frac{\varepsilon_p + \varepsilon_m}{\varepsilon_p + \varepsilon_m^R} \quad \text{(D12)}$$

From the above expression, one can express the expected change in absorption for one solution, if solution of the other solution is known:

$$\Delta D_{CF}^{R} = \Delta D_{CF} \cdot \frac{\varepsilon_p + \varepsilon_m}{\varepsilon_p + \varepsilon_m^{R}} = \Delta D_{CF} \cdot f \qquad \text{(D13)}$$

This expression was used to calculate the absorption of photochrome mixed with nitrochalcone at one concentration (that would have the same optical density as THB) from the experimental data of the absorption of photochrome mixed with nitrochalcone at a different concentration (that would have the same optical density as the model compound).

APPENDIX E: DELTA SCAN METHOD FOR NON-SQUARE LASER PULSES

The equation for three point method (or delta method) has been derived for the case of square shaped laser pulses. Here it will be shown that same equation can be used for any other laser pulse shape. To do so, a simple theorem has to be introduced and demonstrated with a special condition.

Theorem:

If for all elements (x_i) of a data set (S) exists such an operation P, that applied on every element in the data set S gives the same result R, then any sum of the elements in the data set S will give the same result R, when operation P is applied on the sum. (E.g. if any number multiplied by zero, gives zero, then a sum of any numbers multiplied by zero will also give zero)

Partial demonstration. Starting condition:

$$\forall x_i (x_i \in S) : \exists P(x_i) = R \qquad \text{(C1)}$$

For the purpose of this dissertation, only a special case of the theorem will be demonstrated, in which the sum of the elements is also an element of the set S:

$$\sum_{i=a}^{b} x_i = x_j (x_j \in S) \qquad \text{(C2)}$$

In this special case, according to C1:

$$P(x_j) = R \qquad \text{(C3)}$$

Substituting the value of x_j from C2 into C3 yields:

$$P(\sum_{i=a}^{b} x_i) = R \qquad \text{(C4)}$$

End of demonstration.

In the case of a non-square laser pulse, the pulse can be imagined as a temporal sum of infinitively small square pulses. The laser intensity of each such pulse (i) is x_i. Intensity of any laser pulse has a value that belongs to positive real numbers (S). For every individual square pulse calculation of the 2PA cross section (operation P) according to the equation (J11) must give the same result β (R). Indeed, 2PA cross section is a molecular parameter and does not depend of the laser intensity used to measure it.

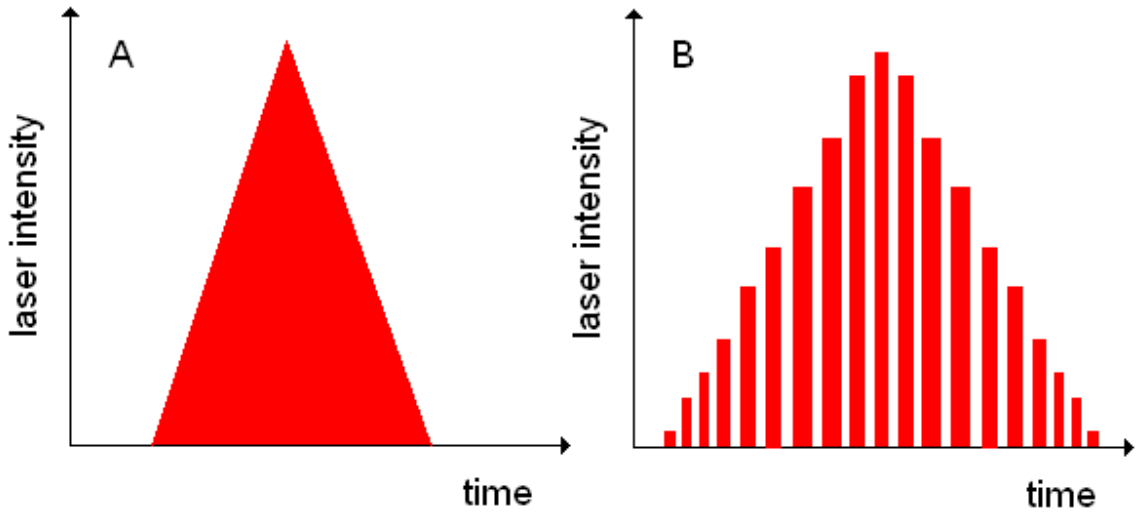

Figure E1. Any pulse shape, e.g. triangular (A), can be viewed as a sum of square pulses (B).

Since every square pulse of any energy gives the same result of cross section, then according to the above theorem, calculation of the cross section from the sum of square pulses (integral pulse of any shape) must give the same result with the same equation. A sum of intensity values of individual square pulses is also a real number, which is included in S (special condition met – C2).

Below an alternative demonstration is presented showing that equation J11 is valid for the particular case of a Gaussian pulse shape (used in Z-Scan).

Three theoretical Z-Scan curves have been simulated with the following common parameters: energy per pulse 50 nJ, laser pulse width 100 fs, w_0 15 μm, scan length 1.57068 cm, laser wavelength 800 nm, sample thickness 0.1 cm. For reference, two theoretical Z-Scan curves correspond to 40 GM, for concentrations 0.01 M and 0.025 M. The third curve corresponds to 55 GM and concentration 0.015 M. The relative cross section coefficient is M = 55 GM / 40 GM = 1.375.

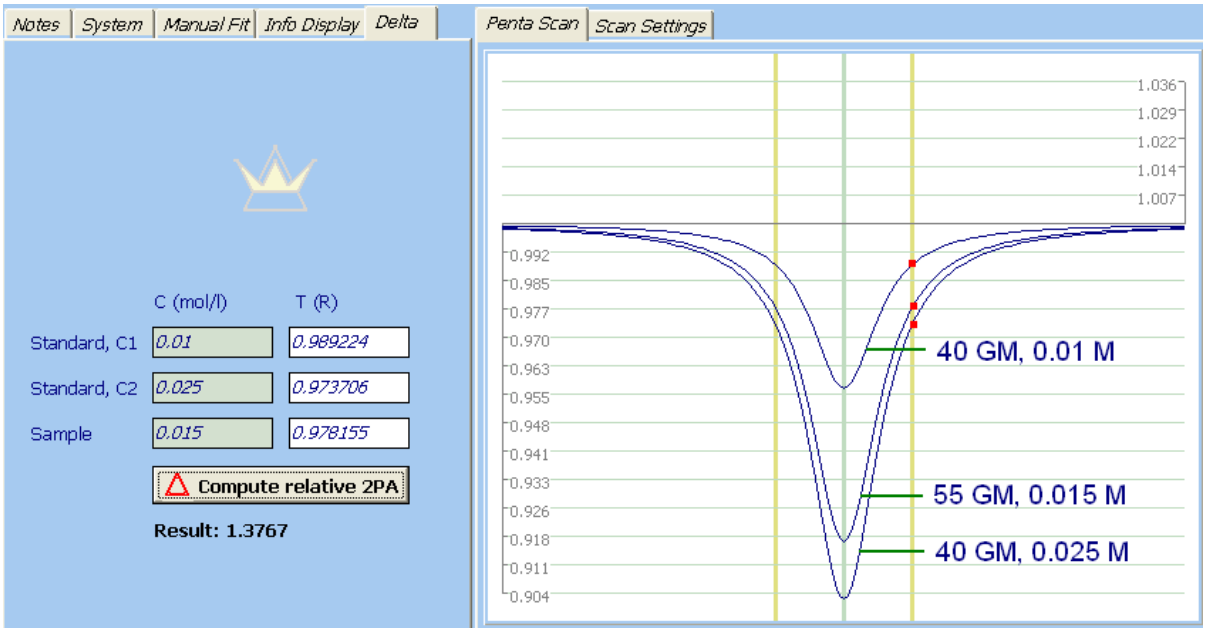

Figure E2. Alice 5.0 software screenshot. Calculated relative 2PA cross section from three theoretical Z-Scan curves using equation J11 (Equation 9). Yellow lines show the selected Z-position, at the intersection with Z-Scan curves laser transmission intensity is registered (marked with red squares): see table of the left side.

It can be shown that in any Z-location (same laser intensity for all Z-Scan curves), equation J11 holds true. In Figure E2, at a random Z-location the transmission values are taken (tabulated on the left side of the picture). As a standard, the 40 GM curves are taken; as a sample the 55 GM curve is considered. The relative cross section coefficient calculated from equation J11 yields M'=1.3767 (0.1% relative error to expected value of 1.375). Note

that coefficients in equation J11 are calculated as: $a=T_1/T_3$ and $b=T_2/T_3$, where T_1 and T_2 are the transmittance values of the standard and T_3 is the transmittance value of the sample.

APPENDIX F: ABSORPTION AND EMISSION SPECTRA OF CHALCONE F

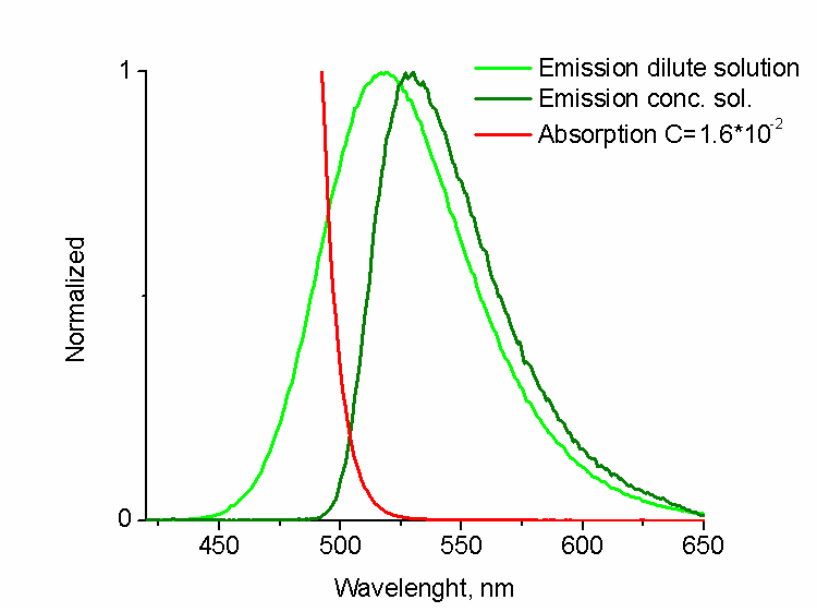

Figure F1. Fluorescence spectral shift due to reabsorption at high concentrations. Concentration of the solutions are $1.6*10^{-2}$ mol/L (concentrated) and 10^{-3} mol/L (less concentrated).

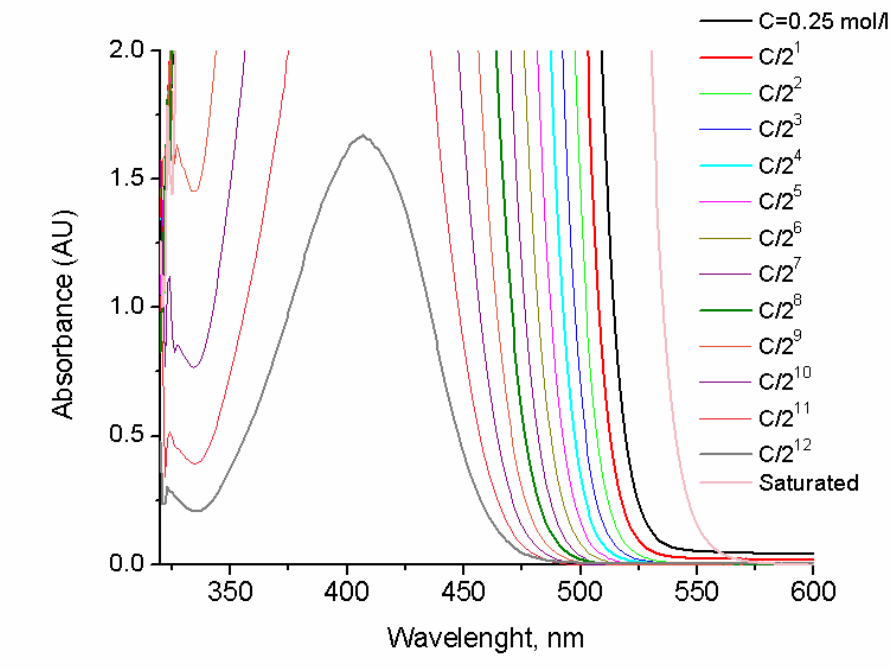

Figure F2. Absorption of the fluorescent chalcone (F) at different concentrations (concentrations are shown on the right side, from C=0.25 M down to $6*10^{-5}$ M).